City Research Online

City St George's, University of London

Citation: Gorasia, Rohit J. (2013). Behaviour of ribbed piles in clay. (Unpublished Doctoral thesis, City University London)

This is the unspecified version of the paper.

This version of the publication may differ from the final published version. To cite this item please consult the publisher's version.

Permanent repository link: https://openaccess.city.ac.uk/id/eprint/2406/

Copyright and Reuse: Copyright and Moral Rights remain with the author(s) and/or copyright holders. Copies of full items can be used for personal research or study, educational, or not-for-profit purposes without prior permission or charge, unless otherwise indicated, provided that the authors, title and full bibliographic details are credited, a hyperlink and/or URL is given for the original metadata page and the content is not changed in any way. For full details of reuse please refer to City Research Online policy.

City Research Online: http://openaccess.city.ac.uk/ publications@citystgeorges.ac.uk

BEHAVIOUR OF RIBBED PILES IN CLAY

by

Rohit Jay Gorasia

A dissertation submitted for the Degree of
Doctor of Philosophy

City University London
Geotechnical Engineering Research Group
School of Engineering and Mathematical Science

May 2013

To my family.

Never fear struggle, pain or hard work for it is these aspects
of life that are ones greatest teacher. – S.P.Gorasia

Contents

List of tables vii

List of figures viii

Acknowledgements xii

Declaration xii

Abstract xii

List of symbols xii

Abbreviations xii

1 Introduction 1

1.1 Background 1

1.2 Objectives 1

1.3 Centrifuge modelling 1

1.4 Summary of thesis 1

2 Literature Review 6

2.1 Introduction 6

2.2 Pile classification 6

2.2.1 Displacement piles 6

2.2.2 Replacement piles 6

2.3 Design of piles 6

2.3.1 Undrained or total stress approach 6

2.4 Pile settlement 6

2.5 Factors of safety 6

2.6 The behaviour of soils 6

2.7 Enlarged pile base 6

2.8 Installation techniques for bored piles 6

2.8.1 Continuous fight auger (CFA) 6

2.8.2 Rotary boring 6

2.9 Individual components of the capacity of a pile 6
2.10 Pile testing 6
2.10.1 Maintained load test (MLT) 6
2.10.2 Constant rate of penetration test (CRP) 6
2.10.3 Rapid load test (RLT) 6
2.10.4 Dynamic load test (DLT) 6
2.10.5 Osterberg load cell 6
2.10.6 Rate effects on pile testing 6
2.11 Interpretation of pile test data 6
2.12 Numerical modelling 6
2.13 Atlas piling system 6
2.14 High capacity shear pile testing – Expanded Piling 6
2.15 Summary 6
3 Geotechnical centrifuge modelling 25
3.1 Introduction 25
3.2 Principles of centrifuge modelling 25
3.3 Scaling laws 25
3.4 Errors in centrifuge modelling 25
3.4.1 Radial acceleration field 25
3.4.2 Vertical acceleration 25
3.4.3 Orientation of model in gravity field 25
3.4.4 Boundary effects 25
3.4.5 Grain size 25
3.4.6 Soil stress errors 25
3.5 The geotechnical centrifuge facility at City University London 25
3.6 Summary 25
4 Model and apparatus design 35

4.1 Introduction 35
4.2 Model design requirements 35
4.3 Apparatus design development 35
4.3.1 Soil container 35
4.3.2 Pile cutters & guides 35
4.3.3 Pile caps 35
4.3.4 Casting of piles 35
4.3.5 Pile loading apparatus 35
4.3.6 T-bar penetrometer and actuator 35
4.4 Testing procedure 35
4.4.1 Sample preparation 35
4.4.2 Model making 35
4.4.3 Test procedure 35
4.5 Summary 35
5 Experimental work 48
5.1 Introduction 48
5.2 Details of tests 48
5.3 Observations and results 48
5.3.1 Preliminary tests - RJG0 and RJG2 48
5.3.2 Apparatus verification tests – RJG5 and RJG6 48
5.3.3 Concentric ribbed pile tests – RJG3, RJG4, RJG7, RJG10, RJG13, RJG14 and RJG21 48
5.3.4 Helical ribbed pile tests – RJG8, RJG9, RJG16, and RJG17 48
5.3.5 Straight piles with equivalent rib diameter test – RJG11 48
5.3.6 Tapered ribbed pile tests – RJG15, and RJG19 48
5.3.7 Under reamed ribbed pile test – RJG22 48
5.3.8 Pore pressures 48

5.4 Summary 48
6 Discussion 58
6.1 Introduction 58
6.2 Soil sample 58
6.3 Comparison to full scale test results 58
6.4 Test data analysis 58
6.5 Pile design framework 58
6.5.1 Longitudinal cross sectional area method 58
6.5.2 Detailed design method 58
6.5.3 The theoretical capacity of a plain pile 58
6.5.4 Concentrically ribbed pile capacity 58
6.5.5 Helically ribbed pile capacity 58
6.5.6 Tapered and under reamed ribbed pile capacity 58
6.6 Comparison of framework to actual test data 58
6.7 Structural capacity of pile rib 58
6.8 Summary 58
7 Conclusions and recommendations for further work 70
7.1 Introduction 70
7.2 Experimental procedure 70
7.3 Conclusions 70
7.4 Limitations and implications of results 70
7.5 Recommendations for further research 70
8 References 77
9 Tables 85
10 Figures 92
Appendix A: Example pile capacity calculation 143

List of tables

Table 2.1 Pile design method for various soil conditions and drainage conditions after Azizi (2007) 85

Table 3.1 Centrifuge scaling laws after Wood (2004)..... 86

Table 4.1 Summary of tests conducted on various resin and filler mixers..... 87
Table 4.2 Soil model consolidation loading schedule..... 87

Table 5.1 Summary of all centrifuge tests 88

Table 6.1 Results of test pile failure analysis for all piles tested..... 89
Table 6.2 Back calculated alpha for plain piles 90
Table 6.3 Summary of theoretically calculated and test rib pile capacity. 91

List of figures

Figure 1.1 Previous pile loading apparatus. 92
Figure 1.2 New pile loading apparatus. 92

Figure 2.1 Summary of pile type (after BS8004:1986). 93
Figure 2.2 Adhesion factors for driven piles, after Tomlinson (1977). 94
Figure 2.3 Adhesion factor for clay tills after Weltman and Healy (1973). 94
Figure 2.4 Schematic diagram of under reaming tool after Tomlinson (1977). . 95
Figure 2.5 Soilmec SR40 CFA and rotary piling rig (courtesy of soilmec.com). 95
Figure 2.6 Pile ultimate failure according to Maxurkiewicz after Fellenius (1980)..... 96
Figure 2.7 Pile ultimate failure according to Chin after Fellenius (1980). 96
Figure 2.8 Comparison of nine failure criteria after Fellenius (1980) 97
Figure 2.9 FEA load settlement curves after Senghani (2008). 97
Figure 2.10 Predictions of volume of concrete for a given load from finite element analysis conducted by Senghani (2008). 98
Figure 2.11 Atlas piling method after Tomlinson (1977). 98
Figure 2.12 Expanded Piling construction issue rib cutting tool. 99

Figure 3.1 Inertial stress in a centrifuge model induced by rotation about a fixed axis and corresponding gravitational stresses in the prototype, after Taylor (1995). 100
Figure 3.2 Comparison of stress variation with depth in a centrifuge model and its corresponding prototype, after Taylor (1995). 100
Figure 3.3 Estimated undrained shear strength profile with depth..... 101

Figure 4.1 Test layout plan. 102
Figure 4.2 Construction details of new cylindrical soil container..... 103
Figure 4.3 Drainage plate. 104
Figure 4.4 Adjustable brass standpipe. 105
Figure 4.5 Straight shafted pile cutting tool. 106

Figure 4.6 Rib cutting tool..... 106
Figure 4.7 Rib cutting tool operation..... 107
Figure 4.8 Pile cutting guide collars..... 107
Figure 4.9 Pile cap (section)..... 108
Figure 4.10 Compressive load tests on Sika Biresein G27 resin with Al_2O_3 filler. 108
Figure 4.11 Compressive load tests on Sika Biresein G27 resin with $Al(OH)_3$ filler..... 109
Figure 4.12 Actuated lead screw and loading beam. 109
Figure 4.13 Load cell and loading pin assembly diagram. 110
Figure 4.14 Optical rotary encoder exploded view. 110
Figure 4.15 T-Bar Penetrometer construction detail..... 111
Figure 4.16 T-bar PCB layout and circuit diagram. 111
Figure 4.17 T-bar Penetrometer photograph..... 112
Figure 4.18 Construction detail and photograph of T-Bar actuator. 112
Figure 4.19 Undrained shear strength with depth for T-bar Penetrometer calibration, (McNamara, 2011). 113
Figure 4.20 Photograph of industrial ribbon blade mixer..... 113
Figure 4.21 Variation of over-consolidation ratio with depth for a kaolin sample consolidated to 500kPa and allowed to swell under 250kPa..... 114
Figure 4.22 Variation of K_0 with depth for over-consolidated kaolin sample.. 114
Figure 4.23 Theoretical vertical and horizontal total and effective stresses for over-consolidated kaolin sample. 115
Figure 4.24 Pore pressure ports and transducer installation equipment. 116
Figure 4.25 Excess soil trimmed with wire cutter. 116
Figure 4.26 PlastiDip used to seal top of soil model..... 117
Figure 4.27 Undrained shear strength with depth for silicon oil and PlastiDip used as surface sealant. 117
Figure 4.28 Top tube mounted to soil container with instrumentation attached. 118

Figure 5.1 Typical pile dimensions. 119
Figure 5.2 Typical exhumed piles (scaled to 10p). 119
Figure 5.3 LVDT arrangement used to detect eccentric pile loading. 120

Figure 5.4 Rib cutting tool developed and used by Witton-Dauris (2008)..... 120
Figure 5.5 Isometric illustration of the tapered rib pile. 121
Figure 5.6 10mm helical rib cutter with ball nut and cutting bucket. 121
Figure 5.7 Manufactured lead screw and ball nut (30mm pitch). 122
Figure 5.8 Load settlement curve, Test RJG0, concentrically ribbed pile with 10mm spacing using existing test equipment. 122
Figure 5.9 Load settlement curve, Test RJG2, concentrically ribbed pile with 10mm spacing. 123
Figure 5.10 Load settlement curve, Test RJG5, 2 straight shafted piles. 123
Figure 5.11 Load settlement curve, Test RJG6, 2 straight shafted piles. 124
Figure 5.12 Load settlement curve, Test RJG3, concentrically ribbed pile with 10mm spacing. 124
Figure 5.13 Load settlement curve, Test RJG13, concentrically ribbed pile with 40mm spacing. 125
Figure 5.14 Load settlement curve, Test RJG21, concentrically ribbed pile with 40mm spacing. 125
Figure 5.15 Load settlement curve, Test RJG4, concentrically ribbed pile with 15mm spacing. 126
Figure 5.16 Load settlement curve, Test RJG7, concentrically ribbed pile with 15mm spacing. 126
Figure 5.17 Load settlement curve, Test RJG10, concentrically ribbed pile with 20mm spacing. 127
Figure 5.18 Load settlement curve, Test RJG14, concentrically ribbed pile with 10mm spacing with ribs only in bottom third of pile. 127
Figure 5.19 Load settlement curve, Test RJG8, helically ribbed pile with 10mm spacing. 128
Figure 5.20 Load settlement curve, Test RJG9, helically ribbed pile with 10mm spacing. 128
Figure 5.21 Load settlement curve, Test RJG16, helically ribbed pile with 20mm spacing. 129
Figure 5.22 Load settlement curve, Test RJG17, helically ribbed pile with 30mm spacing. 129
Figure 5.23 Load settlement curve, Test RJG11, 19mm diameter straight shafted pile. 130

Figure 5.24 Load settlement curve, Test RJG15, tapered ribbed pile with 15mm spacing. 130
Figure 5.25 Load settlement curve, Test RJG22, under reamed pile with 15mm spacing. 131
Figure 5.26 Typical PPT response during pore pressure equalisation. 131

Figure 6.1 Undrained shear strength with depth as profiled by the T-bar 132
Figure 6.2 Load settlement curves from Expanded-Arup tests, Ground Engineering (2003). 132
Figure 6.3 Load settlement curve, Test RJG4, concentrically ribbed pile with 15mm spacing. 133
Figure 6.4 Normalised load settlement curves for all pile tests. 134
Figure 6.5 Normalised load settlement curves for concentric ribs and helical ribs with similar spacing. 135
Figure 6.6 Normalised load settlement curves for 10mm spaced ribs and the tapered rib. 136
Figure 6.7 Normalised load settlement curves for the 19mm plain pile and the 10mm spaced ribbed piles. 137
Figure 6.8 Normalised load settlement curves for the 19mm plain pile and a pile with the bottom third concentrically ribbed. 138
Figure 6.9 Average normalised load settlement curves for helical and concentric rib types. 139
Figure 6.10 Plain pile ultimate capacity against soil sample average undrained shear strength for all successful tests. 139
Figure 6.11 Percentage increase in pile cross sectional area (K) against the percentage increase in ultimate bearing capacity (M). 140
Figure 6.12 The end bearing plastic failure envelope for perfectly rough deep piles as presented by Meyerhof (1951). 140
Figure 6.13 The proposed end bearing plastic failure envelope for concentric ribs. 141
Figure 6.14 Helix angle factor (η) against the helix angle (θ) for helical ribs... 141
Figure 6.15 Tapered rib pile – rib height for shear calculation. 142

Acknowledgements

Working toward this Ph.D. has been a wonderful and often overwhelming experience. I have been fortunate that my involvement with the Geotechnical Engineering Research Group at City University London has enabled me to work closely with a group of highly dedicated people who have always been willing to provide help, support and encouragement whenever needed.

I am indebted to many people for making the time working on my Ph.D. an unforgettable experience.

First of all, I am deeply grateful to my supervisor, Dr Andrew McNamara. Working with Andrew has been a real pleasure. He has been a steady influence throughout my Ph.D. career; and has oriented and supported me with promptness and care, and has always been patient and encouraging in times of new ideas and difficulties. Without his commitment and understanding especially when faced with difficult problems, I could not have completed this research. He has been an unending source of motivation, practical ideas and solutions.

Furthermore, I have been very privileged to get to know and to collaborate with many other great people who have become friends over the last few years. I learned a lot from them about life, research, how to tackle new problems and how to develop techniques to solve them. Professor Neil Taylor, Professor Sarah Stallebrass and Dr Richard Goodey have always given me much encouragement, been willing to help with problems and discuss ideas. They have all enthusiastically provided guidance throughout my time here. Their help has been invaluable and is very much appreciated.

Thanks are also due to the School of Engineering and Mathematical Sciences technical staff, in particular Mr Melvyn Hayes and Mr Keith Osborne, for their assistnce in designing, manufacturing and assembling the testing apparatus. Both Melvyn and Keith have taught me many practical skills which I am sure will be of use in the years to come.

Working at the Geotechnical Engineering Research Group has been made an enjoyable experience by all of the members of the group who have created an atmosphere of friendship and good humour at all times. Thanks are therefore due to Mr Sam Divall for his insightful comments, for his support, and for many motivating discussions. I am also grateful to my colleagues Mr Hitesh Halai, Mr Neil Phillips, and Dr Alexis Rose who have provided insightful discussions about the research and always supported me.

I am grateful that, during various stages of the project, I have received useful guidance and support from Mr Dinesh Patel of Arup Geotechnics, Mr Martin Blower and Dr Toby Hayward of Expanded Piling and Dr Adam Pellew of RKD Consultants Ltd. I am also thankful to City University London for funding the project.

Thanks go to my parents and brother, for their continual support. Finally, thanks to my wife Preeti who has always supported me and believed in me. This thesis would not have been started and could not have been completed without her help and understanding.

Declaration

I grant powers of discretion to the University Library to allow this dissertation to be copied in whole or part without further reference to me. The permission covers only single copies made for study purposes, subject to normal conditions of acknowledgement.

Abstract

This research concerns the influence of ribs on the ultimate capacity of a bored pile in overconsolidated clay. Ribbed bored piles are known to give increased shaft capacity in comparison to conventional straight shafted bored piles. The commercial benefit of greater pile capacity is more economical foundations. Significant environmental benefits will also accrue from the use of efficient foundations that are able to carry higher load, leading to less excavation, reduced concrete in construction and less spoil removal requiring disposal. Moreover, redevelopment of urban sites often requires removal of existing deep foundations owing to clashes in position of old and new foundations. Higher capacity piles offer potential for greater flexibility in foundation layout owing to their reduced size, making them easier to install around existing piles. The investigation sought to explore the effectiveness of ribs at increasing the ultimate of capacity of a pile, and furthermore to understand how this enhanced capacity is derived.

Experimental data were obtained from a series of 23 centrifuge model tests undertaken at 50g. The geometry of the model was such that it was possible to test two piles with each test. Of the two piles tested one was always a plain pile, this allowed for direct comparison to the ribbed pile in the same test and hence any inconsistency in the soil sample to be accounted for. The performance of several rib designs and spacings were investigated, whilst the pile inner diameter and length remained constant. A series of datum tests were conducted to verify the accuracy and repeatability of the testing equipment. Four rib types were tested; concentric ribs, helical ribs, tapered ribs and under reamed ribs. The use of ribs was found to always increase the ultimate capacity of a pile. Of all the rib profiles tested the helical profile was shown to be the most effective.

The data collected from the test series has been analysed using several industry standard methods. A plastic failure envelope for the base of the pile rib has been identified and is derived from that of the end bearing of a pile, proposed by Meyerhof (1951). This envelope assumes two failure zones; the elastic zone, and the radial shear zone. This plastic failure envelope has been used to provide a detailed design solution for the ultimate capacity of the concentrically ribbed pile. The design solution is simple and requires a summation of the constitutive contributions from each rib and from the base and shaft of the pile. A modification factor (Γ) has been proposed to allow for correction of the rib angle generated by the helix. This correction factor allows the same design solution to be used for all helically ribbed piles. This detailed design method has been used successfully to predict the ultimate capacity of any pile tested to within +/- 8%.

List of symbols

A_b	Cross sectional area of the pile base
A_s	Area of pile shaft
B	Pile width
d	Pile core diameter
E_p	Elastic modulus of the pile material
L	Pile length
N_c	Bearing capacity factor
p	Pile perimeter
Q_a	Safe working capacity of the pile
Q_b	Ultimate base resistance
Q_p	Ultimate resistance of the pile
Q_{rb}	Ultimate base resistance from each rib
Q_{rs}	Ultimate skin friction along the rib shaft
Q_s	Ultimate skin friction capacity
Q_u	Ultimate pile capacity
S_u	Undrained shear strength
W	Pile self weight
W_b	Load on the pile base
W_s	Load on the pile shaft
α	Adhesion factor
γ	Unit weight
K	Percentage increase in the longitudinal cross sectional area
M	Percentage increase in capacity when compared to a plain pile
η	Helix angle factor
a	Acceleration
g	Acceleration due to gravity
h	Height in the model
H	Drainage path length
N	gravity scaling factor
N_b	T-bar factor
P	Force per unit length on T-bar
r	Radius from point of rotation
R_e	Effective radius for the model

R_t	Radius to the top of the soil
t	Time
T_v	Dimensionless time factor
Z	Depth in the model
ω	Angular velocity
ρ	Material density
C_v	Coefficient of consolidation
E_b	Deformation modulus of the soil beneath the pile base
I_p	Influence factor related to the ratio of soil L/B
K_0	Coefficient of earth pressure at rest
γ_w	Unit weight of water
M	Stress ratio at critical state (q'/p')
N_γ	Bearing capacity factor
N_q	Bearing capacity factor
υ	Poisson's ratio
OCR	Over consolidation ratio
ϕ'	Friction angle
σ'_h	Horizontal effective stress
σ'_v	Vertical effective stress
σ_{vm}	Vertical stress acting in model
σ_{vp}	Vertical stress acting in prototype

Abbreviations

ASTM	American society for testing and materials
ATH	Aluminium Trihydrate
BEA	Boundary element analysis
BS	British standard code of practice
BSP	British standard pipe thread
CFA	Continuous flight auger
CRP	Constant rate of penetration

DLT	Dynamic load test
EC	European code of practice
FEA	Finite element analysis
FOS	Factor of safety
HCSP	High capacity shear pile
LVDT	Linearly variable differential transformer
MLT	Maintained load test
OCR	Overconsolidation ratio
OD	Outside diameter
PC	Personal computer
PIV	Particle image velocimetry
PPT	Pore pressure transducer
RLT	Rapid load test
rpm	Revolutions per minute

1 Introduction

The past decade has seen the construction of buildings and infrastructure increase rapidly. In urban areas developers aim to build taller structures in more confined spaces. As buildings increase in height with varying design, shape and structure, one aspect remains constant, their foundations, which invariably involve some sort of piling, especially where ground conditions are not suitable for shallow foundations. It is therefore necessary for these foundations to carry larger loads. To accommodate greater loads engineers have no option but to bore deeper and wider piles, at closer spacing. Eventually, this becomes unfeasible.

Moreover, many modern buildings when decommissioned leave behind a set of deep foundations and the foundations for new buildings have to be installed through and between this detritus (Qerimi, 2009). Geotechnical engineers therefore have an increasingly difficult task when finding locations for additional piles and providing sufficient capacity (Chapman et al., 2001). The addition of slimmer ribbed piles to the designers' arsenal can only help in this regard. This research aims to improve these foundations.

1.1 Background

In 2002 Expanded Piling and Arup Geotechnics agreed to co-operate in a jointly funded programme of research consisting of a limited number of full scale field trials, undertaken by Expanded Piling and supported by numerical analyses conducted by Arup Geotechnics. The field trials involved construction of several ribbed piles which in turn required preliminary development work on a special tool used for profiling the shaft. The analyses and tests yielded promising results and suggested that pile capacity could be increased by 30 – 40%. The project was featured in an article in Ground Engineering (2003), the magazine of the British Geotechnical Association, in December 2003. The test data and finite element analysis were considered commercially sensitive and could not be provided to allow comparison with the findings of this project. However comparisons have been made to the available material.

Conventional pile capacity is known to be sensitive to the construction process. 'Over auguring' during pile excavation appears to reduce pile capacity because the soil at the concrete/soil interface is extensively disturbed and remoulded as reported by Burland (1973). Whilst the technique of providing a mechanically rough pile/soil interface has demonstrated increased shaft capacity in the field, and this has been confirmed by numerical analyses, there is a need to test a wider range of geometries in various soil conditions to establish how the additional capacity that such piles offer is derived.

1.2 Objectives

Given the obvious potential for commercial exploitation of ribbed piled foundations, a fundamental study of the factors affecting behaviour at the pile shaft/soil interface has been undertaken. In order to understand how increases in pile capacity can be optimised and to develop guidelines for the important factors affecting design and construction of high capacity piles. The following are identified as the main objectives of the research and form the basis for the discussion and conclusions:

1) Apparatus development to enable scaled construction and centrifuge testing of a variety of ribbed pile profiles and geometries.
2) Development of instrumentation capable of profiling the soil samples undrained shear strength in flight.
3) Assessment of test piles ultimate capacities.
4) Formulation of detailed ribbed pile design framework.
5) Back analysis and calculation of test piles ultimate capacity using the proposed frame work.

This has been achieved by conducting a series of high quality physical model tests using a geotechnical centrifuge and comparison with full scale field trials. The main element of the project was the physical model testing, designed to model important aspects of the pile construction and provide data to evaluate the effectiveness of a pile. The series of tests explored the load displacement characteristics of a range of ribbed profiles in comparison with straight-shafted piles. As part of this work some tests were aimed at understanding the influence that forming ribs in a continuous helix has compared to discrete ribs.

Experimental procedures were developed during the early stages of the project leading to the series of tests in the geotechnical centrifuge which were compared with field trials carried out by Expanded Piling. The aim was to develop a clear understanding of the way in which ribbed piles can provide increased capacity in comparison with straight-shafted piles thereby helping to establish acceptance of their use.

1.3 Centrifuge modelling

Apparatus has been developed that is capable of simultaneously loading two piles within a sample of overconsolidated clay, with a view to exploring the ultimate capacities of the piles. Though the piles were loaded simultaneously, the apparatus was devised such that it was possible to obtain independent load and settlement data. Furthermore, associated tooling has also been developed allowing profiling of a pile shaft and profiling the undrained shear strength of a soil model in flight. In each test a

plain pile was tested to allow for normalisation and hence resolve any issues of inconsistencies between soil models.

Each of the piles tested had a core diameter of 16mm and length of 180mm, the tests were conducted at 50g. This scales to prototype piles with a core diameter of 800mm and length of 9m. The rib outstand and rib height was maintained at 1.5mm by 1.5mm or 75mm by 75mm at prototype. This dimension was chosen as it represented an unreinforced rib height and outstand capable of resisting shear forces expected at prototype scale. The spacing between ribs was varied from 10mm to 40mm, the rib profile was also varied. See Figure 5.1 for typical pile dimensions.

Previous pile research conducted at City University (Qerimi 2009) made use of vessels filled with fluid which were used to axially load the pile (Figure 1.1). The focus of the research was to load, unload and reload the piles and this was achieved by controlling the amount of fluid within the vessel via a series of remotely operated solenoid valves. Though this method proved very effective for the project it was felt that a motor and lead screw type arrangement would be more advantageous for this project. The fluid filled vessel was designed primarily for a maintained load type of test. Constant rate of penetration tests were more difficult since this was a function of the rate of flow of the fluid into, or out of the vessel. Consequently a revised loading apparatus was designed (Figure 1.2) which better suited constant rate of penetration testing.

A total of 23 tests were undertaken testing two piles in each test one of which was always straight shafted or plain. Model preparation time was kept to a minimum and was typically under 1.5 hours. Once the model was installed into the centrifuge the sample was allowed to come into pore pressure equilibrium, which typically took 50 hours. The piles were then loaded to 3mm settlement; once loading was complete the undrained shear strength of the soil sample was profiled using a T-bar penetrometer. For each test the pre-consolidation pressure, soil type, pile length and principle pile diameter were kept constant. Measurements of the piles settlement and the load applied were recorded.

1.4 Summary of thesis

This thesis details the approach to the research, describes the development and commissioning of the model testing apparatus and explains and interprets the response of test piles in the series of tests conducted. There are several techniques used to enhance the capacity of a bored pile and furthermore several techniques to quantify this enhancement in the literature. This has enabled a comprehensive literature review to be undertaken in Chapter 2 that establishes the problem and explains the factors that may influence the ultimate capacity of a bored pile.

Chapter 3 discusses the history and relevant merits of geotechnical centrifuge modelling. Also explained are the principles used within geotechnical centrifuge modelling and the associated scaling laws. As with any model testing technique there are inherent errors involved these have been discussed and typical solutions have been identified. Details of the geotechnical centrifuge facility at City University London are also presented.

The design and development of the centrifuge testing apparatus coincided with the literature review to enable more efficient use of time. A single test was conducted using existing pile testing apparatus to identify limitations and allow for modifications to be made to better suit this test series. It was decided to design and construct an entirely new set of apparatus specifically designed for the project, to streamline the testing process. This work is described in detail in Chapter 4 where the solutions to the practical problems that were encountered are described.

Centrifuge model testing was carried out over a period of about 18 months however this included a period of around 5 months when the centrifuge was out of commission. In Chapter 5 the results from all tests are presented in a manner that enables a stage by stage understanding of how the test series evolved and why certain rib profiles were tested. The results are presented pre-analysis and hence in an unprocessed form. The general quality of data from the instrumentation is assessed and discussed. The trends of behaviour identified from the load settlement curves are also discussed.

A summary of the significant findings from the series of centrifuge tests undertaken is presented in Chapter 6. The observed behaviour of the test foundations has been discussed. To enable the results to be of maximum use the results are presented within a context relating to the specific problem of establishing the trends of behaviour of ribbed bored piles in stiff clay. Comparisons to full scale testing conducted by Arup and Expanded and been made. The data obtained from the testing series has been analysed using several industry standard methods and the results of these analyses are presented and discussed. Trends in the data are identified and analysed and the

significance of the test results highlighted. A ribbed pile design framework has been proposed and has been shown to be able to predict the ultimate capacity of any rib pile tested to within +/- 8%.

Chapter 7 summarises the main findings of the research project, final conclusion are drawn with reference to the applicability and accuracy of the results. Recommendations are made for further research that will enable a better understanding of the parameters influencing the behaviour of ribbed pile foundations. The implications of the results of this research on design and on the use of ribbed pile foundations at prototype scale are discussed

2 Literature Review

2.1 Introduction

Within this chapter, the key literature important to the understanding of the behaviour of ribbed bored piled foundations is presented and reviewed. Firstly, piled foundations are classified, and the design of piled foundations explained. This is followed by a review of work related to pile installation technique, load testing and analysis, numerical modelling and finally pile capacity enhancement techniques. The limitation of the literature review are discussed in the chapter summary.

2.2 Pile classification

The earliest example of piling in Britain dates back to the Roman Empire, where timber piles were used in bridge works and riverside settlements (Tomlinson, 1977). Since then piles have been developed extensively and nowadays piles can be broadly classified into three categories:

- Small displacement piles,
- Large displacement piles, and
- Replacement piles.

Figure 2.1, after BS8004:1986 provides a detailed classification of pile type.

2.2.1 Displacement piles

These piles are usually made of steel or concrete, though sometimes timber, and can be precast or cast-in situ. Larger displacement piles are usually closed ended, whilst smaller displacement piles are quite often open-ended and can make use of structural steel sections. The process of driving the piles into the soil displaces and compacts the surrounding soil, hence their name. If displacement piles are to be cast-in situ a closed tubular section is used to compact the soil. This forms a void that is filled with concrete whilst the section is withdrawn.

2.2.2 Replacement piles

Replacement piles, otherwise known as non-displacement piles are installed by first removing the soil by a drilling process and then constructing the pile by placing concrete or some other structural element into the drilled hole. The simplest form of construction consists of drilling an unlined hole and filling it with concrete. However, complications may arise such as difficult ground conditions, the presence of ground water, or restricted access. Such complications have led to development of specialist piling plant for drilling holes and handling lining tubes. Though unlike the driven piles, very few proprietary piling systems have been promoted (Tomlinson, 1977).

2.3 Design of piles

Tomlinson (1977) stated; that for practical design purposes engineers must base their calculations of carrying capacity on the application of the load at a relatively short time after installation. The reliability of the calculations can then be assessed by a loading test, which is also conducted a relatively short time after the installation. The effects of time on a piles capacity should be appreciated and is discussed in Section 2.3.1.

The ultimate loading capacity of a single vertical pile when subject to an axial load is shown below. The interpretation shown is based upon the static method of analysis.

$$Q_u = Q_s + Q_b - W \tag{2.1}$$

Where: Q_u – ultimate loading capacity of the pile,

Q_s – ultimate skin friction,

Q_b – ultimate base resistance, and

W – pile self weight.

However, in conventional pile analysis the weight of the pile is taken to be the same as the weight of soil it displaced and its effect is therefore negated. These forces are usually small compared with the applied loads. Which are often in the range of 500 to 5000 kN and could perhaps be considerably larger (Atkinson, 1993).

Burland and Cooke (1974) recommend the use of a factor of safety of 2.0 on the combined shaft and base capacity, or, for under reamed piles, the use of partial factors of unity on the shaft capacity and 3.0 on the base capacity. The safe working load related to the ultimate load of Equation (2.1) can therefore be calculated from the following equation:

$$Q_a = \frac{Q_s + Q_b}{2} \tag{2.2}$$

Where: Q_a – safe working capacity of the pile.

A pile should be designed to withstand the most unfavourable loading conditions. It therefore follows that the ultimate capacity of the pile should be derived using the least favourable ground conditions. This may depend on the excess pore water pressures generated during pile installation.

Table 2.1, after Azizi (2007), details the various scenarios.

Table 2.1 suggests a drained or effective stress analysis be conducted for piles installed in heavily over-consolidated soils such as for the soil model proposed. However for tests reported in this project it was considered more representative to undertake an undrained or total stress analysis since the loading event within the centrifuge test is undrained.

2.3.1 Undrained or total stress approach

The ultimate capacity of an axially loaded pile, under undrained conditions, in clay can be calculated from Equation (2.1). The ultimate skin friction Q_s in homogeneous isotropic clay is given by:

$$Q_s = A_s \alpha S_{u(avg)} \tag{2.3}$$

Where: Q_s – ultimate skin friction,

A_s – shaft area,

α – adhesion factor, and

$S_{u(avg)}$ – average undrained shear strength of the clay along the pile shaft.

The adhesion factor is the ratio of skin friction mobilised on the pile shaft to the undrained shear strength of the undisturbed clay. This is to allow for the disturbance of the soil caused by the boring process. Graphs compiled by Tomlinson (1977) relate the undrained shear strength of the soil and the pile length and breadth to provide a value for **α** and are reproduced in Figure 2.2. Another frequently used chart for estimating the adhesion factor is that produced by Weltman and Healy (1978), which relates the undrained shear strength of the soil to the installation technique (Figure 2.3). For overconsolidated clay a value of < 0.5 would commonly be used for **α**. Skempton (1959) suggests the primary reason for **α** being less than unity is due to the near shaft soil absorbing water during the drilling and concreting process. This may be partially explained by the routine addition of water to the pile bore during the tripod piling of this time.

Work by Burland and Twine (1988) shows that Constant Rate of Penetration (CRP) tests over predict the bearing capacity of bored piles in London Clay due to the rapid nature of the test. This was verified by Patel (1992), with work that involved the analysis of 45 pile loading tests of bored piles in London Clay. The conclusions were that important rate effects can occur in the values of **α** determined from CRP failure loads. These may increase the values of **α** by up to 20% for long piles in London Clay,

when compared to maintained load tests. Patel (1992) shows that **α** obtained from a maintained load test had a range of 0.4 to 0.5 with an average of 0.45. Whilst **α** obtained from a constant rate of penetration test had a range of 0.5 to 0.8 with an average of 0.6.

If the undrained shear strength of the soil does not vary linearly with depth, an average may give an exaggerated estimate of the ultimate skin friction and Equation (2.3) will need to be revised to:

$$Q_s = \int_0^L p\alpha S_u \, dz \tag{2.4}$$

Where: L – pile length, and

p – pile perimeter.

The ultimate base resistance of the pile can be estimated from:

$$Q_b = A_b(S_{u(base)}N_c + L\gamma N_q) \tag{2.5}$$

Where: A_b – cross sectional area of the pile base,

$S_{u(base)}$ – undrained shear strength at the pile base,

N_c– bearing capacity factor,

N_q – bearing capacity factor equal to 1 for undrained clay,

γ – unit weight of the concrete

L - pile length and,

d- pile diameter.

Fleming et al. (1992) suggests that a linear interpolation should be made between N_c = 6 for the case of the pile just reaching stiff stratum, and up to N_c = 9 where the pile base penetrates the stiff layer by three diameters or more. By substituting values for N_q and N_γ Equation (2.5) becomes:

$$Q_b = A_b(N_c S_{u(base)} + \gamma L) \tag{2.6}$$

Combining Equations (2.1), (2.3), (2.6) and noting $A_b\gamma L$ is equal to the weight of the pile, W, the ultimate load capacity of a pile is given by:

$$Q_u = \alpha A_s S_{u(avg)} + N_c A_b S_{u(base)} \tag{2.7}$$

2.4 Pile settlement

The ultimate capacity of a pile, the load at which it fails is often assumed to be the load which causes a settlement of 10% of the piles diameter. For a 600mm diameter pile this is 60mm of vertical settlement. In practice a building or civil engineering structure would rarely be able to accommodate such a differential settlement, however global settlements of this magnitude may be acceptable.

Often settlements are a result of excess pore pressure dissipation around a newly loaded pile. These excess pore pressures give rise to hydraulic gradients that cause seepage flow at a rate governed by the permeability of the soil. The result is compression and hence reductions in soil volume due to the seepage flow and changes of effective stress.

Using pile test data to understand the ultimate capacity of a pile is obviously very important. However, arguably the most significant factor is the amount a pile will settle under its working load; it is the acceptable working settlement that often governs pile design.

Skempton (1959) was the first to highlight the fact that the shaft resistance is fully mobilised at significantly smaller settlements than the base resistance, this was verified by Whitaker and Cooke (1966). Base resistance is only fully mobilised at a settlement of 10-20% of the diameter of the pile, whilst shaft friction is often fully mobilised when settlement is about 0.5% of the diameter of the pile. To account for this Burland et al. (1966) presented a simple stability criterion for bored piles in clay. It states that the maximum load on a pile should be the lesser of either half of the ultimate capacity of the pile or a third of the ultimate base capacity of the pile in addition to the ultimate shaft capacity.

Tomlinson and Woodward (2007) define the pile head settlement by the sum of the elastic shortening of the shaft and the compression of the soil beneath the base, as follows:

$$\rho = \frac{(W_s + 2W_b)L}{2A_s E_p} + \frac{\pi}{4} \cdot \frac{W_b}{A_b} \cdot \frac{B(1-\nu^2)I_p}{E_p} \tag{2.8}$$

Where: W_s and W_b - loads on the pile shaft and base respectively,

L - the shaft length,

A_s and A_b - the cross sectional areas of the shaft and base respectively,

E_p - the elastic modulus of the pile material,

B - the pile width,

ν - the Poisson's ratio of the soil,

I_p - the influence factor related to the ratio of soil L/B, and

E_b - the deformation modulus of the soil beneath the pile base

I_p is taken as 0.5 for a Poisson's ratio of 0 - 0.25 and L/B > 5. The elastic modulus of the pile material, E_b, can be obtained from plate loading tests at pile base level or from empirical relationships and laboratory testing.

2.5 Factors of safety

Tomlinson and Woodward (2007) describe safety factors or partial safety factors as 'factors of ignorance' rather than absolute values and summarise the need for safety factors as follows:

- To provide for natural variations in the strength and compressibility of the soil,
- To provide for uncertainties in the calculation method used,
- To ensure that the working stresses on the material forming the pile shaft are within the safe limits,
- To ensure that the total settlement(s) of the single isolated pile or the group of piles are within tolerable limits, and
- To ensure that the differential settlements between adjacent piles or within groups of piles are within tolerable limits.

Burland et al. (1966) present a stability criterion which states the maximum safe load on the pile is the lesser of $\left(\frac{1}{2}Q_p\right)$ or $\left(Q_s + \frac{1}{3}Q_b\right)$.

Where: Q_p - the ultimate resistance of the pile,

Q_s - the ultimate resistance of the shaft, and

Q_b - the ultimate resistance of the base.

The first expression is generally dominant for plain piles, whilst the second expression often governs piles with enlarged bases.

Design codes such as EC7, the European Code for Geotechnics, are generally based on limit state design. In which design loads, soil parameters, and calculated resistances are factored with partial safety factors. The partial factors are applied to characteristic values to obtain design values. The problem is then analysed to ensure that the total effect of all the factored applied actions does not exceed the available resistance calculated from the factored values of soil strength (i.e. the calculations use the 'design values'). Partial factors of unity may be applied to given characteristic values depending on the particular Eurocode Design approach that is adopted (Fleming et al., 2009). Although the codes are fairly prescriptive, the actual method used for design is still a free choice and there is no intention to stifle innovation. Therefore, the ribbed pile design framework proposed in Chapter 6.0, can be incorporated into the current codified approach to pile design.

2.6 The behaviour of soils

A prerequisite to understanding the performance and behaviour of a piled foundation is an understanding of the surrounding soil, for the case of this study, overconsolidated clay. It is generally accepted that the behaviour of overconsolidated clay is a function of its current stress state and stress history. Overconsolidated clay is created in nature by the process of swelling and recompression. This is the result of erosion, deposition of soil, and changes in sea level (Stallebrass & Taylor, 1997). Since the overconsolidation ratio is defined as; $\left(\frac{\sigma_{v\,MAX}}{\sigma_{v\,CURRENT}}\right)$, it follows that this ratio, and hence the behaviour of the soil stratum, will change with depth. This variation will need to be reproduced for any laboratory testing.

Traditionally, estimates of the shaft capacity of a pile are expressed in terms of total stresses and based on the undrained shear strength of the 'undisturbed' soil (i.e. prior to installing the pile). As previously mentioned, these estimates made use of an **α** factor (Wroth et al., 1980). Several authors relate pile behaviour to effective stress in the surrounding soil (Burland, 1973; Parry and Swain, 1977; Randolph et al., 1979). Wroth et al. (1980) state that once the stress history of soil stratum is understood the problem can be considered in three stages:

- Pile installation,
- subsequent consolidation of the soil around the pile, and
- pile loading.

It follows therefore that pile modelling should involve installation of piles at the correct effective stress level. If the stresses acting around the pile immediately before installation can be predicted then the change in effective stress as a result of loading can be observed. Unwin and Jessop (2004) highlighted how pile ultimate capacity is sensitive to the pile construction process, particularly the time for which a pile bore was left open between boring and concreting. As the bore is excavated a pore pressure differential is generated allowing water seepage into the pile bore, however this seepage is significantly hindered by the relatively low permeability of clays. In most circumstances the bore is filled with fluid concrete in a short period of time, and the hydrostatic fluid pressure resists the pore water flow. It follows therefore that if for any reason a delay in concreting occurs the pore fluid has a greater amount time to seep into the excavation. This in turn will soften the soil at the pile soil interface and ultimately result in a reduction of the adhesion factor. Anderson et al. (1985) reported on tests of bored cast in situ piles in both normally and over consolidated clays. The authors concluded that during pile excavation the horizontal effective stress reduced dramatically due to the negative pore pressure generated by the excavation. This however recovered to 90% of the initial at rest effective stress after only 30 days.

2.7 Enlarged pile base

In stiff clays enlarged bases can be formed using specially designed tools. This process is known as under reaming and is designed to increase the end bearing resistance of the pile by providing a greater surface area. Figure 2.4, after Tomlinson (1977), shows a bottom hinged and top hinged under reaming tool. The process of under reaming can significantly improve the ultimate capacity of a pile. However, under reaming is notoriously slow and requires a stop in the auguring for a change of tool and a slow process in the actual under-reaming operation. For this reason coupled with stability issues, designers and or contractors often prefer to use deeper straight shafted piles. Although in recent years commercial organisations have developed tools capable of optimising the under-reamed pile construction process, since under-reamed piles offer the possibility of avoiding existing piles, while simultaneously providing single points of highly concentrated load carrying capacity (Suckling, 2007).

2.8 Installation techniques for bored piles

In soils such as the London clay the two most common techniques for installing bored cast-in situ piles are the Continuous Flight Auger (CFA) method and the rotary auger method. Both systems make use of purpose built crawler mounted augers fabricated by manufactures such as Bachy Soletanche, Bauer, Casagrade, or Soilmec. The larger sized rigs make use of a standard crawler crane base with an auxiliary power pack to drive the auger. Both rigs are shown in Figure 2.5.

2.8.1 Continuous fight auger (CFA)

This piling technique has been used in the United Kingdom since the 1960's. An auger with a continuous flight and hollow stem is used to bore a hole in the soil. Once the required depth is reached a high slump concrete is pumped through the stem and into the bottom of the pile bore. The auger is simultaneously withdrawn at a controlled rate, thus replacing the soil with a shaft of fluid concrete. At this point a reinforcement cage can be pushed into the fluid concrete. In this case 12 m is considered the maximum length of cage without the assistance of cage vibrators. CFA pile diameters range from 450 - 1200 mm with depths up to 30 m at limited diameters, and provide ultimate capacities in the range of 7.5 MN, depending on ground conditions. Some rigs make use of small sections of auger that can be screwed together. This allows for relatively deep piles even in sites with low head room. Modern machines make use of sophisticated instrumentation and computer control to monitor, control and record the CFA pile installation.

2.8.2 Rotary boring

Rotary piling rigs make use of a short auger often 4 or 5 turns of flight attached to a telescopic 'Kelly' bar. The auger is screwed into the ground until fully embedded and then retracted to the surface. The auger can then be rotated at high revolutions to spin off the spoil attached to the flights. This process is repeated until the desired depth is reached. Casings are often used near the surface where the stratum is likely to be weak and highly disturbed. Moreover, casing can be extended to further depths if the ground is found to be water bearing, loose or otherwise unstable. A substitute for this is the use of a Bentonite support slurry, which supports the excavation and prevent ground water from entering the pile bore. This can later be displaced by the concrete placing process. Reinforcement cages can be craned into the bore and can extend the full depth of the pile. The concrete is placed using a hopper and short tube, in the case of a dry pile bore, otherwise a full length tremie pipe is required. Rotary bored piles can range from 0.6 - 3 m diameter and 55 m depth with a standard double extension Kelly bar. This depth can be extended to 72 m with triple telescopic Kelly bars (Skanska Cementation, n.d.)

2.9 Individual components of the capacity of a pile

The proportion of the ultimate capacity of a pile derived from shaft and base resistance will, for obvious reason, depend on the geometry of the pile and the profile of the soil. End bearing piles are those that penetrate a relatively soft layer of soil to found on a firmer stratum, and hence derive the majority of their capacity from base resistance. This is also true of under-reamed piles. If it is not possible to found the pile on firmer stratum the ultimate capacity of the pile will be predominantly derived from shaft friction. Piles which derive the majority of their capacity in this way are often referred to

as floating or frictional piles. Fleming (1992) noted that the shaft capacity of a pile is mobilised at much smaller displacements of the pile, typically 0.5 - 2 % of the pile diameter. Whilst the base resistance may require displacements as large as 5 - 10 % of the pile diameter in order to be fully mobilised.

Determining the settlement response of a pile under working load is a complex issue. It is important to understand the variation between load deformation characteristics of the pile shaft, that of the pile base and how the load is divided between the two.

This is best illustrated by an example after Fleming (1992); a single pile with an ultimate capacity of 7MN may derive 60% of its capacity from shaft friction. However, at a working load of 3.5MN, perhaps 95% of the load will be carried by the shaft, with only 5% reaching the base. This is further confirmed by Unwin and Jessep (2007) who conduct Osterberg cell tests on full scale piles at the London Heathrow Terminal 5 site. The data shows that a load equivalent to 50% of the piles ultimate capacity is applied before any significant pile base movement occurs.

2.10 Pile testing

Currently in the UK there are two main methods of load testing piles. These are the Maintained Load Test (MLT) and the Constant Rate of Penetration (CRP) test; both of which are discussed in detail below. There are also several other methods designed to test piles in cyclic conditions (the Statnamic method) or even to separate shaft friction from base resistance (the O-cell test method).

2.10.1 Maintained load test (MLT)

As the name suggests in the MLT the load is applied to the pile in discrete increments and the resulting settlement is measured. The subsequent load increments are only applied when a specified time period has elapsed and the rate of settlement is below the specified criteria. Normal practice in the UK is to load the test pile up to the design verification load and then to completely unload the pile. Several subsequent cycles then load the test pile to specified values above the design verification load. The testing can take up to 48 hours with an additional 48 hours for erecting and dismantling testing apparatus. The MLT method is normally regarded as the most suitable in determining the load-settlement performance of a pile under working loads and at 1.5 times the working load conditions (FPS, 2006).

Fellenius (1980) describes the American Society for Testing and Materials (ASTM) ‘standard loading procedure’ as one where the pile is loaded in eight equal increments up to a maximum load. This is usually twice the predetermined allowable load. Each increment is maintained until zero settlement is reached, defined as 0.244 mm/h. The final load, known as the 200 % load, is maintained for 24hours.

In an attempt to speed up the standard MLT authors such as Mohan et al. (1967) have proposed tests where the load (jacking pressure) is allowed to drop rather than be maintained by pumping. To allow an analysis of pile settlement with time Housel (1966) proposes that each of the eight increments of loading be maintained for exactly one hour regardless of having reached zero settlement or not. This has reduced the MLT to a full day and has now been incorporated into the ASTM Designation. Fellenius (1980) suggests an improvement to the Housel method where by the load is applied in 16 equal increments over 30 minutes. This reduces the time dependant influence as far as reasonably possible and, in clay soils can be considered an undrained test.

2.10.2 Constant rate of penetration test (CRP)

The CRP test was first proposed internationally for piles by Whitaker (1957 and 1963) and Whitaker and Cooke (1961). The load required to cause a pile to penetrate into the ground at a constant rate is monitored until either the maximum specified test load is achieved or 'failure' of the pile occurs (FPS, 2006). The definition of pile failure is discussed in section 2.11. Normal practice is to force the pile to settle at a rate of 0.5 mm/minute and then conduct the test to a maximum penetration of 50 - 75 mm or to the maximum capacity of the testing apparatus. Measurements of the load are typically taken every two minutes. This test is considerably quicker than the MLT with testing taking two to three hours per pile and 24 hours for erection of the apparatus.

The CRP testing method provides a better determination of the load-settlement curve when compared to that of the MLT. It is therefore often used to determine the ultimate capacity of the test pile. This testing method is particularly effective for frictional piles constructed in stiff clay as they derive their capacity mainly in shaft friction. Though, it should be noted that due to the high rate of loading, the measured maximum soil resistance may over-predict the ultimate capacity.

2.10.3 Rapid load test (RLT)

Traditional static pile tests are carried out using methods similar to the MLT or CRP. These provide reliable results but require substantial temporary infrastructure which increases with pile ultimate capacity. Conversely, dynamic load testing (discussed in section 2.10.4) requires only minimal infrastructure but in practice are complicated to analyse. Rapid load tests such as the Statnamic method aim to circumvent these shortcomings. In the Statnamic test method a gas producing fuel is rapidly burnt in a pressure chamber (Middendorp, 1993). The gas then accelerates a reaction mass upwards at a maximum peak acceleration of about 20g. This in turn imparts a downward load on a test pile, (Brown et al., 2006). The load and duration are controlled by the quantity of fuel and the venting of the gas. The requirement for complex wave

equation analysis is negated by ensuring the length of the stress wave is sufficiently long to encompass the whole pile (FPS, 2006).

2.10.4 Dynamic load test (DLT)

The DLT method was initially developed for use with driven piles and is now universally accepted for testing cast-in place piles. Dynamic load testing is widely used to predict the static soil resistance and pile load-settlement behaviour. The pile head is subjected to hammer blows, either by a piling rig hammer or by a separate drop weight, the response of the pile to the stress wave propagation can be analysed. A typical DLT on a cast-in place pile can take 30 minutes and requires relatively little on-site infrastructure. It should be noted that owing to the very high rates of applied loading, dynamic load testing cannot take into account time related effects such as consolidation, relaxation or creep (FPS, 2006).

2.10.5 Osterberg load cell

Of the many pile testing methods and variations thereof, few offer the possibility of separating ultimate capacity into components of skin friction and end bearing. Moreover, conventional static loading tests are only able to show load-movement for the pile head.

An innovative low cost testing method has been developed by Osterberg (1998) to overcome this problem, the Osterberg Cell (O-cell for short). The O-cell is essentially a sacrificial bellow or jack, which is installed at or near the pile base. The test consists of applying load increments to the O-cell causing it to expand pushing the pile shaft upward and the pile toe downward. The pressures in the O-cell (the load), its expansion, and the upward and downward movements are recorded. The O-cell load plotted against the upward movement of the top and the downward movement of the base are the load-movement curves of the pile shaft and the pile toe respectively (Fellenius, 2001). The weight of the pile above the O-cell is subtracted from the O-cell load to obtain the load-movement for the pile shaft. It is however, included in the load-movement for the pile toe. Since the O-cell uses the end bearing of the pile to react against skin friction, and vice versa, the test is limited by whichever is first to fail. Hence, if the failure of both skin friction and end bearing is required then extrapolation techniques must be used during the test analysis.

2.10.6 Rate effects on pile testing

The rate at which the pile is loaded is known to affect its failure load, as is the type of test conducted. Pellew (2002) observed tests on aged steel piles in London Clay which gave capacity increases of approximately 5 % per log cycle of increased rate of displacement. Lyndon et al. (1994) also found a 15 % capacity increase per log cycle of rate for CFA piles in soft Bothkennar clay over test rates of 0.0002 - 0.1 mm/min.

Several authors warn of the pitfalls of relying generally on quick loading tests. However, these tests may be appropriate in circumstances where piles experience sudden loading with high live-to-dead load ratios.

2.11 Interpretation of pile test data

The interpretation of data from load tests to assess the ultimate capacity of a pile is a complex problem, which requires careful consideration of a number of factors. Including the soil strength, the soil stiffness profile, pile installation method, contribution of friction and end bearing, and the possibility of negative skin friction.

Davisson (1972) states that “load tests do not provide answers – only data to interpret”, and this statement is verified by observations of a number of authors work concentrating in this area.

The British Standard for foundations (BS8004:1986) defines the ultimate capacity of a pile as the load at which the resistance of the soil becomes fully mobilised. At a load greater than the ultimate capacity the soil undergoes shear failure, allowing the pile to penetrate into the ground. It is suggested that for practical purposes the ultimate bearing capacity maybe taken to be the load applied to the head of the pile that causes it to settle by 10 % of the pile diameter. Unless the value of the ultimate bearing capacity is otherwise defined by some clearly recognisable feature of the load-settlement curve.

The ultimate load capacity of a pile can be easily ascertained from a constant rate of penetration test since it can be defined as the peak value. However, identifying the failure load of the pile is somewhat more complicated. Brinch Hansen (1963) presents a 90 % failure criterion where failure is defined as the load giving twice the movement at the pile head as is recorded for 90 % of that load. This failure criterion is able to provide results that are independent of the judgement of the interpreter by assuming the test curve is hyperbolic at failure.

Fuller and Hoy (1970) propose pile failure to be defined as the load corresponding to the point on a load-movement curve where the gradient is equal to 0.14 mm/kN.

De Beer (1968) suggests plotting load settlement values in a double logarithmic diagram thereby constructing two straight lines. The intersection of which corresponds to the failure load. However, Raju and Ghandi (1986) found this method to be overly conservative when compared to other techniques.

A useful element of the method proposed by Mazurkiewicz (1972) is that the failure load can be extrapolated, even if the maximum test load is smaller than the failure load.

This is obviously beneficial since smaller load testing infrastructure is required. This method assumes the load settlement curve is parabolic at failure. A set of equal settlement lines are chosen and the corresponding load lines constructed. From the intersection of each load line with the load axis a 45° line is drawn, to intersect the next load line. These intersections fall approximately on a straight line, the failure load is where this line intersects the load axis. This is best illustrated in Figure 2.6 which shows a hypothetical Mazurkiewciz diagram.

Davisson (1972) proposed a load limit defined as the load corresponding to the movement that exceeds the elastic compression of the pile by an offset of 4 mm plus a value equal to the diameter of the pile divided by 120.

Chin (1970 and 1971) proposed a method where by each load value is divided with its corresponding movement value and the resulting value plotted against the movement. The Chin failure load is then the inverse slope of the aforementioned line. In practice there is some initial variation before a line can be drawn as shown in Figure 2.7. Fellenius (1980) urges users of the Chin method to exercise caution since it is easy to arrive at a false failure load. This can be the case if the Chin method is applied too early into the test. Fellenius (1980) suggests that, as a rule, the Chin failure load is about 20 - 40 % greater than the Davisson (1972) limit.

Fellenius (1975) describes eight methods for defining failure of a pile, including the 90 % criterion, Mazurkiewicz (1972) and the De Beer (1968) method and it shows that, whilst all the examined methods are viable, the interpreted variation in failure load differs by up to 40 %.

It is difficult to make a rational choice of the best criterion to use, because the one preferred is heavily dependent on one's past experience. The main objective of having a strict criterion is to enable a set of compatible reference cases to be established. Fellenius (1980) prefers to use not one but three or four of the criteria presented in Figure 2.8. For this project, pile test data will be analysed using the Chin, Fuller & Hoy, Hansen and BS8004 methods. The British Standard method has been chosen as it is the codified approach used by many practicing engineers, at least in the first instance. Fellenius (1980) recommends the use of the Chin method as it allows a continuous check on the tests, if a plot is made as the test proceeds, and a prediction of the maximum load that would be applied during the test. Sudden kinks or slope changes in the Chin line indicate that something is amiss with either the pile or with the test arrangement. This however will not be of significance in a centrifuge test owing to the short duration of a pile test in comparison to a prototype scale test. However, the Chin value is less sensitive to the imprecisions of the load and movement values, and this is

advantageous. The Hansen criterion is chosen because it usually gives an ultimate capacity value which is close to what one subjectively accepts as the true ultimate failure value. The value is typically smaller than the Chin value. However, the criterion is more sensitive to inaccuracies of the test data than is the Chin criterion. The Fuller and Hoy method has been chosen primarily as it yields a failure value approximately in the middle of the numerous failure analyses presented in Figure 2.8.

2.12 Numerical modelling

In recent years, numerical modelling techniques such as finite element analysis (FEA) and boundary element analysis (BEA) have become valuable tools in understanding complex geotechnical problems. Such analyses are particularly useful for modelling geometrical problems, such as the geometry of ribs on a pile. Since this is a symmetrical problem, only a portion of the pile requires analysis. Another useful feature is the ability to model construction sequences.

Numerical studies on straight-shafted piles have shown that the ultimate capacity of a pile is dependent on parameters such as the pile geometry and soil stiffness. Cooke (1974) suggests that a pile may be considered as surrounded by concentric cylinders of soil with shear stresses on each cylinder. For vertical equilibrium the magnitude of the shear stress on each cylinder must decrease inversely with the surface area of the cylinder. Consequently only the soil in close proximity to the pile shaft is ever highly stressed. Fleming et al. (2009) suggests significant deflections can extend up to one pile length away from the pile.

Senghani (2008) conducts a series of Finite Element Analyses to observe the effect of ribs on bored piles in clay. It was reported that the addition of ribs increased the ultimate load capacity of the pile to values close to those observed in piles with effective diameters equal to that of the shaft diameter plus the rib width. This can be seen in Figure 2.9 which shows the 800mm pile load-displacement curve is significantly closer to the 1m diameter plain pile than to the 800mm diameter plain pile. Moreover, it was also observed that using a fewer number of ribs, or large rib spacing, did not significantly hinder the load carrying capacity of the pile when compared to the larger piles. The failure plane of the pile was observed to be some distance from the pile/soil interface and toward the soil/rib interface. It follows that the soil at this location would be less disturbed by the pile construction process and hence stronger. Senghani (2008) plots pile load capacity against volume of concrete (See Figure 2.10). The load capacity for the volume of concrete for a ribbed pile is always greater than for the volume of concrete for a plain pile. This further highlights the possible economic and environmental benefits of ribbed pile technology. The contoured displacement plots are

not of sufficient resolution to observe the soil flow around the pile ribs, this limits predictions of the failure mechanism.

2.13 Atlas piling system

The ‘screw-in’ Atlas pile is a reinforced, cast in-situ, displacement pile, and is claimed to have many benefits over a standard bored or CFA pile. Namely; minimum noise and vibration during installation, minimum spoil production, an enhanced shaft capacity and an increased capacity from lateral compaction of soil. The Atlas pile is installed using a specially modified piling rig and tools. A casing is attached to an enlarged screw with a single helix and a pile shoe, which is screwed into the ground under controlled torque and thrust. At the required depth a reinforcement cage can be attached to the pile shoe. However as with the CFA method, the reinforcement cage is often placed after concreting. Concrete is placed, under pressure into the pile bore; the steel shoe is then uncoupled from the casing by means of reverse rotation. The concrete is then able to fill the voids left by the upward moving casing. The diameter of the casing is typically 0.36 - 0.56 m and that of the pile screw is typically 0.46 - 0.66 m (Able Piling, 2010). The pile capacities are greater than for traditionally constructed bored piles, although the restricted diameter of the reinforcement cage can be a disadvantage if the pile is required to resist high bending stresses. Figure 2.11, after Tomlinson (1977) illustrates the pile construction process.

2.14 High capacity shear pile testing – Expanded Piling

In early 2002, Expanded Piling and Arup Geotechnics began to develop a revolutionary adaption of the traditional bored pile. This new pile was dubbed the ‘High Capacity Shear Pile’ or HCSP for short. If successful this pile would provide increased load carrying capacity whilst simultaneously reducing cost and environmental impact. The innovation proposed by the team was the addition of concentric ribs along the pile shaft. The High Capacity Shear Pile should not be confused with the Atlas pile (described above) or similar cast in place screw piles. Such piles are relatively small in diameter, and should be considered as displacement piles. This is because the Atlas pile ribs are laterally formed by compaction of the surrounding soil.

The collaborative research project proposed to investigate how well the ribs could be formed with a standard rotary piling rig, and how much capacity could be gained with the addition of these ribs. In December 2002, a testing site was prepared at the Grimsby depot of Expanding Piling. A detailed site investigation was conducted alongside laboratory tests. The site was found to consist of Glacial Clay overlain by a thin layer of superficial deposits. Chalk bedrock was known to exist at a depth in

excess of 20 m below ground level and hence well below the toe of the proposed research piles.

Two straight shafted piles were constructed adjacent to two High Capacity Shear Piles, all of identical length. A void of 250 mm was maintained with the use of a low density foam at the toe of all four piles, to ensure that no base resistance could develop. The rib cutting tool underwent several iterations before the construction issue design (Figure 2.12).

The piles were installed using a conventional 750 mm bladed auger, and bored to a depth of 7.05 m below ground level. The ribs of the High Capacity Shear Piles were then cut using the specially designed tool. Casings were used to form a voided annulus at the top 1.5 m of each pile to ensure no skin friction developed in the superficial deposits.

Each pile was tested to ultimate capacity by a maintained load test followed by a constant rate of penetration test (described in Section 2.10.1 and 2.10.2 respectively). The research team conducted detailed numerical analysis of the results based on the work of Chin (1970). The team found that, in general, a High Capacity Shear Pile compared to a straight shafted pile of identical length and internal diameter showed an increased ultimate load capacity of some 30 % (Expanded, 2002). The test data and finite element analysis were considered commercially sensitive and could not be provided to allow comparison with the findings of this project. However comparisons have been made to the available material.

The focus of the Expanded/Arup research project was on the efficiency of the rib cutting tool, and therefore provides little insight as to the optimal geometry of the concentric ribs. Moreover, an investigation to optimise the rib geometry would benefit from an academic approach utilising a geotechnical centrifuge and detail analysis. Full scale testing would be extremely costly and time consuming.

2.15 Summary

In this chapter the background and previous material related to high capacity piles has been presented. This included a detailed discussion of pile classification and design. Papers relating to single pile settlement have been presented. It is evident that installation technique and workmanship clearly influence the load carrying capacity of a pile. Unfortunately, the majority of a pile will remain underground for its working life. Therefore the workmanship can only be checked for by pile load testing or exhumation. The latter of which is expensive and therefore rarely conducted.

In order to understand the stress history and current stress state in the soil surrounding piles there was a review of accepted soil behaviour and particularly that of overconsolidated clays.

A variety of pile loading tests have also been outlined. The review has focused on the maintained load and constant rate of penetration tests as these are most relevant to centrifuge modelling. Of these methods, constant rate of penetration testing and been selected for pile tests in this project. The constant rate of penetration testing is considered to be the most controllable and repeatable form of pile testing within the limits of Geotechnical centrifuge modelling and more specifically within the limits of current equipment available at City University. In order to evaluate the effectiveness of a ribbed pile it will be necessary to compare the load settlement characterises of a pile to that of a plain pile. Moreover, one must specify when a pile has failed and hence reached its ultimate capacity. Several pile test analysis techniques have been reviewed and discussed. The merits of each are presented.

The key to unlocking the potential of ribbed piles is a better understanding of the difference in failure mechanisms created with the addition of ribs.

There are a number of published cases for the need to increase the capacity of piled foundations. However, little work has been conducted with reference to increasing the capacity of a bored pile by means of shaft profiling although the Atlas pile, which has been outlined, has similar concepts to that of the proposed piles. However significant differences exist in the installation as the Atlas pile displaces the soil within which it is installed whilst the proposed pile replaces the soil.

No work has been presented on pile group interaction and pile group behaviour. Whilst work in this area will be important for ribbed piles in the future, it is considered outside of the scope of this project which focuses on the capacity of a single green field pile.

Research relating to the installation of piles though multi layered stratum, clay with differing over consolidation ratios, pile bending, shear, and tension capacities is not presented here, and is consider outside the scope of this project.

A limited review of literature pertaining to Finite Element Analysis of ribbed piles has been conducted owing to the lack of work in this area. Furthermore, a more general review of the Finite Element Method has not been presented and is considered outside the scope of this project.

The Expanded-Arup joint research programme is the only available instance of research on bored, cast in-situ, profiled piles. The research shows promising results with an increase in capacity of up to 40 %. Unfortunately, the majority of the work conducted remains confidential owing to its commercially sensitive nature and therefore is not available for comparison.

3 Geotechnical centrifuge modelling

3.1 Introduction

Edouard Phillips, a French engineer was the first to recognise the potential of the centrifuge for modelling geotechnical problems. He recognised the significance of self-weight forces and he developed appropriate scaling laws, Craig (1995). The first actual use of a centrifuge for modelling geotechnical problems was in Columbia, where the integrity of mine roof structures in rock was tested. The majority of the early development of the technique occurred in Russia in the early twentieth century. By 1969 the technique had become popular; the International Society for Soil Mechanics and Foundation Engineering (ISSMFE) held its 7th annual conference in which several papers relating to centrifuge work were presented, from England (Avgherinos and Schofield, 1969), Japan (Mikasa et al., 1969) and the USSR (Ter-Stepanoan and Goldstein, 1969) all relating to slope stability.

Today, geotechnical centrifuges are widely used by commercial, educational and military establishments (though in the UK all centrifuges are operated by the education sector) in order to model the behaviour of various geotechnical structures and events. Small scale models are subject to inertial radial acceleration fields many times that of the earth's gravity. This allows self weight stresses and gravity dependant processes to be accurately reproduced. In practice centrifuge tests are often used to validate numerical analyses. Geotechnical centrifuge modelling provides a much quicker and cheaper solution when compared to full scale onsite testing.

3.2 Principles of centrifuge modelling

It is a well established fact that soil behaviour is a function of stress level and stress history and that in-situ stresses change with depth. For this reason it becomes difficult to model scale geotechnical problems at 1g, though various methods do exist. By accelerating a model of scale 1:N to N times earth gravity, a stress similarity at homologous points can be realised if the stress history of the soil is similar to that of the prototype and the same soil is used. Typically clay models are subject to a similar stress history to that of the prototype by means of a consolidation press. The press is used to apply a vertical stress to the kaolin slurry, often 500 kPa. Usually the sample is then allowed to swell by reducing the consolidation pressure to 250 kPa. This has become standard centrifuge practice at City University. The resulting soil sample is one which is overconsolidated, sufficiently stiff to allow for easy model making but not so stiff as to provide a sample which will be difficult to load or penetrate.

This forms the basis of the principle scaling law; a centrifuge model of scale N subject to an inertial radial acceleration equal to N times earth's gravity will have a similar vertical effective stress at depth h_m to that in the corresponding prototype depth h_p, if:

$$h_p = N h_m \tag{3.1}$$

Newton's Second Law of motion states that pulling a mass out of a straight path into a radial path will impose a radial acceleration towards the centre of rotation of:

$$a = \omega^2 r \tag{3.2}$$

Where: a – acceleration (m/s^2),

r – radius from point of rotation (m), and

ω – angular velocity (rad/sec).

Since the earth's gravity can be assumed uniform for the range of depths encountered in civil engineering (9.81m/s^2):

$$a = Ng \tag{3.3}$$

Where: a – radial acceleration (rads/sec^2),

N – gravity scaling factor, and

g – acceleration due to gravity (9.81 m/s^2).

With careful planning of model dimensions and radial acceleration, prototype stress profiles can be closely simulated.

No form of modelling is without flaw, each will have their limitations and errors, and centrifuge modelling is no exception. Scaling laws and scaling errors owing to a non-uniform radial acceleration to name one.

3.3 Scaling laws

As explained above, the key principle of geotechnical centrifuge modelling is reproducing the stress distribution of the prototype. Hence, for a soil of density ρ the total vertical stress σ_{vp} acting at depth h_p in the prototype is given by:

$$\sigma_{vp} = \rho g h_p \tag{3.4}$$

Since density of the soil in the prototype is the same as that of the model, and the model is subject to N times the earth's gravity, then the vertical effective stress σ_{vm} acting at depth h_m in the prototype is given by:

$$\sigma_{vm} = \rho N g h_m \tag{3.5}$$

For stress similarity between the model and the prototype:

$$\sigma_{vm} = \sigma_{vp} \tag{3.6}$$

Thus:

$$\rho N g h_m = \rho g h_p \tag{3.7}$$

$$\frac{h_p}{h_m} = N \tag{3.8}$$

Therefore the scaling factor for linear dimensions is 1:N (model:prototype), this applies to all geometrical components of the model. Since this scale factor applies to displacement, it follows that strains will have a scale factor of 1:1.

Wood (2004) gives a detailed list of scaling factors applicable to centrifuge modelling, summarised in Table 3.1.

The scaling law for seepage and consolidation is often considered as one of the more beneficial aspects of centrifuge modelling. This is the dimensionless time factor T_v which scales at 1/N^2. T_v for consolidation is defined as;

$$T_v = \frac{C_v t}{H^2} \tag{3.9}$$

Where: C_v – coefficient of consolidation,

t – time (s), and

H – drainage path length (m).

Therefore, the same time factor in the model and prototype is:

$$\frac{C_{vm} t_m}{H_m^2} = \frac{C_{vp} t_p}{H_p^2} \tag{3.10}$$

and:

$$\frac{H_m^2}{H_p^2} = \frac{1}{N^2} \tag{3.11}$$

Thus:

$$t_m = \frac{1}{N^2} \frac{C_{vp} t_p}{C_{vm}} \tag{3.12}$$

Assuming the same soil in the model as in the prototype the scale factor for time is 1/N^2. With the physical dimensions of the model significantly reduced and the increasing speed of time dependant processes, the centrifuge modeller can observe processes that occur over years at prototype scale in minutes at model scale.

3.4 Errors in centrifuge modelling

The centrifuge is a valuable tool in investigating geotechnical problems; however certain problems arise owing to the rotation of the swing about a fixed axis, Taylor (1995). Since the horizontal acceleration imparted at any depth of the model is a function of the radius, (See Equation (3.2)) the model is subjected to an increasing acceleration with depth. Furthermore, trying to replicate prototype events will increase the chance of errors within the testing procedure. It is for this reason that physical

model tests rarely aim to reproduce prototype events, and instead aim to model a generic prototype event or provide a series of realistic events that can be compared to each other or to some form of numerical analysis.

3.4.1 Radial acceleration field

Stewart (1989) described the radial acceleration field acting in a direction that passes through the axis of the centrifuge. This introduces a horizontal component of acceleration into the model, which increases with the distance from the centreline. This lateral acceleration is greatest at the boundaries of the model, since this is the farthest from the centreline. For this reason, it is considered good practice to keep major events as close to the centreline as possible. For the series of tests proposed a distance of +/- 105mm from the centreline would result in an error of about 5% of the vertical.

3.4.2 Vertical acceleration

The vertical stress at any point in the centrifuge model, as in the prototype is a function of the weight of soil above that point. In the centrifuge the acceleration field acting on the soil above that point varies linearly (due to the changing radius), for this reason average acceleration, and hence the acceleration midway between the point of consideration and the model surface is used. Careful model design can ensure that the under stress at the model surface and the over stress at the model base are restricted to acceptable limits. The vertical stress distributions for both the model and prototype are shown in Figure 3.1, after Taylor (1995). By comparing the under stress (r_u) and over stress (r_o) to the prototype stress at the same depth, it can be shown that the least variation between the two occurs when the required acceleration is set at 1/3 of the model depth. This gives the correct vertical stress at 2/3 of the model depth as shown in Figure 3.2. In the prototype the vertical effective stress at a given depth is given by:

$$\sigma_{vm} = \rho g h_p = \rho g N h_m \tag{3.13}$$

The scale factor N is calculated at an effective radius R_e, (3.2) becomes:

$$Ng = \omega^2 R_e \tag{3.14}$$

Where: R_e – effective radius for the model

If the radius between the centre of rotation and the top of the soil is R_t, then:

$$\sigma_{vm} = \int_0^Z \rho\omega^2(R_t + z)dz = \rho\omega^2 z\left(R_t + \frac{z}{2}\right) \tag{3.15}$$

Where: Z – is the depth in the model,

R_t – is the radius to the top of the soil, and

ω– angular velocity (rad/sec).

If the vertical stress in the model and in the prototype is identical at depth Z = h_i then:

$$R_e = R_t + \frac{h_i}{2} \tag{3.16}$$

A convenient rule for minimising the error in stress distribution is derived by considering the relative magnitude of under and over stress, Taylor (1995), as shown in Figure 3.2. The ratio of the maximum under stress, r_u which occurs at model depth $0.5h_i$, to prototype stress at the same depth can be expressed as:

$$r_u = \frac{0.5h_i\rho gN - 0.5h_i\rho\omega^2\left(R_t + \frac{0.5h_i}{2}\right)}{0.5h_i\rho gN} \tag{3.17}$$

Combining equations (3.14) and (3.16) this reduces to:

$$r_u = \frac{h_i}{4R_e} \tag{3.18}$$

The ratio between maximum over stress which occurs at the base of the model h_m, and the prototype stress at the same depth, can be expressed as:

$$r_o = \frac{h_m - h_i}{2R_e} \tag{3.19}$$

Equating the expression for under stress (3.18) and over stress (3.19) the following is obtained:

$$\frac{h_i}{4R_e} = \frac{h_m - h_i}{2R_e} \tag{3.20}$$

$$h_i = \frac{2}{3} h_m \tag{3.21}$$

Therefore:

$$R_e = R_t + \frac{h_m}{3} \tag{3.22}$$

3.4.3 Orientation of model in gravity field

As explained in section 3.4.1, it was necessary to have the pile foundations offset from the model centre line by +/- 105mm. This therefore resulted in the piles being inclined to the resultant acceleration direction. It may have been possible to mitigate this effect by installing the piles at inclination, but this would have resulted in the piles being inclined to the principle direction of soil swelling and consolidation (parallel to the walls of the soil container or perpendicular to the base), which would likely cause more complication. To reduce the effect of this problem the foundation loading was orthogonal to the axis of the pile. Therefore the only non axial load on the foundation was from the weight of the pile which is considered small compared to the axial load. Furthermore since this non-axial load is the same for both piles, as they are the same distance from the centre line, all tests remained internally consistent.

3.4.4 Boundary effects

In model tests it is necessary to contain the soil sample, boundary effects are the phenomena whereby the behaviour of a soil is influenced by the boundary it is contained within. Phillips (1995) gave guidance on containers and stated that side wall friction is always present to some extent, it is therefore essential for the model to be sufficiently wide that the boundaries do not create significant problems. Craig (1995) suggests that for a pile foundation test, a minimum distance of 5 pile diameters from the boundaries is sufficient to minimise boundary effects.

3.4.5 Grain size

The scaling laws mentioned in Section 3.3 apply in the same way to both model dimensions and soil grain size. This would mean clay with a particle size of 2 microns would scale to 0.2mm at 100g. Taylor (1995), states that, in this way, clay could be

thought of as representing fine sand and that since the stress-strain characteristics of clay and fine sand are very different this argument is flawed. Moreover, for coarse grained soils; only where grain size exceeds 1/30th of an important model dimension does a significant grain size effect occur; see for example Fuglsang and Ovesen (1988).

It is accepted practice that speswhite kaolin is generally used for tests in clay soils. This is owing to its high permeability, which allows samples to be consolidated relatively quickly when compared to other clays, and also reaches pore pressure equilibrium at an accelerated rate. Moreover the soil characteristics of speswhite kaolin are well researched, e.g. Al-Tabbaa & Wood (1987) and others.

3.4.6 Soil stress errors

Typically, for centrifuge tests using over-consolidated clays a consolidation press is used to consolidate clay slurry with water content of 120%. The slurry is placed in a strong container and subjected to a vertical consolidation pressure p'_{max}. In general the pressure at the top of the sample is reduced a day before testing resulting in an over-consolidated sample. It can be assumed that the surface for the model has the same stress history as that of the prototype, where the prototype is a full scale sample of kaolin clay. Accordingly the difference between the model and the prototype can be defined in terms of permeability and strength.

3.4.6.1 Permeability

Al-Tabbaa (1987) concludes that for speswhite kaolin clay; permeability is a function of voids ratio. The model comprises a more uniform specific volume profile with depth than the prototype and therefore the reduction in permeability with depth is not as rapid as in the prototype.

3.4.6.2 Strength

Several authors have published empirical solutions to estimating the undrained shear strength of centrifuge models. The empirical solutions all take the form:

$$S_u = a\,\sigma'_v\,OCR^b \tag{3.23}$$

Where a and b are empirically derived constants and OCR is the over-consolidation ratio. Wroth (1984), Stewart (1989), and Garnier (2002) all suggest a value of 0.22 for a and 0.49, 0.57, and 0.706 for b respectively. Whilst Springman (1989) recommends 0.19 and 0.59 for a and b respectively. The difference in a and b values can likely be attributed to dissimilar methods of measuring the undrained shear strength. Stewart (1989) plots $\frac{C_u/\sigma_v'}{0.22}$ against the log of OCR on σ_v' for data obtained from triaxial tests and in flight shear vanes. Springman (1989) derives the parameters from in-flight shear

vane data of speswhite kaolin with an OCR of 1. Whilst Garnier (2002) uses both in-fight shear vane and CPT data. The undrained shear strength can also be calculated theoretically by using Equation 3.24 to determine the failure on the critical state line.

$$S_u = \left(\frac{M}{2}\right) exp\left[\frac{\Gamma - \nu}{\lambda}\right] \tag{3.24}$$

Figure 3.3 shows the estimated undrained shear strength profile with depth for the given stress history, g-level and soil type; using the above equations. The empirical solutions were used to verify the undrained shear strength profile obtained from the T-bar. The comparison is presented in Section 4 and is of significance since the measured undrained shear strength profile was used to calculate the theoretical capacity of each pile tested.

3.5 The geotechnical centrifuge facility at City University London

The Geotechnical Engineering Research Group at City University makes use of an Acutronic 661 beam centrifuge, described in detail by Schofield and Taylor (1988). The centrifuge has been designed to accommodate a wide variety of strong model containers which are either rectangular boxes or cylindrical tubs. The permitted package volume is 500mm x 700mm in plan and 500mm height, however a usable height of 970mm is available in the central area of the swing between the pivots. A maximum package mass of 400kg can be accommodated at 100g and this capacity reduces linearly with acceleration to give a package mass of 200kg at the maximum acceleration of 200g. The centrifuge can therefore be classed as a 40g/tonne machine. The swing platform is at a radius of 1.8m when horizontal and is balanced by a 1450kg counterweight that can be adjusted radially on a screw mechanism.

Strain gauged sensors are used to detect any out-of-balance in the base of the centrifuge. These sensors are monitored in real time by the centrifuge flight computer, which will automatically shut down the centrifuge if an out-of-balance of more than the pre-set 15kN is detected. This safety feature enables unmanned overnight running of the machine, which is often required during pore pressure equalisation.

The centrifuge has a fibreglass clamshell enclosure that helps to reduce air resistance and this is aided by an aerodynamic fairing on the leading edge of the swing. A sacrificial block wall designed to absorb the energy of any projectile that may come off the centrifuge surrounds the clamshell and is itself encased by a reinforced concrete structure.

Electrical and hydraulic connections are supplied through a stack of slip rings. Electrical slip rings are used to transmit transducer signals to the control room once being converted from analogue to digital and amplified by the onboard computer. Other

electrical slip rings are used to transmit video feeds, supply power for lights, motors and solenoid valves as required. The fluid slip rings can be used for water, oil or compressed air and are rated at 15bar.

The data acquisition and motor control systems on the centrifuge are in the process of being upgraded. The new system makes use of a second in-flight computer, supplied by National Instruments which will capture video feeds, real time instrumentation data, control motor speeds, and lead screw feeds. The National Instruments computer will conduct its operations in flight, and will make use of a solid state hard disk to store data. Real time feeds will be available in the control room via a remote desktop connection to the National Instruments computer over a dedicated wireless network. The new system should not hinder this research project provided all instrumentation is re-calibrated, which is proposed for each test.

3.6 Summary

The Geotechnical centrifuge generally and more specifically the facility at City University London has been described. The history, key principles, applications and limitations of the geotechnical centrifuge have been discussed. Relevant scaling laws have also been derived, and explained and their relevance to the project discussed. Errors inherent in geotechnical centrifuge modelling and relevant to this project have also been highlighted and discussed.

4 Model and apparatus design

4.1 Introduction

It was necessary to design an experiment and test series to investigate the effect ribs would have on the ultimate capacity of a pile. This chapter discusses the centrifuge model requirements and the design of the experiment. The design and construction of the apparatus required to conduct such experiments is also detailed. Several custom-made tools and instruments have been used and are discussed here. The model making and centrifuge testing procedure has also been outlined.

4.2 Model design requirements

The centrifuge is a widely used and well documented tool for modelling single piles and pile group behaviour. The research centre at City University London has recently been involved in tests concerned with the reuse of piles in urban environments (Qerimi, 2009) and with micro piles (Rose, 2010). Existing single pile loading equipment at City University makes use of vessels mounted above the piles. These can be filled with liquid to provide a constant or varying load. The liquid contained within the cylinder can be dumped and then refilled to simulate an un-loading and re-loading event. For the tests proposed in this project it was considered more beneficial to have a constant rate of penetration. A maintained load test would require either accurate control of fluid in a vessel or feedback from a load cell to the motor controller. Both were considered to be unnecessarily complicated. Furthermore, a constant rate of penetration was thought to be simple, effective and repeatable. For this reason new pile loading apparatus was designed that used a lead screw and actuator. The new pile loading apparatus is discussed in more detail below.

An existing stainless steel cylindrical tub measuring 420mm diameter by 415mm depth was available to use. The proposed tests required a sample depth of 300mm and would require some trimming of the clay after removal from the consolidation press. This is normally carried out using ‘box’ cutters, thin wall tubes and scrapers. It is notoriously difficult to obtain an undisturbed level surface. Moreover, this process is time consuming and undesirable on two fronts. Firstly, swelling commences immediately after removal from the consolidation press and secondly, the sample may begin to dry out. A new two stage cylindrical soil container was designed and manufactured to address these points. This container allowed for easy trimming of the sample height and also quick installation of testing apparatus and measuring equipment.

The test procedure involved boring and casting the test piles at 1g on the lab floor before centrifuge spin up and in-flight loading. An in-flight four-axis robotic manipulator, such as that used by Ng et al. (2002), was thought to be too complex a system to develop for installing and loading the test piles. Especially since it would have to work in conjunction with a system capable of mixing and pouring the resin used to cast the piles. Moreover, little would be gained by installing the pile in-flight.

Pile cutting tools were designed and manufactured to bore the piles and profile ribs whilst minimising soil disturbance. A guide system was also designed to allow the piles to be installed with a good vertical and horizontal alignment. Details of the designs are discussed in Section 4.3.2.

The capacity of a pile, both in skin friction and end bearing, is proportional to the undrained shear strength of the soil within which it lies. Whilst it was possible to estimate the undrained shear strength from known parameters such as the soils stress history, permeability and overconsolidation ratio (OCR). It was considered beneficial to have a direct measurement for the undrained shear strength with depth. To date Pilcon hand shear vane readings have been taken at discrete depths and then adjusted using the BS1377 calculation. This method is thought to provide a reasonably accurate measurement but is not able to profile S_u with depth. A further complication is that this tool is used at 1g post testing and therefore the soil is not subject to an accelerated gravitational field. To limit this Pilcon hand shear vane readings are typically conducted immediately after spin down. A T-bar penetrometer has been developed based on Stewart & Randolph (1991) which is able to profile the samples undrained shear strength with depth. The T-bar penetrometer has been extensively used for this research project and also by colleagues at the Geotechnical Engineering Research Centre.

4.3 Apparatus design development

Each test consisted of three testing sites within the soil container. Two of the sites were used for piles and the third for the T-bar penetrometer. Since the soil container was a cylindrical tub it was decided to locate each test site on a pitch circle diameter of 240mm. This ensured that each site was sufficiently far away from the boundaries of the tub and from adjacent test sites to minimise any influence they may have had on each other. Craig (1995) suggests that for a pile foundation test, a minimum distance of 5 pile diameters from the boundaries is sufficient to minimise boundary effects. For the main series of tests using 16mm diameter by 180mm long piles, a spacing of at least 6.5 pile diameters was maintained between all boundaries. Furthermore the sides of

the soil container were lubricated with water pump grease to minimise the skin friction at the boundaries. Figure 4.1 shows the test layout in plan.

4.3.1 Soil container

A new soil container has been designed and manufactured and is shown in Figure 4.2. The container consists of two cylindrical tubes with flanges at the top and bottom. The shallower tube is attached to the deeper tube that in turn is attached to a base plate. The walls and flanges of the tubes are 8mm and 10mm thick respectively. The tubes have bosses which are tapped with a ¼" BSP thread internally and ¾"BSP thread externally. The bosses are intended to allow the installation of instrumentation such as pore pressure transducers and have been positioned to provide a choice of locations.

The tubes were manufactured by rolling a sheet of stainless steel to the required diameter. Stainless steel rings were then welded to the top and bottom flanges. The Author is grateful to Skanska Cementation for rolling the plate, welding of the flanges and bosses at their Bentley Works. Cementation also faced the flanges and turned the bore of the tubes to ensure they were completely perpendicular. The inner bore of the tubes were also honed in order to achieve a surface roughness of no greater than 4 microns, designed to keep the boundary effects to a minimum.

The bottom flange of each tube was machined with a groove in order to receive an o-ring, allowing a watertight seal between each tube and the base.

An aluminium drainage plate was also manufactured to allow free drainage at the bottom of the sample as shown in Figure 4.3. The drainage plate was connected to taps at either end which allowed excess water to be removed during consolidation or to provide a static head during centrifuge flight.

A standpipe had also been constructed from brass and is shown in Figure 4.4. It consisted of an adjustable overflow pipe that was used to maintain the head of water. The standpipe was also equipped with quick connect fittings to allow for easy installation.

4.3.2 Pile cutters & guides

The piles used in the tests were 16mm in diameter by 180mm long; at 50g this scales to an 800mm diameter by 9m long pile. For the ribbed piles the shaft diameter remained constant at 16mm, the ribs protrude radially outwards. For all tests the rib outstand remained constant at 1.5mm. For the helical and concentric rib profiles the rib height was also maintained at 1.5mm

The straight-shafted piles were cut using a hypodermic tube with an external diameter of 16mm and wall thickness of 0.5mm. The hypodermic tube was mounted onto a knurled brass handle to allow for easy cutting (as shown in Figure 4.5).

The pile cutting tube was guided using collars to maintain positional tolerance and verticality; the guide system is discussed below. Several steps were taken to reduce the friction on the cutter and minimise soil disturbance within the pile bore. These included the use of a spray lubricant inside the pile bore to allow the cut soil to move more freely inside the tube and a sharpened edge on the tool. Moreover, the boring of the pile took place in three equal stages.

The ribbed piles were formed by initially boring a hole in the clay using the straight-shafted pile cutter (Figure 4.5). A specifically designed tool was then dropped into the bore and used to profile the ribs. The tool is shown in Figure 4.6 and its operation illustrated in Figure 4.7.

The tool was made of a brass tube with a section of the wall removed. A rotating rod was mounted with an interchangeable toothed plate positioned to one side of the tube. The cutting tool could then be inserted into the bore with the rib cutting teeth retracted. The inner rod was then rotated exposing the teeth and therefore beginning the cutting of the rib. The entire tool was then rotated within the pile bore. Once the rib had been formed the inner rod was retracted back into the tool thereby forcing any spoil into the tube. The tool had been designed to make use of the same guide system used by the straight-shafted pile cutter. This reduced the time for model making and also aided in maintaining accuracy.

The helically ribbed piles were formed with the use of a single cutting tooth and spoil collection bucket mounted to a lead screw, which controlled the pitch (See Figures 5.6 and 5.7). The pitch was altered by changing the lead screw. The rib cutting process was therefore inherently different to concentric ribbing tool, as the concentric ribbing tool profiled all ribs simultaneously, whilst the helical ribbing tool profiled the shaft from the top to the bottom of the pile.

Owing to the way the piles were loaded it was imperative that the piles were installed in the correct horizontal alignment and with good verticality. The pile cutting tools were guided in order to achieve this. The guide system made use of a plate mounted on top of the soil container with two collars (Figure 4.8). The collars had a good fit with the outer diameter of the cutting tools and were sufficiently long to restrict horizontal movement.

The development of these tools and guides ensured the pile forming and installation process was repeatable for each test but also allowed the time from removal from the press and installation into the swing to be kept to a minimum. The typical duration for this was in the order of one and a half to two hours, this was consistent across the testing series.

4.3.3 Pile caps

A pile cap is the component of a foundation that provides the connection between the superstructure and substructure. Pile caps can be designed to only transmit specific types of load. In this case, a study about the axial capacity of the foundation, it was necessary for the pile cap (Figure 4.9) to only transfer vertical load and not horizontal loads or moments.

The load cells were equipped with bull nose loading pins which sat in a matching recess in the pile cap (Figure 4.9). The lack of mechanical connection and the bull nose profile at the point of contact ensured only axial force was transmitted to the pile. The pile cap was equipped with a shelf to allow a thin metal plate to be attached. The plate was fixed with a small amount of cyanoacrylate adhesive before each test and provided a horizon for the LVDT legs. This allowed measurement of the pile settlement and also provided a check as to the verticality of the pile loading. The pile cap was cast into the model pile using a two-part resin as discussed in Section 4.3.4. The underside of the pile cap was kept at 10mm above the top of the pile to ensure sufficient room for the test pile to settle.

4.3.4 Casting of piles

McNamara (2001) experimented with several resins in an attempt to source a material that was capable of being poured at room temperature and could cure without excessive exotherm whilst providing good resistance to shrinkage and fast setting. McNamara (2001) decided on a polyurethane resin called Sika Biresein G27 which is a two part ‘fast cast’ resin used commercially for complex and rotational moulding. The resin consisted of two parts that were first mixed with an aluminium trihydrate (ATH) filler and then mixed together. The casts were observed to shrink less than 1% during curing. The exotherm was also measured and found to be negligible. McNamara found a mixture of 100g of filler to 100g of resin resulted in an easily pourable fluid which was capable of filling the pile holes and leaving few if any voids. The fluid was found to have a pot life of 2 minutes and a curing time of 20 minutes.

Some preliminary tests of the Sika G27 resin were conducted to check the viability of the resin for the proposed tests. A simple resin delivery system was used whereby an 8mm nylon hose was attached to a funnel. This hose assisted in delivering the resin to the bottom of the pile bore. The initial mix of one Part A of the resin, to one Part B, to

one part filler was trialled. This was found to be too viscous for even the resin delivery system. A second mix of 1.5:1.5:1 was used and was found to have a good viscosity. This mixture showed good contact with the clay and was fluid enough to form the small intricate ribs required. Samples of this mixture were taken. The results of a series of tensile and compressive tests are shown in Figure 4.10. The material was found to have an average Young's Modulus of 574MPa. A 50ml hypodermic syringe and suitably long needle was chosen to deliver the resin required to cast the pile to the bottom of the pile bore.

Some air bubbles were observed at the top surface of the pile during the testing of the resin. Upon further investigation it has become apparent that these bubbles are a result of the individual components of the resin being exposed to air for an extended period of time. The liquid components of the resin remove moisture from the surrounding air and therefore the containers should not be left open for any longer than necessary. Smaller containers of the resin were sourced to be consumed more quickly in order to avoid this.

The 1.5:1.5:1 mixture described above was used for some of the preliminary tests. However, it was found to have a density less than that of water. This clearly was undesirable as the pile would be subject to some up thrust from its buoyant nature. Although this was small it was considered to be unrepresentative. This prompted an investigation into the ideal resin mix. Both Aluminium Trihydrate and Aluminium Oxide were trialled as fillers with varying ratios. Table 4.1 summarises the findings. A ratio of 1:1:3, where the larger part was Aluminium Trihydrate filler was chosen for the main testing series. This mix was shown to have a density of around 1800kg/m^3 and a pot life of 3.5 minutes. The results of a series of compressive tests are shown in Figure 4.11. The material was found to have an average Young's Modulus of 586MPa. This is very similar to the Young's Modulus of the previous resin (an increase of 2%) and is not considered significant. Moreover this demonstrates that the heavier filler only increased the piles mass and not its structural properties.

4.3.5 Pile loading apparatus

The piles were driven simultaneously with independent measurements for load and settlement. The most robust way of achieving this was by using an actuated lead screw connected to a loading beam (Figure 4.12). The loading beam had been designed to be sufficiently stiff and therefore would not bend from being subjected to differential loads at its extremities. The loading beam had a threaded load cell attached at the location of the piles. Each load cell was equipped with a loading pin threaded on to it. The loading pin was spherical where it met the pile head. This was in order to provide a

single point of contact and therefore minimise any horizontal loading of the pile (Figure 4.13).

To ensure the loading beam descended vertically, and in the correct position two 8mm linear bearings with matching shafts were utilised.

The screw jack manufactured by Zimm was capable of providing 5kN of axial force, and had a maximum stroke of 250mm with a stroke per revolution of 1mm. It had been built such that the lead screw did not rotate. A Maxon motor and planetary gear head, with a gearbox ratio of 1:156, capable of providing 15Nm of torque drove the screw jack. The motor was equipped with a digital optical encoder which fed information about the speed of the motor to the centrifuge motor controller. This in turn adjusted the current to the motor in order to maintain the desired speed. The digital optical encoder operated by converting the rotating motion of the motor into a sequence of digital pulses. A light shone on a rotating disk within the encoder which was perforated at specific locations such that the light could pass through and be detected by a receiver. The receiver could then count the number of passes and therefore, compute the revolutions per minute (illustrated in Figure 4.14).

4.3.6 T-bar penetrometer and actuator

Since the soils undrained shear strength is a function of stress history and stress level and hence g-level, it was considered necessary to profile the undrained shear strength with depth in flight.

An instrumented T-bar penetrometer was designed and constructed based on Stewart & Randolph (1991), Figure 4.15 shows the construction detail. A 7mm diameter rod was connected to a hollow tube via a short length of thin walled hypodermic tube. The strain gauges were attached to this hypodermic tube. The T-bar used four strain gauges in a full bridge circuit to compensate for bending and only measured axial strain whilst simultaneously compensating for temperature changes, lead wire resistance and Poisson's ratio effects. A brush on neoprene coating was applied to the strain gauges to protect from dirt and moisture.

During construction of the penetrometer a small imbalance in the bridge circuit was generated. This was likely to be due to the difficulty of attaching extremely small strain gauges to a curved surface. The imbalance caused an output voltage at zero load. Which, when amplified to the necessary gain, was found to be too close to the maximum range of the centrifuge data logging equipment. A subsequent redesign of the bridge circuit included a 10 Ohm multi-turn potentiometer. The potentiometer was positioned such that its resistance could be split between each arm of the bridge thus allowing any imbalance of the circuit to be corrected. The revised circuit and circuit

board were housed in a small brass container at the top of the T-bar. Figure 4.16 shows the strain gauge circuit and the printed circuit board layout and Figure 4.17 shows the completed T-bar.

The T-bar was calibrated for force on a Budenberg dial calibration system, such that a specific number of bits equate to 1N of force. A gain of 500 times was found to give a satisfactory change in voltage over the expected range of loading. From the force on the T-bar, the shear strength was estimated using the following simple expression:

$$\frac{P}{S_u d} = N_b \tag{4.1}$$

Where: P – force per unit length acting on the cylinder (kN).

d – diameter of the cylinder (m).

S_u – undrained shear strength of the soil (kPa).

N_b – bar factor.

Randolph and Houlsby (1984) recommend that an intermediate value for N_b of 10.5 could be adopted for general use.

Some preliminary tests were conducted using the T-bar, driven via a 10kN Zimm screw jack and a Maxon motor. Test showed a reasonable correlation between the T-bar and the shear vane at 1g. Upon post flight inspection an enlarged void was observed at the entry location for the T-bar. The most likely cause for this is the T-bar being driven at an inclination. The length of the T-bar (300mm) also made it difficult to use with generic test apparatus. For these reasons it was decided a dedicated T-bar actuator was required which allowed for easy incorporation into any test arrangement whilst also ensuring good verticality.

The T-bar actuator is shown in Figure 4.18. A Maxon motor drove a 1:156 planetary gear head which was connected to a 15 toothed, module 1.25 spur gear. This spur gear drove an 18 toothed idler cog which was free to rotate on a shaft. The idler cog would then turn another 18 toothed cog mounted to a lead screw. The lead screw had a multi-start thread with a pitch of 5mm. The entire system of gears including the planetary gear head had a gear box ratio of 187.2:1. This equates to 187.2 rotations of the motor for a 5mm vertical moment of the T-bar. The T-bar was mounted on a platform that was attached to the lead screw via a ball nut. The platform was also equipped with a linear bearing which ran on a shaft parallel to the lead screw in order to guarantee verticality.

The T-bar and associated actuator have been incorporated into tests by other researchers within the research group. A series of 20g tests were conducted for an unrelated project, with the T-bar being driven in-flight and Pilcon shear vane measurements taken immediately after spin down. Figure 4.19 shows graphs from two tests conducted by McNamara et al. (2011). Both tests show a very good correlation between the Pilcon shear vane at 1g and the T-bar in-flight. The tests conducted were quick undrained tests and hence the pore pressures may have not necessarily equalised. For this series of testing the shear vanes was used in conjunction with the T-bar. The primary reason for this was to allow estimations of the undrained shear strength profile to be made in instances where the T-bar failed.

4.4 Testing procedure

4.4.1 Sample preparation

The clay samples for the tests were prepared from slurry at a water content of approximately twice the liquid limit, as per standard practice, which for speswhite kaolin is 120%. Clay was recycled from previous tests where possible. Mixing of the dry kaolin powder, recycled clay and distilled water was conducted using an industrial ribbon blade mixer (see Figure 4.20).

Approximately 600mm of kaolin slurry at 110% water content was required to provide a 320mm sample after consolidation in the soil container. This equated to a volume of 83 litres of slurry in the soil container and represented 70% of the maximum capacity of the mixer. However, the mixer was always filled to its capacity and any excess slurry left behind since it was difficult to fully empty the mixer.

Mixing of the slurry and verification of its water content took a full day depending on the portion of recycled clay and the amount of time to soak.

The soil container was prepared by coating the walls with waterproof grease. The slurry was then sandwiched between a layer of filter paper and 3mm porous plastic, at either end, in combination with the aluminium drainage plate, described in Section 4.3.1 and shown in Figure 4.3. This arrangement was found to provide an effective drainage system, which also prevented the loss of clay slurry during the early stages of consolidation.

Since the required slurry height (600mm) was much greater than the height available in the soil container (300mm), an extension was required. Such an extension with a depth of 300mm and the same plan dimensions as the tub was available. An O-ring grove was machined into the bottom flange of the extension to allow for effective sealing.

Although the slurry was at a water content of 110% post mixing it was still too viscous to be poured into the soil container without the use of special equipment. It was therefore carefully placed into the soil container with the use of a scoop and spatula to prevent the entrapment of air. Once the slurry had been placed and levelled the top filter paper and porous plastic were positioned to enable top drainage.

A hydraulic consolidation press with a tight fitting loading platen was used to consolidate the sample. The platen was fitted with an O-ring during the early stages of consolidation to prohibit any slurry loss. A dial controlled the pressure in the ram to which the platen was attached. The actual pressure in the ram was also displayed and it was noted that this often lagged behind the desired pressure. The pressure in the ram was not accurately controlled at the lower ranges, it was therefore necessary to manually lower the ram to achieve the first 25kPa in increments of 5kPa. After which time the loading was switched to computer control. The applied pressure was then rapidly increased to 125kPa and left to consolidate for 5 hours. At this point the loading pressure was set to 250kPa and doubled the following morning. The sample remained at 500kPa for 6 days after which time the pressure was reduced to 250kPa, to allow for swelling. During the swelling process the pipes connected to the drainage taps remained immersed in water so as to prevent air from entering the sample.

Consolidation took place over a 10 day period, including 1 day of swelling. McNamara (2001) found that after approximately one week the vertical movement of the ram was negligible, for a sample of similar height. A detailed loading schedule is shown in Table 4.2.

Colleagues at City have observed an increase in the soil stiffness when a sample remains in the consolidation press for an extended period of time. Some tests using much smaller soil containers are being conducted to verify this observation (Musbahi, 2012). At the time of writing the only conclusions that have been drawn suggest that a difference in slurry water content can cause varying stress profiles. For this reason, not only was the total time for consolidation regulated, but also the time in-between loading increments. The consolidation-loading schedule set out in Table 4.2 was strictly adhered to. To further ensure consistency every effort was made to ensure the time between removal of the sample of the press and centrifuge spin up was consistent and in the range of one and a half to two hours.

A consolidation pressure of 500kPa followed by swelling to 250kPa resulted in a sample at 50g with an over-consolidation ratio variation with depth as shown in Figure 4.21. The variation of K_0 with depth (Figure 4.22) was calculated using Equation (*4.2)* after Mayne and Kulhawy (1982):

$$K_0 = (1 - sin\emptyset')OCR^{sin\emptyset'} \quad (4.2)$$

The consequent theoretical vertical and horizontal total and effective stresses are shown in Figure 4.23.

4.4.2 Model making

Pore pressure transducers (PPTs) were installed on the day swelling commenced through plugged holes in the walls of the soil container. The transducers were installed in the centre of the tub and were guided with a collar that screws on to the tub (Figure 4.24). The core of soil that was removed in order to install the transducer was replaced with de-aired kaolin slurry with a water content of 120%.

The soil container was removed from the consolidation press and the extension un-bolted. At this point the clay sample was protruding out of the soil container by 20-30mm. This was trimmed to the level of the soil container using a wire cutter (Figure 4.25). The edge of soil nearest to the boundary could then be depressed using a fingertip. It is normal practice at this stage to seal the surface of a clay model with silicone oil or similar to prevent drying during flight. However, preliminary trials showed that oil could easily be drawn into the void created around the pile ribs. The use of brass bunds reduced this phenomena, but not to a satisfactory level. In view of this it was decided that the top of the clay should be sealed by an alternative means. A product used for this is commercially known as PlastiDip, a multipurpose synthetic rubber coating. The spray on membrane sticks to the top of the clay and once dried (3-4 minutes) can be cut with a sharp scalpel. The cured membrane has been measured to be 400 microns thick. The PlastiDip was removed at both the pile test and T-bar sites, so as not to influence the test (Figure 4.26). A bead of silicone grease around the edge of the tub ensured the sample remained sealed during any swelling of the clay.

Figure 4.27 shows a plot of undrained shear strength with depth obtained from the T-bar during the early tests. Also plotted are predicted undrained shear profiles derived from empirical relationships (Wroth, 1984; Springman, 1989; Stewart, 1989; Garnier; 2002). Tests RJG2 and RJG3 were sealed with silicon oil whilst Tests RJG4, RJG5, and RJG8 were sealed with PlastiDip. The PlastiDip tests all show good correlation with the majority of empirical solutions.

At this point the pre-assembled pile cutting guides were mounted to the soil container as illustrated in Figure 4.8. The piles could then be bored and cast as detailed in Section 4.4.2.

With the piles fully installed the top tube could be mounted to the soil container (Figure 4.28). This was pre-configured with the remaining apparatus attached. The LVDTs

were then aligned with the pile caps. Next the model was weighed and placed on the swing of the centrifuge where the instrumentation and the standpipe were connected. The drainage plate could then be flushed with water to remove any air that may have been trapped. Next the loading beam was lowered such that the loading pins were just above each pile cap.

Once the counterweight had been adjusted, the centrifuge clamshell was closed and the centrifuge was accelerated to 50 gravities.

4.4.3 Test procedure

Once the centrifuge had reached 50 gravities it was left for 50 hours to allow the pore-water pressures to reach equilibrium. Pore pressure equalisation was verified by real time monitoring of the installed pore pressure transducers (PPT). Once fully hydrostatic pore pressures were established the testing of the piles could commence.

The piles were loaded simultaneously at a rate of 0.25mm/min for at least 12 minutes or 3mm of settlement. A loading rate of 0.25mm/min at 50g scales to a loading rate of 0.3mm/hr or 7.26mm/day. This is comparable to constant rate of penetration tests conducted at prototype scale.

Lehane et al. (2009) describe results from a centrifuge investigation into the rate dependence of T-bar and ball penetrometer resistance in kaolin. During this extensive investigation several parameters were varied including; T-bar diameter, penetration rate and over consolidation ratio. Lehane et al. (2009) showed how the penetration resistance for any given penetrometer velocity and diameter is related to the mechanical and hydraulic properties of the soil. For this series of testing the T-bar was driven at a rate of 60mm/min to a depth of approximately 200mm. Chung et al. (2006) found the tip resistance of an advancing penetrometer to decrease as the rate of penetration decreases, provided the conditions around the advancing penetrometer were undrained due to viscous effects. Conversely, once the penetration rate has reduced sufficiently for partial consolidation to occur the tip resistance increased as the penetration rate was decreased. Stewart & Randolph (1991) suggest a use of 1mm/second for a 35mm by 7mm T-bar used in-flight.

4.5 Summary

The design and development of apparatus suitable to investigate the effect of pile ribs has been explained. This included the soil container, pile cutting, rib forming and loading apparatus. The soil container has been designed to minimise the time between removal of the sample from the consolidation press and centrifuge spin up. Whilst being designed for this series of testing a significant number of features built into the soil container will prove to be of use to future researchers at the Geotechnical

Engineering Research Centre. The pile cutting and rib forming equipment operated at a high level of accuracy, this is evident from the quality of the exhumed piles. The principles of the new loading apparatus has described and explained. Guide collars, jigs and pile caps have been designed and constructed to assist in achieving high positional accuracy of pile cutting, casting and loading.

A T-bar penetrometer has been design, built and commission. The ability to profile the undrained shear strength of a soil sample in-flight is a valuable tool for a centrifuge modeller. Leading research centres such as the University of Western Australia's, Centre for Offshore Foundation Systems have long since had the ability to profile undrained shear strength with depth. The advent of this tool brings the City University London, Geotechnical Research Centre in line with such institutions.

The resin used for casting of model piles has been presented and its key characteristics discussed. The initial resin and filler combination was found to have too small a density and hence a second combination was sourced. The structural properties of both resin and filler combinations have been derived from the conducted structural tests and are presented. The soil type and stress history of the sample was chosen to enable measureable pile settlement whilst preserving the essential characteristics of stiff over consolidated clay.

A new centrifuge testing practice has been identified that makes use of a spray on plastic membrane to seal the soil sample, as opposed to silicon oil which is typically used. This method of sealing a clay sample was required to alleviate issues with the silicon oil lubricating the pile shaft and hence hindering its performance. Furthermore, from the tests conducted with silicon oil it appears the oil fails to effectively seal the sample.

The model making and testing procedure adopted for this test series has also been explained. Every effort has been made to reduce the time between removal of the sample from the consolidation press and centrifuge spin up. Furthermore, the developed equipment has aided in keeping this time consistent and, generally to under two hours. This is considered to be relatively quick when compared to other centrifuge model making operations both at this institution and at others.

5 Experimental work

5.1 Introduction

This chapter describes in detail the tests that were conducted and their fundamental results. A total of 23 centrifuge tests were carried out, each with two model foundations. For the most part each test consisted of a plain pile versus a ribbed pile. The intention was to use the plain pile load settlement data to normalise out any inconsistencies in sample preparation. Sample preparation, model making and centrifuge testing took two weeks per test. The tests were generally run back to back subject to centrifuge availability. This time constraint dictated that only rib spacing and rib type be varied. The rib height and outstand remained constant for all tests. Details of the tests conducted and performance of test apparatus are presented in Table 5.1.

5.2 Details of tests

For all tests the soil sample was prepared from kaolin slurry with 110% water content. Typically a water content of 120% is used for centrifuge tests in kaolin, however for this test series and over consolidation ratio a water content of 120% would result in too shallow a sample. The soil container consisted of a centrifuge tub and extension, the height of the tub had been designed to provide a convenient location to trim the soil. The slurry was placed into the soil container in layers; care was taken to ensure no air became trapped. The samples were consolidated to 500kPa and allowed to swell under 250kPa. The soil was prepared in an identical manner for each test. Upon removal from the consolidation press the extension was removed and excess clay trimmed using a wire cutter. The sample was sealed before model making commenced in order to prevent drying, see Section 4.3.2. All piles tested were 180mm long and had a diameter of 16mm. The rib height and outstand was maintained at 1.5mm for all tests. Typical pile dimensions can be seen in Figure 5.1. The pile castings are considered to be of very high quality and generally consistent, Figure 5.2 shows typical exhumed piles.

In all tests instrumentation consisted of six Linear Variable Differential Transformers (LVDT), three Pore Pressure Transducers (PPT), two load cells and a T-bar penetrometer. Two LDVTs were used on each pile to measure pile head settlement and check for any non-axial pile head settlement (Figure 5.3). The remaining two LVDTs were used to measure soil surface movement during pore pressure equalisation and pile loading. PPTs were installed in the centre of the soil container at depths of 50mm, 150mm and 250mm from soil surface level. The PPTs were used to verify hydrostatic pore pressures and were considered to be too far from the zone of

influence to detect pore pressure changes due to pile loading. Load cells were equipped with bull nose loading pins to provide a single point of contact and hence provide only axial loading. The T-bar was developed as part of the project and used to obtain an undrained shear strength profile of the soil in every test. However, there was a varying success rate due to the preliminary nature of the instrument. Cameras were used to assist in rapidly moving the loading apparatus close to the pile caps and ensuring contact was not made prematurely.

Tests RJG5 and RJG6 were used as calibration tests and hence modelled two plain piles in the same soil to observe any relative difference. Test RJG11 was used to compare a plain pile against one of a diameter equal to the rib outer diameter (19mm). The 19mm pile was bored in the same way as the ribbed pile. This meant using a blank plate on the ribbing tool as opposed to a toothed plate and provided the same level of mechanical roughness between the pile shaft and clay as with the other ribbed piles.

- Test RJG0

This test was intended as a preliminary test and was used to gain insight into the likely issues that would need addressing with the development of apparatus for the main test series. Existing pile loading apparatus (Qerimi, 2009) was used to load the piles (Figure 1.1). An existing shaft profiling tool (Witton-Dauris, 2008) was used to cut pile ribs. This tool made use of a wedge shaped plate which when moved in the vertical plane exposed or retracted the rib cutting teeth (Figure 5.4).

This test also provided an opportunity to test resin delivery systems. Several methods were tested using syringes, tubes and funnels. The optimum for the given resin and filler mix was found to be a small funnel attached to an 8mm OD pipe. This allowed the resin mix to be delivered effectively to the bottom of the pile.

The existing rib pile cutters, whilst effective at profiling the pile shaft made little allowance for spoil collection. Furthermore, the design of the cutting plate made varying the rib dimensions somewhat difficult. This resulted in the development of a new profiling tool which made use of an interchangeable toothed plate for varying rib profiles. A rotating rod to which the cutting plate was mounted was used for exposing and retracting the cutting teeth.

The existing loading apparatus made use of fluid filled vessels which could be filled or emptied to allow for loading or unloading. Whilst it was felt that this apparatus could be used for constant rate of penetration tests, it would be best suited to maintained load testing. Loading apparatus better suited for CRP testing was designed and is explained in Section 4.2.5.

The existing pile loading and instrumentation rack made use of four M8 threaded rods which allowed vertical movement to accommodate for changes in sample height. This was thought to be cumbersome and time consuming. Moreover problems occurred when ensuring the platform was level. Trimming the clay for each test to the correct level was also time consuming and rather arduous. This inspired the design of a new two stage tub used for the main test series. The bottom tube was a soil container whilst the top tube was used to mount all apparatus and instrumentation. The interface between the two was designed to provide a convenient location for trimming of the sample with a wire cutter. This significantly reduced the model preparation time for the main test series.

It was also decided that a camera focused on the pile cap would aid in verifying whether contact had been made or give an indication as to the distance to contact.

-Test RJG1

Test RJG1 was the first test to use the new two part soil container, pile cutter, casting and loading apparatus. The consolidation and model making appeared to be successful. However, before centrifuge spin up it became apparent that the base drain had become blocked. This was likely to have resulted from a poor seal between the porous plastic and soil container or from a rapid succession of loading increments during the early stages of consolidation. Attempts were made to purge any soil from the drain using water and then air. This proved to be unsuccessful owing to the extent of the blockage and the test was aborted. The base drain was periodically flushed using a 50ml syringe, during consolidation for every test post RJG1. The loading increments were also reduced during the early stages

- Tests RJG2, RJG3, RJG4 and RJG7

In tests RJG2, RJG3, RJG4 and RJG7 the influence of concentric ribs on a pile shaft was investigated. Test RJG3 was a repeat of RJG2. In all tests both piles were loaded to a settlement of 3mm, significantly in excess of the 10% of the pile diameter which is generally considered failure. Subsequent investigation of tests RJG2 and RJG3 showed small amounts of silicon oil near to the pile shaft. It was thought this would be detrimental to the performance of the pile. For all tests after and including RJG4 PlastiDip (Section 4.4.2) was used to seal the surface of the soil sample. G27 resin with aluminium oxide filler was used to cast the piles in a ratio of 3 parts resin to 1 part filler.

- Tests RJG5 and RJG6

In order to establish the repeatability of the testing apparatus, it was necessary to conduct a test whereby both piles were identical. In Test RJG5 two plain piles were tested. During in-flight consolidation it had become apparent that the loading pins had made contact with the top of the pile caps. This was verified by the load cells which detected a small compressive load. Test RJG6 was identical to RJG5 and conducted to verify the observations made in test RJG5. G27 resin with aluminium oxide filler was used to cast the piles in a ratio of 3 parts resin to 1 part filler.

- Test RJG8 and RJG9

The previous tests were focused on either verifying the test equipment (RJG5 and RJG6) or focused on the effects of concentric ribs. Tests RJG8 and RJG9 looked at the effects of 10mm helical ribs. A helical rib cutting tool was designed and constructed. The tool made use of a 10mm pitch lead screw and ball nut (Figure 5.6). The tool was therefore only capable of producing a helical rib with 10mm spacing. At the time of designing the tool it was envisaged that only a 10mm helical spacing would be investigated, owing to the considerable cost of manufacturing a new tool for every variation in rib spacing. Before Test RJG8 several helical piles were cast in unused clay samples in order to gain experience with the cutting tool. This also resulted in several variations in the spoil collection bucket and rib cutting tooth. The decision was made to further investigate the helical rib profile, given that the 10mm helical ribs showed significant merit.

- Test RJG10 RJG13 and RJG21

In Tests RJG10, RJG13 and RJG21 the effectiveness of wider concentric rib spacing was investigated. Test RJG10 was conducted with a 20mm concentric rib spacing whilst Test RJG13 and RJG21 used a spacing of 40mm. All tests post Test RJG10 made use of an Aluminium Trihydrate (AL_2O_3) filler. Two parts resin to three parts filler was found to have a density of around 1800kg/m^3. This was preferred since the previous resin/filler mix had a density close to that of water resulting in a pile that was either buoyant or close to buoyant. During centrifuge spin up of Test RJG10 the data logger ceased functioning. The data logger was reset once the centrifuge was at the required g-level. The consolidation pressure on the sample for Test RJG13 reduced over the subsequent two days before the test, which coincided with a weekend owing to an equipment malfunction. This was likely to have been a result of insufficient hydraulic oil in the reservoir of the pump. The pressure was reinstated early on Monday, which resulted in the sample swelling and PPT installation not taking place

until that evening. Test RJG21 was a repeat of test RJG13 testing a concentrically ribbed pile with a 40mm spacing.

- Test RJG11

All tests previous to RJG11 were aimed at either comparing a ribbed pile to a plain pile or comparing two plain piles for the purpose of equipment verification. In Test RJG11 a plain 16mm diameter pile was compared to a plain 19mm diameter pile. The 19mm pile was bored with the same tool used to profile ribs. However in this case a blank plate instead of a toothed plate was used. The purpose of this was to ensure the same mechanical roughness between the soil and pile as with the ribbed piles. The ribbed piles had an outer diameter of 19mm and hence the 19mm plain pile represented a ribbed pile with zero spacing between ribs. Any improvement in normalised failure load provided by a ribbed pile would mean that the ribbed pile was in fact better than a pile with a diameter equivalent to the outer ribs. The T-bar failed during the test, although it was shown to work pre-flight, suggesting that the problem with the drive equipment was related to the additional force it was subjected at a high g-level.

- Test RJG12

Test RJG12 was conducted with a 40mm concentrically ribbed pile and a plain shafted pile. Model making was successful and hydrostatic pore pressures were achieved during flight. Once the loading of the piles commenced it became apparent that neither of the load cells were functioning correctly. The pile displacement was increasing whilst the load remained constant. After further investigation it became clear that the apparent lack of load increase was attributable to an incorrect gain setting for the load cell channels. This resulted in the test being discarded.

- Test RJG14

The tests previous to RJG14 investigated the behaviour of piles with the entire length of shafted profiled in some fashion. It was decided to model a pile with only the bottom third profiled, since the ideal situation would be to increase load bearing capacity with the minimum amount of work or additional time spent. A 10mm concentric rib profile was chosen resulting in five ribs at the bottom third of the pile.

- Test RJG15 & RJG19

All tests prior to Test RJG15 made use of square ribs (1.5mm by 1.5mm), for Tests RJG15 & RJG19 a tapered rib profile was tested. A tapered rib can be described as one where the rib starts at the same diameter as the pile and ends at the rib outer diameter (or in section, half of an arrow pointing downwards) (Figure 5.5). The

motivation for this type of rib was simply that a wedge shaped pile (pointing downwards) would perhaps perform much like a door wedge, where the resistance would increase as embedment increases, if it were possible to construct such a pile. This tapered or wedge shaped rib profile was an extension of this principle.

- Test RJG16 & RJG17

It was decided to further investigate helical ribs, owing to the significant increase in ultimate pile capacity demonstrated by the 10mm helical rib test piles in Tests RJG8 & RJG9. The tool used to cut the 10mm helical ribs made use of a commercially available lead screw and a custom made spoil collection bucket with a single cutting tooth. The key benefit of using an off-the-shelf lead screw was that it was relatively quick and easy to incorporate into the profiling tool. It was decided that simply purchasing further lead screws in order to vary the helical rib spacing was not economical. Moreover, lead screws with large pitch (20-30mm) and small core diameter (less than 15mm) were not available since they would have little or no commercial use. For this reason two single start lead screws were manufactured. They made use of a 15mm diameter silver steel rod with a 5mm groove cut helically around the rod. A ball nut was manufactured by using a tight fitting collar and single 5mm roll pin which ran in the 5mm grove and hence guided the movement of the cutting tool (Figure 5.7). The tool made use of the same spoil collection bucket and single cutting tooth as the 10mm helical rib cutter. For Test RJG16 a 20mm helically ribbed pile was tested whilst a 30mm helically ribbed pile was tested in RJG17.

- Test RJG18 & RJG20

Test RJG18 was the second of the tapered ribbed pile tests. Model making was successful however; during centrifuge spin up it became apparent that the data logger failed to respond. After several hours attempting to repair the data logger it was decided to abort the test. Test RJG20 was also discarded due to a separate issue with the data logger.

- Test RJG22

Test RJG22 compared a straight shafted pile to a pile with concentric under reamed ribs. The rational for this rib shape was simply that under reams are often used to enhance a piles base capacity, and perhaps they would have a similar effect for the base capacity of a pile ribs.

5.3 Observations and results

A total of 23 centrifuge test have been performed. Following preliminary tests the main programme of experimental work sought to explore effect of varying the rib spacing and profile:

Test type:	Test ID:
Preliminary	RJG0 and RJG2
Apparatus verification	RJG5 and RJG6
Concentric ribbed pile	RJG3, RJG4, RJG7, RJG10, RJG13, RJG14 & RJG21
Helical ribbed pile	RJG8, RJG9, RJG16, and RJG17
Straight piles with equivalent rib diameter	RJG11
Tapered and under reamed ribbed pile	RJG15 and RJG22

The tests that were aborted provided valuable experience into centrifuge modelling, however are not presented here since no data was obtained.

5.3.1 Preliminary tests - RJG0 and RJG2

Both Tests RJG0 and RJG2 were considered preliminary; Test RJG0 was conducted using existing equipment with a view of gaining insight into apparatus and tools that may be required for the main series of testing. Test RJG2 was the first successful test with the new centrifuge soil container and testing apparatus. The intention of Test RJG2 was to gain experience with the new apparatus and to identify possible areas in the testing procedure that could be streamlined.

Figure 5.8 and Figure 5.9 show the load settlement curves for test RJG0 and RJG2 respectively. Both tests modelled a pile with 10mm concentric ribs compared with a plain pile. Piles in Test RJG0 were cut and profiled using tooling developed by Witton-Dauris (2008) and hence may have possessed different properties to piles in subsequent tests. During loading of Test RJG0 it was also apparent from the LVDT data that the piles were being loaded eccentrically. The data showed an upward movement of one LVDT and a downward movement on the other. This indicates a tilting of the pile cap. Figure 5.8 shows that the 10mm concentrically ribbed pile performed significantly better than the plain pile in Test RJG0. The ribbed pile only began displacing after 200N of load was applied which is approximately a quarter of the maximum load applied in that test. This is due to an averaging of LVDT data that were not consistent due to the eccentric loading caused by the apparatus.

Test RJG2 (Figure 5.9) shows the 10mm concentrically ribbed pile had very similar stiffness to that of the plain pile. At a pile head settlement of 0.8mm the plain pile clearly failed where the settlement at the pile head rapidly increased as the load decreased. Conversely the ribbed pile at the same point continues to settle under the same load.

5.3.2 Apparatus verification tests – RJG5 and RJG6

Test RJG5 was intended to compare the load-settlement response of two identical piles in the same soil. This was intended to isolate any inconsistencies in the pile forming and loading process. Figure 5.10 presents the load settlement curve for test RJG5. At a pile head settlement of 1.6mm there was an 8% difference in load. In Test RJG5 it was noted that the loading pins were left too close to the pile caps during centrifuge spin up and pore pressure equalisation. This resulted in the piles becoming preloaded as the soil sample swelled. This was also verified by the presence of a compressive load on both load cells prior to pile loading.

It was decided to repeat Test RJG5 since the effect of preloading the piles was unquantifiable. Moreover, Test RJG5 was thought to be significant since it was an important aspect of validating the test apparatus and test series. Test RJG6 was a repeat of Test RJG5, again with two plain piles. The load settlement curve for test RJG6 is presented in Figure 5.11. As in Test RJG5 both piles behaved in a similar manner. At a pile head settlement of 1.6mm there was a 7% difference in load between the two straight shafted piles.

In Test RJG5 the maximum load measured was approximately 300N whilst in Test RJG6 this was approximately 480N. Both soil samples were prepared in an identical manner. The difference in maximum load can be explained by the premature contact and hence premature loading of the piles in Test RJG5

5.3.3 Concentric ribbed pile tests – RJG3, RJG4, RJG7, RJG10, RJG13, RJG14 and RJG21

Tests RJG3, RJG4, RJG7, RJG10, RJG13, RJG14, and RJG21 all compared concentrically ribbed piles with plain piles. In Tests RJG3, RJG4, RJG7, RJG10, RJG13 and RJG21 the rib spacing was varied. Test RJG14 consisted of a pile with only the bottom third ribbed, a 10mm concentric spacing was used for the ribs since at had been shown to be the optimum for the arrangements tested to date. The increase in pile load capacity at a pile head settlement of 1.6mm decreased from 38% in Test RJG3 (Figure 5.12) with a 10mm spacing, to 7% in Test RJG13 (Figure 5.13) with a 40mm spacing. Test RJG21 (Figure 5.14) also tested a 40mm concentrically ribbed pile, which also showed a 7% increase in load capacity. The 15mm spacing in Test RJG4 and RJG7 (Figure 5.15 and 5.16) showed a 20-22% increase in pile capacity,

whilst the 20mm spacing in Test RJG10 (Figure 5.17) showed a 10% increase in capacity for the same pile head settlement. The pile with only the bottom third ribbed in Test RJG14 (Figure 5.18) was shown to have an increase in capacity of 15% compared with the plain pile in the same test.

5.3.4 Helical ribbed pile tests – RJG8, RJG9, RJG16, and RJG17

Tests RJG8, RJG9, RJG16, and RJG17 all compared helically ribbed piles with plain piles. The pitch or spacing of the helix was varied. Test RJG8 and RJG9 used a 10mm pitch whilst Tests RJG16 and RJG17 used 20mm and 30mm spacing respectively. In all cases the helical pile performed better than the plain pile. Figures 5.19 and 5.20 show the load settlement curves for tests RJG8 and RJG9. In both cases the initial stiffness of the plain and ribbed pile appear similar. At a pile head settlement of 1.6mm the helically ribbed pile in Test RJG8 generated 45% more capacity than the plain pile in that test. Whilst in Test RJG9 the helically ribbed pile generated 35% additional capacity when compared with the plain pile. Figures 5.21 and 5.22 show load settlement curves for Tests RJG16 and RJG17 respectively. The relative increase in performance between the plain pile and the helically ribbed pile decreased as the rib spacing increased. At a pile head settlement of 1.6mm the 20mm spaced helically ribbed pile in Test RJG16 was subject to 14% extra load whilst the 30mm spaced helically ribbed pile in Test RJG17 was subject to a 2% increase in load when compared to the plain pile.

5.3.5 Straight piles with equivalent rib diameter test – RJG11

Test RJG11 compared a regular 16mm diameter plain pile to a 19mm diameter plain pile. A 19mm plain pile was chosen as it represented the outer diameter of the ribbed piles. Figure 5.23 shows the load settlement curve for Test RJG11. The 19mm plain pile was found to have a marginally stiffer response and at a pile head settlement of 1.6mm the 19mm pile generated 25% extra capacity.

5.3.6 Tapered ribbed pile tests – RJG15, and RJG19

Isolating and quantifying the base and shaft resistance of a pile rib would provide an insight into how ribs function and the mechanism for generating additional capacity. Tests RJG15 and RJG19 compared plain shafted piles to piles with tapered ribs. Figure 5.24 shows the load settlement curve for Test RJG15 initially both piles have a similar response in terms of stiffness. At a pile head settlement of 1.6mm the tapered rib pile was subject to 40% greater load. Upon analysing the data from the instrumentation from Test RJG19 it became apparent that the load cells had made premature contact with the pile caps, this was likely due to them not being set sufficiently high enough to accommodate the swelling of the soil sample during pore pressure equalisation. For this reason the test was discarded.

5.3.7 Under reamed ribbed pile test – RJG22

Test RJG22 (Figure 5.25) tested a pile with under reamed ribs. These ribs were the opposite of the tapered rib. The under reamed ribbed pile has a similar initial response to that of the plain pile. At a pile head settlement of 1.6mm the under reamed rib pile was subject to 30% greater load.

5.3.8 Pore pressures

Druck PDCR81 Pore Pressure Transducers were installed at 50mm, 150mm and 250mm below the soil surface. The transducers provided real time pore pressure measurements at the above horizons. The principle purpose for the PPTs was to establish when the model had reached pore pressure equilibrium. The target or equilibrium pressure for each horizon would be equal to the hydrostatic pressure of the water head. In cases when the PPTs failed in-flight the model was left spinning for a sufficient amount of time to ensure hydrostatic pore pressures were established. All of the soil samples were of the same height since the tub was used as a guide for trimming. This meant the time required for pore pressure equilibrium was well known and in the range of 50 hours. A typical response of the three PPTs during pore pressure equalisation is shown in Figure 5.26.

5.4 Summary

The programme of tests conducted has been described. Load settlement curves for each test have been plotted and the difference in load capacity relative to a plain pile at a pile head settlement of 1.6mm has been presented. Observations of significant events that may impact the results of tests have been examined. No complex analysis has been presented in this Chapter, data has been presented in its raw form as far as reasonably possible. More detailed analysis forms the basis of Chapter 6.0.

Generally ribbed piles behaved differently when compared to plain-shafted piles. Rib spacing was varied from 10mm to 40mm. A reduction in the ribbed piles performance was clearly visible as the rib spacing increased helically ribbed piles generated the greatest increase in capacity. Of all the piles tested the 10mm helically ribbed pile showed the greatest increase in capacity.

6 Discussion

6.1 Introduction

The purpose of this chapter is to present a summary of the significant findings from the series of centrifuge tests undertaken and to provide an explanation of the behaviour observed. To enable the results to be of maximum use, the results are presented within a context relating to the specific problem of establishing the trends of behaviour of ribbed bored piles in stiff clay.

The enhancement of the capacity of bored piles by the addition of ribs is a relatively novel concept; therefore its use in practice has been limited. However, some numerical and field research has been conducted verifying the plausibility of the technique.

Contractors and clients alike are keen to make use of innovative techniques which support their green credentials. Moreover, ground congestion is fast becoming a genuine concern and therefore more efficient foundations will soon become an obvious choice.

The rationale behind the addition of ribs on bored piles is twofold. Firstly this could, if spaced correctly, move the plane of shear failure radially away from the pile/soil interface to somewhere further into the soil where there has been less disturbance caused by the auguring process. Secondly, the ribs will also result in an additional component of base capacity along the underside of each rib. The viability of increasing a plain pile's capacity with the addition of ribs is not contested. The aim of this research is to optimise this phenomenon and develop a framework to enable detailed design. If a relationship between the type and spacing of rib exists in the model then this could be used to indicate how similar measures used at prototype scale could influence displacements. It therefore follows that in determining the relative effects between the model and the prototype the influence of ribs should be viewed in terms of an overall effect in the model and then an estimate made of the likely effect in the prototype.

6.2 Soil sample

Several, if not all modelling techniques are subject to some level of idealisation. This project is concerned with how the ribs on the shaft of a pile can increase its capacity. It therefore follows that an in-depth understanding of the soil and its behaviour within which the piles are installed is essential.

Soil behaviour is a function of stress history, current stress and water content. Several authors have proposed relationships between current vertical effective stress and the overconsolidation ratio (OCR).

Springman (1989) conducted shear vane tests on Kaolin within the geotechnical centrifuge and proposed the following relationship

$$S_u = 0.19\,\sigma'_V\,(OCR)^{0.71} \tag{6.1}$$

Phillips (1987) proposed the following relationship between undrained shear strength, overconsolidation ratio and vertical effective stress:

$$S_u = 0.19\,\sigma'_V\,(OCR)^{0.67} \tag{6.2}$$

Garnier (2002) suggested the following relationship for Speswhite Kaolin clay:

$$S_u = 0.19\,\sigma'_V\,(OCR)^{0.59} \tag{6.3}$$

Stewart (1989) proposed a similar equation for estimation of the undrained shear strength of a centrifuge soil sample:

$$S_u = 0.22\,\sigma'_V\,(OCR)^{0.57} \tag{6.4}$$

Figure 6.1 shows the measured undrained shear strength profile of the soil model with depth after equilibrium has been reached at 50g in the centrifuge for every test in which the T-bar functioned successfully. In Figure 4.2.7, Equations 6.1-6.4 have been used to calculate the respective profiles. Also plotted on the same axis are selected results from the T-bar penetrometer. Springman (1989) appears to marginally over predict the undrained shear strength profile. Whilst the profiles calculated using relationships proposed by Phillips (1987), Stewart (1989) and Garnier (2002) all show good correlation with the measured undrained shear strength profiles, where Plastidip was used to seal the model. The shear strength profiles where silicon oil was used to seal the sample show little variation with depth and perhaps further verify the influence of the silicon oil on such results. From the data presented is appears that the silicon oil is ineffective at sealing the soil sample. This could be for a variety of reasons, the most plausible being a slight loss of oil into the sample, resulting in the curved free surface of the oil (due to the Coriolis Effect) being under the clay surface (in the centre of the model) allowing water in the sample to evaporate. The measured undrained shear strength profile from the T-bar was used for the majority of the pile test analysis. However where the T-bar failed an estimation of the profile was made using the shear vane result.

6.3 Comparison to full scale test results

In 2002, Expanded Piling and Arup Geotechnics collaborated in a joint research venture looking at the effect of concentric ribs on the performance of a bored pile in clay. As part of this venture several full scale tests were conducted supported by finite element analysis. The project featured in an article in the industry press, Ground Engineering (2003). Figure 6.2 shows the load settlement data of one of the prototype scale tests. This test compared a concentrically ribbed pile to a plain pile. The rib dimensions and spacing were not reported and this information remains confidential. However, the ribbed pile showed a 30% increase in load capacity. This can be compared to Figure 6.3 which shows the load-settlement curve for test RJG4. The 15mm spaced concentrically ribbed pile provided a similar increase in load carrying capacity, approximately 30%. It should be noted that although the magnitude of the increase in load capacity between the Expanded-Arup tests and the tests presented here are similar, the load-settlement curves are different in shape, indicating a different response. The Expanded-Arup test piles were constructed in glacial till with a voided base to avoid generating any base resistance. This may, in part, explain the difference in shape of the load-settlement curves; furthermore the Expanded-Arup piles were not tested to failure.

6.4 Test data analysis

Data obtained from each pile load test has been analysed using several techniques to better define the behaviour of the test pile and allow for comparison between plain shafted piles.

The first technique used was to normalise the load settlement behaviour of a ribbed pile against the plain pile used in the same test. This allowed for any inconsistencies in the soil sample to be accounted for including any variation in undrained shear strength profile. It can be assumed that two identical piles in the same soil sample, subject to the same load will respond in the same way. It follows therefore that the behaviour of a ribbed pile can be compared to that of the plain pile to ascertain any relative improvement.

Figure 6.4 shows the normalised load settlement curves for each test. In each case the ribbed pile load data has been normalised against the load data of the plain pile used in the same test.

To allow for comparison Figure 6.4 has been broken down into several simpler graphs shown in Figures 6.5, 6.6 and 6.7. The dashed lines in Figure 6.5 represent helically ribbed piles, which in all cases exhibited an improvement over concentrically ribbed piles with the same spacing. For both helical and concentric ribs the 10mm spacing has

been shown to be the most effective in increasing the piles ability to carry load at the lower settlement ranges. The normalised increase in capacity decreased as the rib spacing increased.

The tapered rib pile was also very effective and almost matched the normalised load of the 10mm helical pile (Figure 6.6). However, this increase in normalised load was only evident after a significant amount of initial settlement whereas the helical piles showed an improvement in normalised load during the initial stages of loading.

Figure 6.7 shows a normalised load settlement curve for the 19mm plain pile, which is a pile with a diameter equivalent to that of the outer diameter of the ribs. By comparing the 19mm plain pile to the other normalised load settlement curves, it can be seen that the 10mm helically ribbed, the 10mm concentrically ribbed and the tapered rib pile all out performed a plain pile of diameter equal to the outer rib diameter.

In Test RJG14 the behaviour of a pile in which only the bottom third was profiled using concentric ribs at 10mm spacing was explored. The normalised load settlement curve (Figure 6.8) shows the performance of the pile was inferior when compared to the plain pile for the majority of the test, however near the maximum settlement the ribbed pile showed a slight improvement. This suggests the additional capacity mobilised by the ribs is contributed by end bearing which is traditionally accepted to be generated after significant vertical settlement.

By normalising the load settlement curve in each test it is evident that the helically ribbed profile provided the most efficient rib form, given that the normalised load for any magnitude of settlement was higher than for a concentrically ribbed pile with similar rib spacing (Figure 6.4). However, this technique provides no insight as to how the additional capacity has been generated.

In order to better understand the behaviour of the ribbed pile it was necessary to define the point at which each test pile had failed. Several methods were considered (Chin, 1980; Fuller & Hoy, 1970; Brinch Hansen, 1963; BS8004:1986) to analyse and define the failure load of every pile tested (Table 6.1). A spreadsheet was setup for each failure criterion and used to calculate the failure load in an identical fashion, thus removing the variable of human interpretation. Of all the various failure analyses techniques used none proved to be more favourable than any other. None of the failure criterion used gave an output constantly higher or lower when compared to another, instead the output from each of the analyses were generally within 10-15%. For this reason a mean average of the four methods was used to define the failure load of the pile. The defined failure load has also been scaled up to prototype scale. The percentage improvement in capacity of the ribbed pile relative to the plain pile in the

same test is also shown. This improvement in load capacity varied from a 3% increase to a 57% increase.

The calculated failure loads for all of the plain piles show some variation. This can probably be attributed to inconsistencies in the soil sample, and also type of resin used to cast the piles. It is therefore necessary to consider the plain pile used in each test when analysing the ribbed pile behaviour. The percentage increase in capacity between the ribbed pile and plain pile varied from 57% to 3%. However in all cases the ribbed pile showed an improvement over the plain pile. The 19mm plain pile showed a 27% increase in load capacity at failure when compared with the plain pile.

The average normalised load capacity has been plotted against the rib spacing for both the concentric and helical rib types (Figure 6.9). Also plotted are the plain pile normalised failure load and the 19mm plain pile normalised failure load. The 19mm plain pile is a pile with a diameter equivalent to the outside rib diameter. Both the 10mm spaced concentric and helical rib piles show a normalised capacity greater than a pile with an outer diameter equal to the rib diameter. The 10mm spaced concentrically ribbed pile also showed increased capacity when compared to the 19mm pile. The remaining concentric and helically ribbed piles all exhibited an improvement over the plain pile but were out performed by the 19mm plain pile.

The ultimate capacity of a pile is evidently related to the undrained shear strength of the soil. To gauge the accuracy of the pile analysis techniques described above, the plain pile ultimate capacities have been plotted against the soil samples undrained shear strength (Figure 6.10) for each successful test. Though there is some scatter a clear trend can been seen confirming that as the samples undrained shear strength increases so does the plain piles ultimate capacity.

6.5 Pile design framework

From the analysis conducted there is a clear trend between the rib spacing and the increase in pile capacity for both helical and concentric ribs. Furthermore, there is a clear distinction between the two different rib formats. Since the trends set out by the helically ribbed piles are different to that of the concentrically ribbed piles, the method of generating the additional capacity must be different. In order to allow for design of these ribbed piles a framework must be established.

6.5.1 Longitudinal cross sectional area method

Figure 6.11 shows a graph of percentage increase in capacity (when compared to the plain pile in the same test) against the percentage increase in sectional area (i.e. the area presented if the pile were cut in half along its length). Also on this plot is a +/- 10% error band. All of the tests show good correlation with the proposed best fit line and all

are approximately within the 10% error band. The best fit line has the following Equation:

$$K = 0.0445M + 95.91 \tag{6.5}$$

Where: K – is the percentage increase in the longitudinal cross sectional area,

M – the percentage increase in capacity when compared to a plain pile.

With this information it is possible to predict the increase in the capacity of a ribbed piles using the increase in longitudinal cross sectional area to an accuracy of +/- 10%.

If this method were to be used to design a ribbed pile it is envisaged the design engineer would first conduct a standard plain pile calculation. A decision would then be made on what additional capacity is required. Equation 6.5 would then be used to calculate the additional cross sectional area required. A rib size and spacing could then be designed to suit the required increase in longitudinal cross sectional area. This would assume square ribs evenly spaced, since this is the range of geometries tested.

This method requires refinement since; a larger diameter plain pile, for example a 19mm diameter pile, will have an increase in cross sectional area of 118.75%. Analysis of test RJG11 suggested such a pile would have an increase in capacity of 127% when compared to a 16mm diameter pile. If this data point were plotted on Figure 6.11 it could be seen that Equation 6.5 does not apply. This is owing to the 19mm diameter pile being thought of as a 16mm diameter ribbed pile with effectively zero rib spacing. The point at which a ribbed pile becomes a plain pile with diameter equivalent to the outer rib diameter is not clear.

6.5.2 Detailed design method

The longitudinal sectional area method described in Section 6.5.1 is an empirical method for geotechnical design of ribbed piles. A more detailed design method would be required before ribbed piles could be justified for use in industry. Since the failure mechanisms of the differing rib styles are likely to be different, it has been decided to present a different design method for each rib type.

6.5.3 The theoretical capacity of a plain pile

In the first instance it was necessary to calculate the theoretical capacity of the plain pile in each test. This would allow for derivation of the adhesion factor which would be required in any ribbed pile design.

The theoretical ultimate capacity of a plain pile can be calculated using the following Equation:

$$Q_u = Q_s + Q_b - W \tag{6. 6}$$

Where: Q_u – ultimate loading capacity of the pile,

Q_s – ultimate skin friction,

Q_b – ultimate base resistance, and

W – pile self weight.

The undrained shear strength profile with depth varied for each test. For the purpose of theoretically calculating the capacity of the pile a best fit line was applied to the measured shear vane readings from each test. From this best fit line it was possible to estimate the undrained shear strength at any depth in any particular test.

6.5.3.1 End Bearing Capacity

The plastic failure envelope presented by Meyerhof (1951) shown in Figure 6.12 consists of 2 zones. Zone ABC remains elastic and acts as part of the foundation. Zone ACD is that of radial shear. The end bearing capacity of a piled foundation can therefore be calculated using the following Equation:

$$Q_b = A_b(N_c S_{u(base)} + \gamma L) \tag{6. 7}$$

Where: A_b – cross sectional area of the pile base,

$S_{u(base)}$ – undrained shear strength at the pile base,

N_c– bearing capacity factor,

γ – unit weight of the concrete

L - pile length.

Fleming (1992) suggested that linear interpolation should be made between N_c = 6 for the case of the pile just reaching the bearing stratum and up to N_c = 9 where the pile penetrates a stiff layer by three diameters or more. Since this study is concerned with piles installed in a single sample of soil, the bearing capacity factor for every test pile can be taken as 6.

Using the undrained shear strength profile obtained from the T-bar, where available, the shear vane readings and an N_c value of 6 it was possible to calculate the theoretical bearing capacity of the plain pile for every test.

6.5.3.2 Shear capacity

From the various failure analyses conducted for each test (detailed in Section 6.3) the ultimate failure load of every plain pile was identified. Using the ultimate failure load obtained from the theoretical base resistance of the plain pile and Equation 6.6 for each test; it was possible to back calculate the shaft capacity of the pile. The adhesion achieved by each plain pile could then also be calculated using Equation 6.8.

$$Q_s = A_s \alpha S_{u(avg)} \tag{6.8}$$

Where: Q_s – ultimate skin friction,

A_s – shaft area,

α - adhesion factor, and

S_u – average undrained shear strength of the clay along the pile shaft.

The value of α achieved in all tests varied from 0.67 to 1. This is within the expected range for the pile material and model preparation method. The back calculated alpha for each plain pile is shown in Table 6.2

6.5.4 Concentrically ribbed pile capacity

Traditional pile capacity calculations are categorised into two constitutive parts, namely the base resistance and shaft resistance. This is because these two components cause very different failure mechanisms within in the soil, and therefore generate the resistance in a different way. A similar approach has been adopted to allow for the design of ribbed pile foundations. Equation 6.6 can be rewritten to include the additional capacity generated by the pile ribs:

$$Q_u = \sum Q_s + Q_b + \sum Q_{rs} + \sum Q_{rb} - W \tag{6. 9}$$

Where: Q_u – ultimate loading capacity of the pile,

Q_s – ultimate skin friction along the plain shaft,

Q_b – ultimate base resistance,

Q_{rs} – ultimate skin friction along the rib shaft,

Q_{rb} – ultimate base resistance from each rib and,

W – pile self weight.

6.5.4.1 Base and shaft capacity of concentrically ribbed piles

For each of the concentrically ribbed piles the base resistance was calculated using the same method as for the base of a plain pile (described in section 6.5.3.1). The shaft capacity was calculated for the space between two consecutive ribs. However, the

average shear strength was calculated across the distance between each set of consecutive rib as opposed to the entire length of the pile. The adhesion factor used in this calculation was the same as that calculated for the plain pile in that test. The sum of these individual shaft capacities were then used, to give a total shaft capacity (Q_s).

6.5.4.2 Rib base and rib shaft capacity of concentrically ribbed piles

The plastic failure envelope of the rib base is likely to be similar to the Meyerhof (1951) plastic failure envelope. The proposed plastic failure envelope for a concentric pile rib is shown in Figure 6.13. An angle of 45 degrees has been used for the undrained plastic failure zone. The plug underneath each rib defined by the triangle ABC remains elastic and fails as part of the foundation. The existence of this intact plug of soil has been verified visually during deconstruction of each test. This small area must therefore not be included in the shaft shear capacity calculation. The area ACD is that of radial shear.

The rib shaft capacity for each rib was calculated using the standard method since the failure mechanism is likely to be the same as the shaft of a plain pile. The adhesion factor used was the same as that for the plain pile in the corresponding reference test and the outer rib diameter was taken as the clay pile shear interface.

An example calculation for the 15mm concentrically ribbed pile can be seen in Appendix A.

6.5.5 Helically ribbed pile capacity

Many of the principles outlined for concentrically ribbed pile capacity calculations (section 6.5.4) can be applied to helically ribbed piles. However, there are some fundamental differences which must be addressed by the framework.

Primarily the concentrically ribbed piles present an axisymmetric problem, however the helical piles cannot be thought of as axisymmetric or plane strain. Since the rib is continuous it is difficult to define a specific undrained shear strength value. For the purpose of design it is proposed to idealise the pile having been cut in half along its length and assume a full rib revolution is equivalent to two discreet ribs (each spanning half a revolution). This allows for the shear strength at the midpoint of each half revolution to be used. A similar technique can be applied to the pile shaft. With these small modifications the concentrically ribbed pile framework can be used, however a key difference not addressed by the concentrically ribbed pile framework is that of the helix angle. The helix angle is defined as the angle between any helix and a line perpendicular to the axis. This angle is what enables a helical rib to travel continuously

from the top to the bottom of the pile, and will vary as the helical rib spacing, or helix pitch, varies. In order to address this it is proposed to apply a helix angle factor to the rib base capacity. The boundary conditions for this factor must be 1 when the helix angle is 0° since this is equivalent to a concentric rib. The factor must also be 0 when the helix angle is 90° since this is parallel to the shaft and hence there can be no base resistance. Figure 6.14 shows the empirical fit for this curve, which can be defined by the following Equation:

$$\eta = -0.222 \ln \theta + 1 \tag{6. 10}$$

Where: η – Helix angle factor and,

θ – helix angle.

The data points on this curve were generated by back calculating the difference in test capacity and theoretical capacity. Using the helix angle factor in conjunction with the concentric rib analyses techniques Equation 6.9 becomes:

$$Q_u = \sum Q_s + Q_b + \sum Q_{rs} + \sum \eta Q_{rb} - W \tag{6. 11}$$

Where: Q_u – ultimate loading capacity of the pile,

Q_s – ultimate skin friction along the plain shaft,

Q_b – ultimate base resistance,

Q_{rs} – ultimate skin friction along the plain shaft,

η – Helix angle factor and,

Q_{rb} – ultimate base resistance from each rib and,

W – pile self weight.

This method was used to calculate the theoretical capacity, for each helical pile tested. The adhesion factor used in the calculation was the same as that for the plain pile in the same test.

6.5.6 Tapered and under reamed ribbed pile capacity

The tapered rib was designed to represent a wedge shaped pile; the philosophy behind this, as with a wedge, is to increase resistance as the embedment increases. The components of the end bearing, shaft friction and rib base capacities can all be calculated using the framework for concentric ribs as a basis, since in this respect both types of pile are identical. A variation is required to define the rib shaft capacity component since with tapered piles this is inclined, unlike the concentric ribs which

have a shaft profile parallel to the main pile shaft. The shear failure plane for this type of shaft cannot be parallel to the slope and instead must be parallel with the main shaft. For this reason the height of the rib shaft used for the rib shear capacity calculation is the rib height parallel to the shaft. This is illustrated in Figure 6.15. The difference between the theoretically calculated failure load and the actual failure load was +5.4% using this framework.

Test RJG22 compared a plain pile to that of a pile with concentric under reamed ribs with a 15mm spacing. As with the tapered pile, the components of end bearing, shaft friction and rib base capacities were calculated in the same manner as for concentrically ribbed piles. The rib shaft capacity component was taken to be the rib height parallel to the failure plane, as used for the tapered pile. The difference between the theoretically calculated failure load and the actual failure load was -3.3%.

6.6 Comparison of framework to actual test data

The various theoretical pile capacity calculation techniques described in Section 6.5 have been applied to every pile tested. Each pile has been surveyed and weighed post-test to confirm the physical properties. Allowances have been made in the theoretical calculations for imperfections to the pile where these existed. Table 6.3 summarises the theoretical capacity as calculated by the above methods. This has also been compared to the actual test capacity of the pile. An example calculation for the 15mm concentrically ribbed pile can be seen in Appendix A. The difference between the actual capacity and the theoretical capacity for concentrically ribbed piles within +/-8%. Similarly for helically ribbed piles the difference is within +/-5%. This is clear evidence that for the range of geometries tested in over-consolidated clay the framework set out in Section 6.5.2 is an effective solution for the theoretical calculation of ultimate capacity of a ribbed pile.

6.7 Structural capacity of pile rib

The addition of ribs has been shown to increase the ultimate capacity of a bored pile in the model scale, with a two part resin used as the construction material. However, if this rib is unable to withstand the forces imparted on to it at prototype scale the technique is of little use. The most likely mode is failure between a concrete rib and the pile shaft and is that of shear failure. The rib dimensions used in this project scale to 75mm square ribs at prototype scale. Assuming the pile is constructed from C40 concrete and the rib remains unreinforced, it can been shown that for the given dimensions the applied shear force is around a quarter of the available shear resistance, and hence well within acceptable limits.

6.8 Summary

The centrifuge model testing has enabled a clear understanding of the model behaviour. A good quality of data has been acquired from the series of tests in which various pile rib designs and spacing's have been tested. This has allowed for a better understanding of the ribbed pile performance when compared to that of a plain pile.

The results of the centrifuge tests have been compared and discussed and reasons for the behaviour of the ribbed piles have been justified. The tests conducted have shown that ribs of any nature will increase the piles ultimate bearing capacity.

In the tests undertaken it was observed that the capacity of a ribbed foundation can increase by as much as 57% when compared to a plain pile. Of all the rib designs and geometries tested the 10mm spaced helically ribbed pile proved to be the most effective.

A simple design method has been developed and tested against each successful test and this has shown that the increased capacity of a ribbed pile can be predicted to within +/- 10%. Possible plastic failure envelopes of the soil around the ribs have been proposed. Furthermore, a detailed design method has also been proposed and tested against every successful test. This has shown that the ribbed piles capacity can be calculated to within +/- 8%. Several new parameters were required to define this design method and these have been explained and justified. It is envisaged that the simple method first be used to decide on the geometric layout of the ribs. The detailed method can then be used to more accurately define the failure load of the ribbed pile taking into account the soil parameters.

7 Conclusions and recommendations for further work

7.1 Introduction

There are obvious advantages for increasing the capacity of a bored pile whilst minimising the spoil removed and therefore the concrete used in construction. This chapter concludes the research undertaken into the behaviour of bored ribbed piles subject to axial load, in overconsolidated clay, and the influence of ribs on the ultimate capacity of such a pile.

The work presented here was conducted to investigate the influence of various rib profiles and geometric arrangements on the ultimate capacity of a bored pile. If this novel pile enhancement technique is to be used by industry it is necessary to critically analyse the behaviour and then develop design methods based on this new understanding. It is worth noting however that an increase in ultimate pile capacity was observed for every type and arrangement of rib pile tested.

In this chapter the experimental approach is summarised and conclusions drawn. The implications and relevance of the conclusions are considered and recommendations for further work are made.

7.2 Experimental procedure

An extensive literature review concerning bored pile behaviour, bored pile load testing, pile load test analysis and modified pile behaviour has been conducted as part of this project. The use of shaft ribs to increase the capacity of a bored pile is not contested. However, the manner in which this additional capacity is generated and how it can be optimised is the primary objective of this research project.

A total of twenty three tests were conducted using the geotechnical centrifuge at City University London. In each test two piles 9m deep at prototype scale were tested, one of which was always a control or plain shafted pile. The first test, RJG0 was conducted using, pile cutting, and pile load apparatus developed and used by previous research projects (Witton-Daruris, 2008; and Qerimi, 2009). This initial test provided a valuable insight into how to optimise the testing procedure. Apparatus was then designed and manufactured to allow for the majority of the test setup to be conducted prior to testing. This resulted in the time from removal of the sample from the consolidation press to centrifuge spin up being less than one and a half hours. The apparatus consisted of a new two stage soil container (Section 4.3.1) to allow for swift model preparation. In addition to several rib profiling tools, toothed plates and spoil collection buckets (Section 4.3.2) to profile the shaft of a pile, and a servo motor controlled pile loading

system. The load was applied to the pile cap via a loading pin attached directly to the load cells.

Miniature pore pressure transducers were used to monitor the changes in pore water pressure during the pore pressure equalisation stage of the centrifuge flight. The displacement of each pile was measured by two independent LVDTs and the average reading was used for the analysis. The difference between the LVDT values was generally around 0.3-0.4mm this verifies that out of vertical loading was not significant and justifies the average values being used in the analysis conducted.

The centrifuge models were made form overconsolidated Speswhite kaolin clay prepared from slurry with 110% water content. Both piles were cut and cast at 1g, any negative effect of boring and casting on the lab floor has been minimised by keeping the duration of model preparation both short and consistent between tests. The loading apparatus was then attached and installed on the swing. The centrifuge was accelerated to 50g and the models were left to reach effective stress equilibrium prior to pile loading.

Of the twenty three tests conducted four tests are considered to be failures, owing to malfunction of the data logger, the centrifuge, loading apparatus or human error. The T-bar penetrometer developed as part of this project, had a varying success rate. On occasion the T-bar failed to penetrate the soil, owing to the drive gears slipping at high g. For the last four successful tests in the series the T-bar provided an unusual output. Upon investigation it became apparent that this may be due to the T-bar cross head being reinstalled in the incorrect orientation after a previous detachment. This could have resulted in an unbalanced strain on the gauges and perhaps explain the anomalous readings.

Four main types of rib were tested; concentric ribs, helical ribs, tapered ribs and under reamed ribs. A straight shafted pile with a diameter equal to the outer diameter of the ribs was also tested.

For every test the load on the ribbed pile was normalised against the load on the plain pile in the same test. This provided an insight into the behaviour of the pile throughout its working settlement range and not only at failure. The ultimate capacity of each test pile was calculated using several pile analysis techniques (Section 6.4). An average of these techniques was used to define the actual ultimate capacity of each test pile which could then be used for comparison.

An empirical relationship has been identified between the percentage increase in the piles cross sectional area and the percentage increase in ultimate capacity (Section 6.5.1). This relationship fits all of the tests conducted to within +/- 10%.

A detailed design method has been identified for concentrically ribbed piles which allows for the unlimited capacity of the ribbed pile to be predicted (Section 6.5.2). Modifications factors and procedures have been included to allow for design of helical, tapered and under reamed ribs. The design method has successfully predicted the ultimate capacity for every ribbed pile tested to with +/- 8%.

7.3 Conclusions

This project has focussed on the performance of ribbed bored piles and the influence of ribs on the ultimate capacity. The use of physical modelling techniques has provided clear insight into the effects of rib on the ultimate capacity of a bored pile in overconsolidated clay.

The behaviour observed in the centrifuge tests has been extremely consistent and therefore the following conclusions can be drawn:

- Any rib profile and geometry will provide some increase in ultimate capacity when compared to a plain pile.
- Helical ribs are by far the most efficient of all those tested.
- The most efficient spacing was that of 10mm or 62.5% of the piles diameter, for both helical and concentric ribs.
- Ribbed piles can, perform better than a pile with a diameter equivalent to the outer diameter of the ribs.
- The majority of the additional capacity is generated by the end bearing contribution of the ribs.

The greatest increase in ultimate capacity when compared to a plain pile was provided by the 10 mm spaced helically ribbed piles, which at failure carried a 55% greater load than the straight shafted pile in that test.

A plastic failure envelope for the base of the pile rib has been identified and is derived from that of the end bearing of a pile, proposed by Meyerhof (1951), Figure 6.12 & Figure 6.13. This plastic failure envelope assumes two failure zones. Namely, the elastic failure zone, and the radial shear failure zone.

This plastic failure envelope has been used to provide a design solution for the ultimate capacity of the concentrically ribbed pile. The design solution is simple and requires a summation of the constitutive contributions from each rib and from the base and shaft

of the pile (Section 6.5.4). A modification factor has been proposed (Γ) to allow for correction of the rib angle generated by the helix (Section 6.5.5). This correction factor allows the same design solution to be used for all helically ribbed piles. Under reamed and tapered ribbed piles can be designed by adjusting the dimensions of the rib base and rib shaft to be in plane with the failure mode (i.e. horizontal for the rib base capacity and vertical for the rib shaft capacity).

From the analyses conducted it can be said that the majority of the additional capacity is derived from the end bearing capacity of the ribs. Test RJG14 where only the bottom third of the pile was ribbed, suggests that it is more effective to provide ribs along the entire length of the shaft. Providing ribs only at the top would not be as effective as at the bottom since the undrained shear strength of the soil is greater at depth and hence will support more load.

Both the tapered and under reamed ribs provided a similar increase in capacity when compared to the plain pile in the same test (around 40%). The tapered rib can be described in section as that of an arrow pointing downward and the under reamed rib described as an arrow pointing upward. Since the rib end bearing component is developed perpendicular to the pile shaft and the rib shaft capacity developed parallel to the shaft, the design method for both rib profiles is the same (Section 6.5.6).

7.4 Limitations and implications of results

As with all modelling techniques, centrifuge modelling has some level of idealisation which may not be completely representative of prototype situations. The behaviour of soil is dependent on its stress state, stress history and permeability. For centrifuge modelling Speswhite Kaolin clay was used, primarily for its high permeability compared to other clays. The high permeability allows the time for model preparation and consolidation to be considerably reduced relative to prototype soils.

The piles were installed at 1g on the laboratory floor rather than a high g environment. At the time of pile installation the pore pressures in the sample were likely to be in suction as the sample had recently been removed from the consolidation press. This is clearly not representative of the prototype scale. Moreover, there were no attempts made to install the piles in flight and thus there is no way of quantifying the effect of 1g pile installation. However the effect of installation is not believed to be significant, primarily as all the tests were subject to the same phenomena and hence remain internally consistent. Secondly, the soil model post pile installation was subjected to a high gravity field for over two days allowing the soil immediately adjacent to the pile to consolidate around the pile. The resin used to cast the piles was also an idealisation. The adhesion between the resin and kaolin clay sample may not be representative of

the adhesion between concrete and London Clay, for example. However, every pile tested was subject to both of these idealisations and hence the test series remains internally consistent, although this poses some difficulty when making comparisons to prototype scale tests.

A piled foundation must perform both geotechnically and structurally. Throughout this research project some has been made to verify whether the pile ribs would fail structurally. The ribs cantilever away from the pile shaft and hence could buckle if the shear force imparted on them is greater than their structural capacity. Possible solutions to this would be to adjust the geometry of the ribs or to include some type of reinforcement. However for the tested geometry at prototype scale the shear force has been calculated to be within acceptable limits.

The tools developed for profiling the shaft are adequate and effective for this project and at this scale. However, at prototype scale the forces and costs involved would probably prohibit the entire shaft being profiled simultaneously. The Expanded tool profiled a short section of pile a time, it is envisaged that any prototype scale tool will operate in a similar manner. The constructability of a rib is highly dependent on the ground conditions. The soil will need sufficient stiffness to allow a rib to be cut without causing any local collapse of the soil. Piles which require installation under a Bentonite support slurry are unlikely to be able to be profiled.

The ribbed bored pile provides several benefits over a conventional bored pile. A smaller diameter and shallower piled foundation would translate to less spoil removal and less concrete use, resulting in a more environmentally friendly foundation, adding to the green credentials of any project. Furthermore, smaller diameter and shallower piled foundations will allow for installation in between other new or existing piles and perhaps even in low headroom applications.

The use of ribbed piles is a clear advancement in piling technology and provides another option to contractors and designer when building foundations for structures. For the technique to become widely used the tooling and machinery must be developed, and manufactured, such that the additional effort and cost required to install the pile ribs is sufficiently reduced in comparison to the cost of boring a deeper and or wider pile.

7.5 Recommendations for further research

Several of the pile rib types and spacings have been shown to have a higher capacity than a plain pile with a diameter equal to the outer rib diameter. It follows, that at some point the rib spacing will become so close that the pile fails as if it were a pile with no

ribs and simply of a diameter equal to the outer diameter of the ribs. This trend can be explored by successively reducing the rib spacing until such time that the increase in pile capacity begins to reduce.

The mechanisms of failure presented here fit well within the current theories and successfully predict the behaviour of a ribbed pile. However, these mechanisms can be confirmed with the use of Particle Image Velocimetry (PIV). Ribbed piles cut in half could be placed in a strongbox container with a Perspex observation window. The PIV would be capable of tracking the movement of soil particles around the pile ribs and would visually confirm the presented plastic failure envelope.

Whilst several rib type and rib geometry parameters have been investigated, no attempt has been made to vary the rib height and rib outstand. The influence of varying these dimensions should be explored. However, the outstand is likely to be limited by the ability of the concrete to resist the shear force adjacent to the pile shaft, and the rib height likely to be limited by the ability of the soil to stand unsupported at depth.

The structural integrity of the pile ribs at prototype scale has not been investigated. The force on the ribs especially at depth is likely to be significant, if the ribs were to fail structurally it is unlikely the ribbed pile would perform as expected. This could be investigated by conducting structural analysis or even finite element analysis based on the forces a rib is likely to experience at prototype scale. The structural implications will limit the distance a rib is able to protrude from the pile.

A programme of interface tests using resin blocks against over consolidated clay in a shear box, would provide valuable insight into the operation of the ribs, and help to further optimise parameters such as geometry and spacing. Furthermore, since the setup and test procedure is somewhat faster than that of a centrifuge tests, a significant number of experiments could be conducted in a short space of time.

The effect of 1g pile installation though not currently thought to be significant, remains unquantified. The development of a new centrifuge modelling technique whereby a pile could be installed in a high g environment would allow for better comparison with the prototype installation procedure. Owing to the complexity of installation for rotary bored piling this is probably unfeasible; the sample is also too soft to allow such a bore to be excavated. However, this may be possible for Continuous Flight Auger (CFA) piles. A test could be conducted where a single pile is installed at 1g and a second pile constructed at high g. The load settlement data could then be compared to quantify the influence of 1g pile installation.

A significant programme of field testing is required to support the theories presented here. This should also be correlated with numerical analyses to provide much needed additional data to enable predictions of ribbed pile ultimate capacities to be made with more confidence.

8 References

Able Piling. (2010). Atlas Screw Piles - The Green Pile. Available: http://www.ablepiling.co.uk. Last accessed 1 July 2010.

Al-Tabbaa, A. (1987). Permeability and stress-strain response of speswhite kaolin. PhD Thesis, University of Cambridge.

Al-Tabbaa, A. & Wood, D.M. (1987) Some measurements of the permeability of kaolin. Géotechnique 37, No.4, 499-503

Anderson, W.F., Yong, K.Y., Sulaiman, J.A. (1985). Shaft adhesion on bored and cast in situ piles. Proceedings of the 11th International Conference on Soil Mechanics and Foundation Engineering, San Francisco, pp 1333-1336.

Atkinson, J.H. (1993), An Introduction to the Mechanics of Soils and Foundations Through Critical State Soil Mechanics, McGraw-Hill International Series in Civil Engineering.

Avgherinos, P.J. and Schofield, A.N. (1969). Drawdown failures of centrifuged models. Proc. 7Th Int. Conf. Soil Mech. Found. Eng., Vol. 2, pp. 497-505

Azizi, F. (2007), Engineering Design in Geotechnics, School of Engineering, University of Plymouth.

Brinch Hansen, J. (1963). Discussion, “Hyperbolic stress-strain response. Cohesive soils”, ASCE, J. SMFO, Vol 89, SM4, pp. 241-242.

Brown, M.J., Hyde, A.F.L. & Anderson, W.F. (2006), Analysis of a rapid load test on an instrumented bored pile in clay, Géotechnique, Vol 56, No. 9 pp. 627-638.

BS1377, British Standard methods of test for soils for civil engineering purposes, (1990). British Stands Institution, BSI London.

BS8004, British Standard Code of Practice for Foundations, (1986). British Stands Institution, BSI Milton Keynes.

Burland, J.B., Butler, F.G. and Dunican, P. (1966) The behaviour and design of large diameter bored piles in stiff clay. Proceeding of the Symposium on Large Bored Piles. Institution of Civil Engineers, Reinforced Concrete Association, London, pp. 51-71

Burland, J.E. and R.W. Cooke (1974) The design of bored piles in stiff clays, Ground Engineering, 7(4): 28–30; 33–35.

Burland, J.B. (1973) Shaft friction of piles in clay – a simple fundamental approach, Ground Engineering, 6(3): 30–42

Burland J.B. & Twine D. (1988) "The shaft friction of bored piles in terms of effective strength", Proc. 1" Int. Geotech. Seminar on Deep Foundations on Bored & Auger Piles, Ghent, ed. Van Impe, Balkema. pp 411 - 420.

Chapman, T., Marsh, B. and Foster, A. (2001). Foundations for the future. ICE Civil Engineering, 144, No. 1, pp 36-41.

Chin, F.K., (1970). “Estimation of the ultimate load of piles not carried to failure”, Proceedings of the 2nd Southeast Asian Conference, on Soil Engineering., pp. 81-90.

Chin, F.K., (1971). Discussion, “Pile tests. Arkansas River project”, ASCE, J. SMFD, Vol. 97, SM6, pp. 930-932.

Chung, S. F., Randolph, M. F. & Schneider, J. A. (2006). Effect of penetration rate on penetrometer resistance in clay. J. Geotech. Geoenviron. Engng, ASCE 132. No. 9, 1188–1196.

Cooke, R.W. (1974), Pile foundations: A survey of research at the building research station. Building Research Establishment

Craig, W. H. (1995). Chapter 1 in Geotechnical centrifuges: past, present and future. Geotechnical centrifuge technology, Taylor, R. N. (Ed) Blackie Academic and Professional, Glasgow.

Davisson, M.T., (1972). “High capacity piles”, Proc. Lect. Series, Innovations in Foundation Construction, ASCE, Illinois Section, pp. 52.

De Beer, E.E., (1968) “Proefondervindelike bijdrage tot de studie van het grensdragg vermogen van zand onder funderingen op stall,” Tijdshrift der Openbar Werken can Belgie, Nos. 1,4,5,6.

Expanded Piling, (2002). “High Capacity Shear Technical Report”, Internal Report.

Federation of Piling Specialist, FPS (2006), “Handbook on Pile Load Testing”.

Fellenius, B.H. (1975), “Test loading of piles. Methods, interpretation and new proof testing procedure”, Proc. ASCE, Vol. 101, GT9, pp. 855-869.

Fellenius, B.H. (1980), “The analysis of results from routine pile load tests”, Ground Engineering, London, Vol. 13, No. 6, pp. 19-31.

Fellenius, B.H., (2001). The O-Cell – An innovative engineering tool. Geotechnical News Magazine, Vol. 19, No. 2 pp 32-33.

Fleming, W.G.K. (1992), A New Method for Single Pile Settlement Prediction and Analysis, Géotechnique, 42 No. 3, pp. 411-425.

Fleming, W.G.K, Weltman A.J, Randolph H.F, Elson W.K (1992), “Piling Engineering”, 2nd Edition, Blackie.

Fleming, W.G.K, Weltman A.J, Randolph H.F, Elson W.K (2009), “Piling Engineering”, 3rd Edition, Taylor and Francis, Abingdon.

Fuglsang, L.D. and Ovesen, N.K. (1988) The application of the theory of modelling to centrifuge studies. Centrifuges in Soil Mechanics. Eds. W.H. Craig, R.G. James and A.N. Schofield, Balkema, Rotterdam, pp. 11-138.

Fuller, F M. and Hoy, H. E. (1970) “Pile Load Tests Including Quick Load Test Method, Conventional Methods, and Interpretations,” Research Record 333, Highway Research Board, Washington, D.C., pp. 74-86.

Garnier, J. (2002). Properties of soil samples used in centrifuge models. Physical Modelling in Geotechnics: ICPMG ’02, Phillips, Guo & Popescu (eds.) 2002 Swets & Zeitlinges Lisse, ISBN 90 5809 389 1. pp 5-19.

Ground Engineering (2003, December) “Getting to grips with friction”. Ground Engineering. Magazine of the British Geotechnical Association.

Housel, W.S. (1966), Pile Load Capacity; Estimates and Test Results, Journal of the Soil Mechanics and Foundation Division, Proc. ASCE, Vol. 94, No. SM4, PP. 1-30.

Lehane, B.M., O'Loughlin, C.D., Gaudin, C., Randolph, M.F. 2009, 'Rate effects on penetrometer resistance in kaolin', Geotechnique, 59, 1, pp. 41-52.

Lyndon A., King G.J.W. & Dickin E.A. (1994) "The behaviour of continuous flight augured piles in soft clay" Conf. Piling & Deep Foundations, Bruges, Belgium, Vol. I, pp 5 -16.

Mayne PW and Kulhawy FH, (1982). K_0 – OCR Relationship in Soil, Proc ASCE J. Geotech Eng. Div. Vol 108 (GT6), June.

Mazurkiewicz, B.K., (1972). Test Loading of Piles according to Polish Regulations, Preliminary report No.35, Commission on Pile Research, Royal Swedish Academy of Eng. Sci, Stockholm.

McNamara, A.M. (2001) Influence of heave reducing piles on ground movements around excavations. PhD Theses, City University.

McNamara, A.M., Rettura, D., & Gorasia R.J., (2011) Press-In Engineering, Proceedings of 3rd International Workshop, Shanghai, pp 25-31.
Meyerhof, G. G., 1951. "The ultimate bearing capacity of foundations." Géotechnique, Vol. 2. pp. 301 332

Middendorp, P., (1993), First experiences with Statnamic load testing of foundation piles in Europe. Proc. 2nd Int. Geotech. Seminar on Deep Foundations on Bored and Auger Piles, Ghent, pp. 265-272.

Mikasa, M., Takada, N. and Yamada, K., (1969). Centrifuge model test of a rock fill dam. Proc. 7Th Int. Conf. Soil Mech. Found. Eng., Vol. 2, pp. 325-333.

Mohan, D, Jain, G.S, & Jain, M.P, (1967), A New Approach to Load Tests, Géotechnique, Vol. 17, pp. 274-283.

Musbahi, O., (2012), Experimental Investigation determining the undrained shear strength of Kaolin. MEng Dissertation, City University.

Ng, C.W.W., van Laak, P.A., Zhang, L.M., and Tang, W.H. (2002). Development of a four-axis robotic manipulator for centrifuge modelling at HKUST. Proc. Int. Conf. Physical Modelling in Geotechnics, St John's Newfoundland. Balkema, Lisse, The Netherlands, pp. 71–76.

Osterberg, J.O., (1998). The Osterberg load test method for bored and driven piles. The first ten years. Proc. 7th Int. Conf. Piling and Deep Foundations, Vienna, Austria, pp. 1.28.1 - 1.28.11.

Parry, R. H. G. and Swain, C. W. (1977). A study of skin friction on piles in stiff clay. Ground Engineering 10, No. 8, pp 33-37.

Patel, D.C. (1992). Interpretation of results of pile tests in London clay. Piling: European practice and worldwide trends. Thomas Telford, London.

Phillips, R. (1995). Chapter 3 in Geotechnical centrifuge technology, Blackie Academic & Professional, Taylor, R. N. (Ed) Glasgow, pp 34-59.

Pellew. A.L. (2002) Field Investigations into Pile behaviour in Clay. PhD Theses, Imperial College of Science Technology and Medicine.

Phillips, R. (1987). Ground deformation in the vicinity of trench heading. Cambridge University PhD thesis.

Qerimi. B.L. (2009) Geotechnical centrifuge model testing for pile foundation re-use. PhD Theses, City University.

Raju, V.S. and Gandhi, S.R. (1986) "How Should Data From Pile Load Tests be interpreted for Design of Piles?" Proceedings of Indian Geotechnical Conference-86, Delhi, Dec.1986, Vol.2, pp165-168.

Randolph, M. F., Carter, J.P. and Wroth, C.P. (1979). Driven piles in clay – the effect of installation and subsequent consolidation. Géotechnique 29, No.4, pp 361-393.

Randolph, M.F. & G.T. Houlsby, (1984), The limiting pressure on a circular pile loaded latterly in cohesive soil, Géotechnique, Vol 34, No. 4, pp. 613-623.

Rose. A.V. (2010) Modelling the performance of linear mini pile groups. Proc. 7th International Conference on Physical Modelling in Geotechnics. Taylor & Francis Group, London, UK, Vol. 2, pp. 891-896.

Schofield, A. N. and Taylor, R. N. (1988). Development of standard geotechnical centrifuge operations. Centrifuge 88, Ed Corte, Balkema, Rotterdam, pp 29-32.

Senghani, P.L., (2008), Finite Element Analysis of Enhanced Capacity Piled Foundations. MEng Dissertation, City University.

Skanska Cementation (n.d), “Large Diameter Bored Piles”, Company services brochure.

Skempton A.W. (1959) "Cast in-situ bored piles in London Clay", Géotechnique, 9, pp 153 - 173.

Springman, S. M. (1989). Lateral loading on piles due to simulated embankment construction. Cambridge University PhD thesis.

Stallebrass, S. E. and Taylor, R. N. (1997). The development and evaluation of a constitutive model for the prediction of ground movements in overconsolidated clay. Géotechnique 47, No. 2, pp 235-253.

Steward, D. I. (1989). Groundwater effects on in-situ walls in stiff clay. PhD Thesis, University of Cambridge.

Stewart D.P., and Randolph M.F., (1991) A new site investigation tool for the centrifuge. Proc. Centrifuge ‘91, Ko (Ed.), Balkema, Rotterdam.

Suckling, T. (2007, January) “Back to the bottom”. New Civil Engineer. Magazine of the Institution of Civil Engineers.

Taylor R.N. (1995), Centrifuges in Modelling: Principles and Scale Effects, Geotechnical Centrifuge Technology, Blackie Academic & professional, Taylor R.N. (Ed), Glasgow, pp 19-33.

Ter-Stepanian, G.I. & Goldsteen, M.N., (1969). Multi-storied landslides and strength of soft clays. Proc. 7Th Int. Conf. Soil Mech. Found. Eng., Vol. 2, pp. 693-700.

Tomlinson, M.J. (1977), Pile Design and Construction Practice, Viewpoint Publication, Cement and Concrete Association.

Tomlinson, M.J. and Woodward, J. (2007), Pile Design and Construction Practice, 5th edition, Taylor & Francis Group, Oxfordshire.

Unwin, H. and Jessep, R.A. (2004), Long-tern pile testing on London Clay: a case study, Proc. Inst Civ. Engrs, Ground Engineering No. 157, Vol. 2, pp.57-63.

Weltman, A.J. and Healy P.R. (1978), “Piling in Boulder Clay and other Glacial Tills”, CIRIA Report PG5.

Whitaker, T., (1957), “Experiments with model pile groups”, Géotechnique, Vol. 7, pp. 147-167.

Whitaker, T., (1963),The constant rate of penetration test for the determination of the ultimate bearing capacity of a pile. Proc. Inst Civ. Engrs, No. 26 (Sept.), pp. 119-123

Whitaker, T., and R.W. Cooke. (1961), “A new approach to pile testing.” Proc. 5th Int. Conf. Soil Mech.

Whitaker T. & Cooke R.W. (1966) "An investigation of the shaft and base resistance of large bored piles in London Clay" Symp. on Large Bored Piles, ICE, pp 7 - 49.

Witton-Daruris, J. (2008). Behaviour of high shear capacity ribbed pile foundations in stiff clay, PhD transfer report, City University, London.

Wood, D.M, (2004). “Geotechnical Modelling”, Spoon Press, Taylor & Francis Group, Oxfordshire.

Wroth, C. P. (1984). The interpretation of in situ soil tests. 24th Rankine Lecture. Géotechnique 34, No. 4, pp. 449 489.

Wroth, C. P., Carter, J. P. and Randolph, M. F. (1980). Stress changes around a pile driven into cohesive soil. In recent developments in design and construction of piles, pp. 345-354. London: Institution of Civil Engineers.

9 Tables

Case	Soil Condition	Drainage condition	Type of analysis
1	Heavily over-consolidated clay, hence pile installation generates negative excess pore water pressure, causing the effective stress in the vicinity of the pile to increase. Therefore the least favorable condition is in the long term when the excess negative pour water pressure has dissipated	Drained	Effective stress
2	Normally consolidated clay, hence positive pore water pressure is generated, leading to a decrease in effective stress around the pile immediately after installation.	Undrained	Total stress
3	Lightly over-consolidated and pile installation generates small excess pore water pressure. The critical soil resistance may occur in either the short or long term. Therefore both conditions should be checked, to see which is less favorable.	Drained & undrained	Total and effective stress
4	Multi-layered clay, whereby the top layer is still undergoing a process of consolidation. This implies an excess pore water pressure exists in the top layer of soil. Any additional pore water pressure generated by pile installation is likely to induce differential consolidation settlement between the pile and top layer of clay. This generates a downward force on the pile and is known as negative skin friction.	Drained	Effective stress

Table 2.1 Pile design method for various soil conditions and drainage conditions after Azizi (2007)

Quantity	Scale Factor
Length	1/N
Mass density	1
Acceleration	N
Stiffness	1
Stress	1
Force/unit length	1/N
Strain	1
Displacement	1/N
Permeability (Darcy's	N
Time (diffusion)	$1/N^2$

Table 3.1 Centrifuge scaling laws after Wood (2004)

Mix	Ratio (by mass)	Ratio (g)	Filler type	Mass (g)	Vol (ml)	Density (kg/m^3)	Pot life
A	1:1:0.75	12:12:9	Al_2O_3	7.46	6.95	1073.4	2:30
B	1:1:0.75	12:12:9	$Al(OH)_3$	10.33	7.56	1366.4	2:30
C	1:1:1	12:12:12	Al_2O_3	7.47	7	1067.1	3:00
D	1:1:1	12:12:12	$Al(OH)_3$	10.78	7.18	1501.4	2:45
E	1:1:0.5	12:12:6	$Al(OH)_3$	10.18	8.14	1250.6	2:10
F	1:1:2	12:12:24	$Al(OH)_3$	12.74	8.15	1563.2	4:00
G	1:1:3	12:12:36	$Al(OH)_3$	27.81	15.7	1765.2	3:30

Table 4.1 Summary of tests conducted on various resin and filler mixers.

Operation	Control	Time	Time since
Begin mixing of		Day 0	
Pour slurry		10:00 – Day 1	
Increase to 5kPa	Manual	11:00 – Day1	1 hrs
Increase to 10kPa	Manual	14:00 – Day 1	3 hrs
Increase to 15kPa	Manual	17:00 – Day 1	3 hrs
Increase to 20kPa	Manual	09:00 – Day 2	16 hrs
Increase to 25kPa	Manual	10:00 – Day 2	1 hrs
Increase to	Computer	12:00 – Day 2	2 hrs
Increase to	Computer	17:00 – Day 2	5 hrs
Increase to	Computer	09:00 – Day 3	16 hrs
Swell to 250kPa	Computer	09:00 – Day 9	6 days
Remove from		09:00 – Day 10	24 hrs

Table 4.2 Soil model consolidation loading schedule

Test reference	Test date	Pile 1 details	Pile 2 details	Method used to seal clay	T-bar Status	Average shear vane S_u (kPa)	Filler type	Comments
Test 0	11/11/2009	10mm concentric ribs	16mm plain pile	Silicon oil	Not used	Not conducted	Aluminium Oxide Al_2O_3	Preliminary test conducted using existing pile loading and cutting equipment. Water bottles used to load piles.
RJG1	09/11/2010	10mm concentric ribs	16mm plain pile	Silicon oil	Not used	Not conducted	Aluminium Oxide Al_2O_3	First test with new soil container, pile cutting and loading apparatus. Test failed owing to blocked base drain from slurry leakage during consolidation.
RJG2	24/11/2010	10mm concentric ribs	16mm plain pile	Silicon oil	OK	Not conducted	Aluminium Oxide Al_2O_3	Successful test, leak developed from lowest PPT port. Centrifuge stopped twice, to deal with leak. Problem remedied with grease, split washer and glue.
RJG3	08/12/2010	10mm concentric ribs	16mm plain pile	Silicon oil	OK	58.21	Aluminium Oxide Al_2O_3	Successful test, in feed for standpipe not adjusted correctly causing excessive water from standpipe overflow.
RJG4	18/01/2011	15mm concentric ribs	16mm plain pile	PlastiDip	OK	52.33	Aluminium Oxide Al_2O_3	Successful test.
RJG5	01/02/2011	16mm plain pile	16mm plain pile	PlastiDip	OK	47.45	Aluminium Oxide Al_2O_3	Successful test, however it was observed that the driving pins had made contact with the pile caps, likely during soil swelling during pore pressure equalisation.
RJG6	16/02/2011	16mm plain pile	16mm plain pile	PlastiDip	OK	55.75	Aluminium Oxide Al_2O_3	Successful test.
RJG7	08/03/2011	15mm concentric ribs	16mm plain pile	PlastiDip	OK	48.29	Aluminium Oxide Al_2O_3	Successful test, leak developed from lowest PPT port. Centrifuge stopped, faulty dowty washer was repaired. Once standard test was complete, piles were unloaded and reloaded.
RJG8	22/03/2011	10mm helical ribs	16mm plain pile	PlastiDip	OK	50.48	Aluminium Oxide Al_2O_3	Successful test.
RJG9	12/04/2011	10mm helical ribs	16mm plain pile	PlastiDip	FAILED	46.27	Aluminium Oxide Al_2O_3	Successful test. T-bar not responding to commands from motor controller.
RJG10	17/05/2011	20mm concentric ribs	16mm plain pile	PlastiDip	FAILED	50.98	Aluminium Trihydrate $Al(OH)_3$	Successful test. T-bar (axis 1) motor not responding. Data logger crash during centrifuge spin up. New resin filler.
RJG11	21/06/2011	19mm plain pile	16mm plain pile	PlastiDip	FAILED	54.34	Aluminium Trihydrate $Al(OH)_3$	Successful test. Centrifuge stopped to investigate possible leak, none found. T bar failed at high-g, though shown to function and 1-g before test.
RJG12	05/07/2011	40mm concentric ribs	16mm plain pile	PlastiDip	FAILED	Not conducted	Aluminium Trihydrate $Al(OH)_3$	Test failed owing to incorrect gain setting on load cell channels resulting in no output from load cells.
RJG13	19/07/2011	40mm concentric ribs	16mm plain pile	PlastiDip	OK	47.28	Aluminium Trihydrate $Al(OH)_3$	Successful test. Consolidation pressure reduced to 300kPa from 500kPa over weekend. Pressure reinstated early on Monday, PPT's installed Monday PM.
RJG14	09/08/2011	10mm concentric ribs along bottom 3rd of pile	16mm plain pile	PlastiDip	OK	50.81	Aluminium Trihydrate $Al(OH)_3$	Successful test.
RJG15	24/08/2011	15mm tapered ribs	16mm plain pile	PlastiDip	OK	45.76	Aluminium Trihydrate $Al(OH)_3$	Successful test.
RJG16	13/09/2011	20mm helical ribs	16mm plain pile	PlastiDip	OK	48.96	Aluminium Trihydrate $Al(OH)_3$	Successful test.
RJG17	02/09/2011	30mm helical ribs	16mm plain pile	PlastiDip	Unusual output	43.24	Aluminium Trihydrate $Al(OH)_3$	Successful test. Centrifuge stopped to investigate leak. Remedied with new split washer. T-bar output significantly higher than usual. Instrument recalibrated and channel gain verified. No significant difference observed.
RJG18	12/10/2011	15mm tapered ribs	16mm plain pile	PlastiDip	Not used	Not conducted	Aluminium Trihydrate $Al(OH)_3$	Test failed owing to a fault with the data logger resulting in no recordable output from instrumentation.
RJG19	22/11/2011	15mm tapered ribs	Plain pile	PlastiDip	Unusual output	51.48	Aluminium Trihydrate $Al(OH)_3$	Successful test. Centrifuge stopped to investigate low pressure in standpipe. T-bar output significantly higher than usual. Instrument recalibrated and channel gain verified. No significant difference observed.
RJG20	01/02/2012	Pile not constructed	Pile not constructed	PlastiDip	Test Failed	Test Failed	Test Failed	Test aborted after consolidation as centrifuge data logger was out of commission
RJG21	24/07/2012	40mm concentric ribs	Plain pile	PlastiDip	Unusual output	35.75	Aluminium Trihydrate $Al(OH)_3$	Successful test. First test with new National Instruments data logger
RJG22	09/08/2012	15mm Under ream ribs	Plain pile	PlastiDip	Unusual output	37.25	Aluminium Trihydrate $Al(OH)_3$	Successful test.

Table 5.1 Summary of all centrifuge tests

Test ID:	Pile #:	Pile Type:	Pile Description	Chin (1980)	BS8004:1986	Fuller & Hoy (1980)	Hansen (1963)	Average	Model Scale (kN)	% Capacity Increase
22	1	Con. Ribbed	O:1.5,H:5,S:15 Under reamed	596.73	532.44	546.94	546.94	555.76	1389.40	
22	2	Straight	L:180	400.48	408.66	378.55	391.22	394.73	986.82	1.41
21	1	Con. Ribbed	O:1.5,H:1.5,S:40	470.34	424.16	444.41	429.78	442.17	1105.43	
21	2	Straight	L:180	405.15	397.22	386.09	398.76	396.81	992.01	1.11
17	1	Helically Ribbed	O:1.5,H:1.5,S:30	526.36	496.97	499.77	500.02	505.78	1264.45	
17	2	Straight	L:180	458.58	485.74	445.07	497.93	471.83	1179.58	1.07
16	1	Helically Ribbed	O:1.5,H:1.5,S:20	624.36	561.59	567.69	561.21	578.71	1446.78	
16	2	Straight	L:180	455.87	483.18	440.84	479.97	464.96	1162.41	1.24
15	1	Con. Ribbed	O:1.5,H:5,S:15 TAPERED	525.43	505.37	501.27	497.42	507.37	1268.43	
15	2	Straight	L:180	344.71	359.34	352.60	388.98	361.41	903.52	1.40
14	1	Con. Ribbed	O:1.5,H:1.5,S:10 (BTM 3rd)	443.34	401.32	410.69	404.53	414.97	1037.42	
14	2	Straight	L:180	388.68	415.56	372.06	427.77	401.02	1002.55	1.03
13	1	Con. Ribbed	O:1.5,H:1.5,S:40	522.63	449.22	485.33	451.08	477.07	1192.67	
13	2	Straight	L:180	401.35	419.03	390.34	440.10	412.71	1031.77	1.16
11	1	Straight	19mm dia L:180	612.82	545.98	544.99	551.34	563.78	1409.46	
11	2	Straight	L:180	469.82	436.61	422.89	441.35	442.67	1106.67	1.27
10	1	Con. Ribbed	O:1.5,H:1.5,S:20	513.68	458.68	485.46	474.75	483.14	1207.85	
10	2	Straight	L:180	382.67	417.28	382.49	432.87	403.83	1009.56	1.20
9	1	Helically Ribbed	O:1.5,H:1.5,S:10	705.11	547.93	586.65	591.40	607.77	1519.43	
9	2	Straight	L:180	382.55	405.15	372.26	404.39	391.09	977.72	1.55
8	1	Helically Ribbed	O:1.5,H:1.5,S:10	585.89	501.38	538.57	544.46	542.57	1356.44	
8	2	Straight	L:180	347.01	344.24	343.47	351.53	346.56	866.41	1.57
7	1	Con. Ribbed	O:1.5,H:1.5,S:15	564.65	467.47	509.70	507.53	512.34	1280.85	
7	2	Straight	L:180	388.88	388.15	374.69	356.74	377.11	942.78	1.36
6	*1*	*Straight*	*L:180*	*427.54*	*443.93*	*415.21*	*444.57*	*432.81*	*1082.03*	
6	*2*	*Straight*	*L:180*	*506.62*	*477.20*	*446.87*	*476.43*	*476.78*	*1191.95*	*0.91*
5	*1*	*Straight*	*L:180*	*241.16*	*272.75*	*237.48*	*304.29*	*263.92*	*659.80*	
5	*2*	*Straight*	*L:180*	*229.85*	*251.33*	*221.13*	*262.34*	*241.16*	*602.91*	*1.09*
4	1	Con. Ribbed	O:1.5,H:1.5,S:15	653.23	559.61	592.12	592.12	599.27	1498.17	
4	2	Straight	L:180	469.25	459.58	449.57	469.07	461.87	1154.66	1.30
3	1	Con. Ribbed	O:1.5,H:1.5,S:10	967.48	845.00	823.29	844.75	870.13	2175.32	
3	2	Straight	L:180	629.30	608.94	615.35	632.16	621.44	1553.60	1.40
2	1	Con. Ribbed	O:1.5,H:1.5,S:10	338.76	334.93	325.75	334.93	333.59	833.98	
2	2	Straight	L:180	234.68	249.63	238.41	324.26	261.74	654.36	1.27

* Where O is the rib outstand, H is the rib height, and S is the rib spacing

Table 6.1 Results of test pile failure analysis for all piles tested.

Test ID	Test type	Rib spacing	Alpha
RJG3	Concentric	10	1
RJG4	Concentric	15	0.9
RJG7	Concentric	15	0.78
RJG8	Helical	10	0.67
RJG9	Helical	10	0.89
RJG10	Concentric	20	0.77
RJG13	Concentric	40	0.95
RJG14	Concentric - Bottom 3rd	10	0.78
RJG15	Tapered	15	1
RJG16	Helical	20	0.96
RJG17	Helical	30	1
RJG21	Concentric	40	0.92
RJG22	Under reamed	15	0.94

Table 6.2 Back calculated alpha for plain piles

Test No	Test Type		Q_b	ΣQ_{rb}	ΣQ_s	ΣQ_{rs}	Theoretical Capacity	Test Capacity	Percentage difference
	Rib Type	Spacing							
14	Btm 3rd Con	10mm	186.77	329.26	561.05	46.25	1123.33	1037.42	7.65
3	Concentric	10mm	184.21	1038.96	850.53	187.91	2261.60	2175.32	3.81
4	Concentric	15mm	178.57	468.01	753.10	76.06	1475.74	1498.17	-1.52
7	Concentric	15mm	168.25	533.19	597.31	75.73	1374.48	1280.85	6.81
10	Concentric	20mm	165.41	333.14	693.93	41.80	1234.27	1207.85	2.14
13	Concentric	40mm	164.46	214.71	786.35	38.82	1204.35	1192.67	0.97
21	Concentric	40mm	169.61	183.19	800.93	41.94	1195.67	1105.43	7.55
8	Helical	10mm	176.97	543.39	570.87	72.77	1364.00	1320.34	3.20
9	Helical	10mm	167.05	494.37	679.90	173.24	1514.55	1519.43	-0.32
16	Helical	20mm	161.95	187.27	1066.68	101.25	1517.16	1446.78	4.64
17	Helical	30mm	147.12	79.53	1155.36	93.58	1475.59	1446.78	1.95
15	Tapered	20mm	151.75	422.25	594.90	209.05	1377.95	1268.43	7.95
22	Under Reamed	20mm	143.78	391.94	546.34	263.51	1345.56	1389.40	-3.26

Table 6.3 Summary of theoretically calculated and test rib pile capacity.

10 Figures

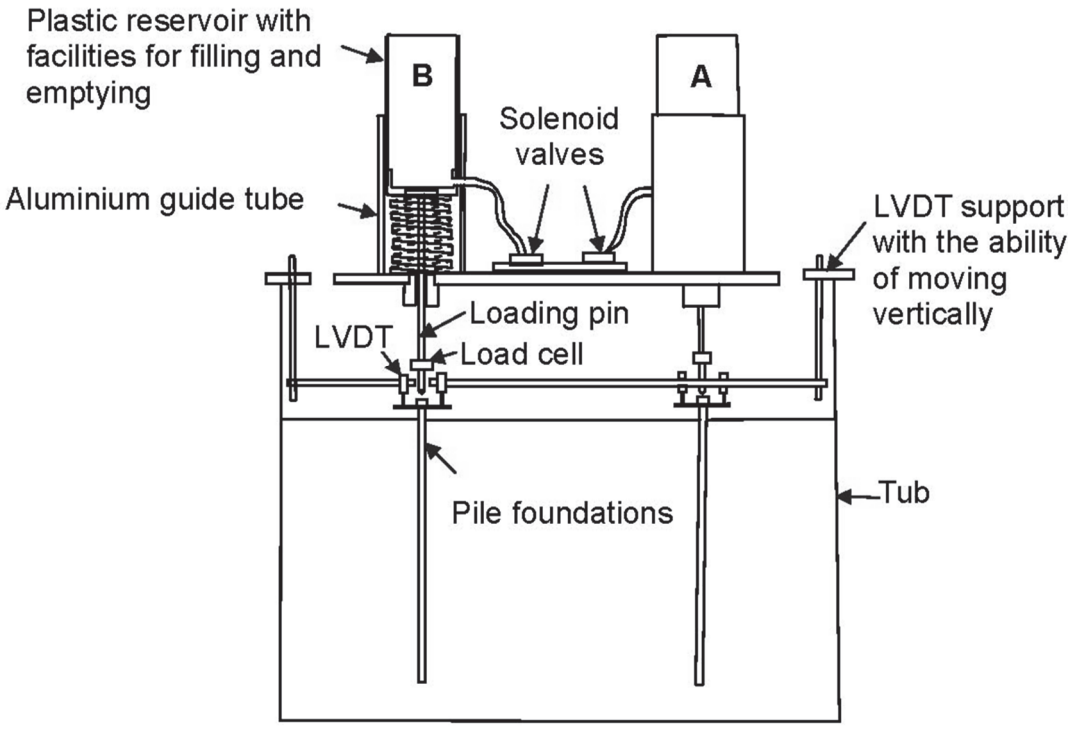

Figure 1.1 Previous pile loading apparatus.

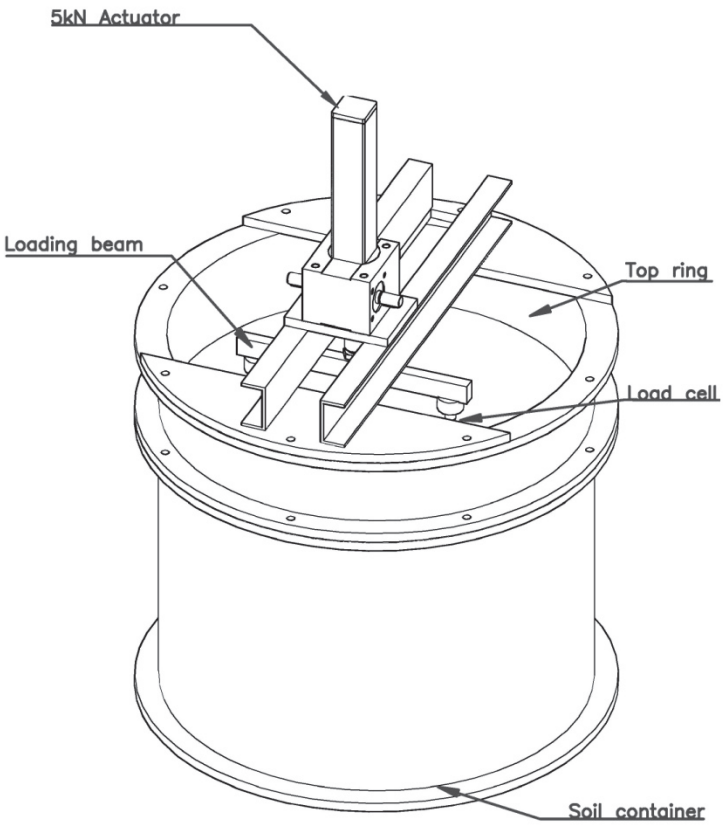

Figure 1.2 New pile loading apparatus.

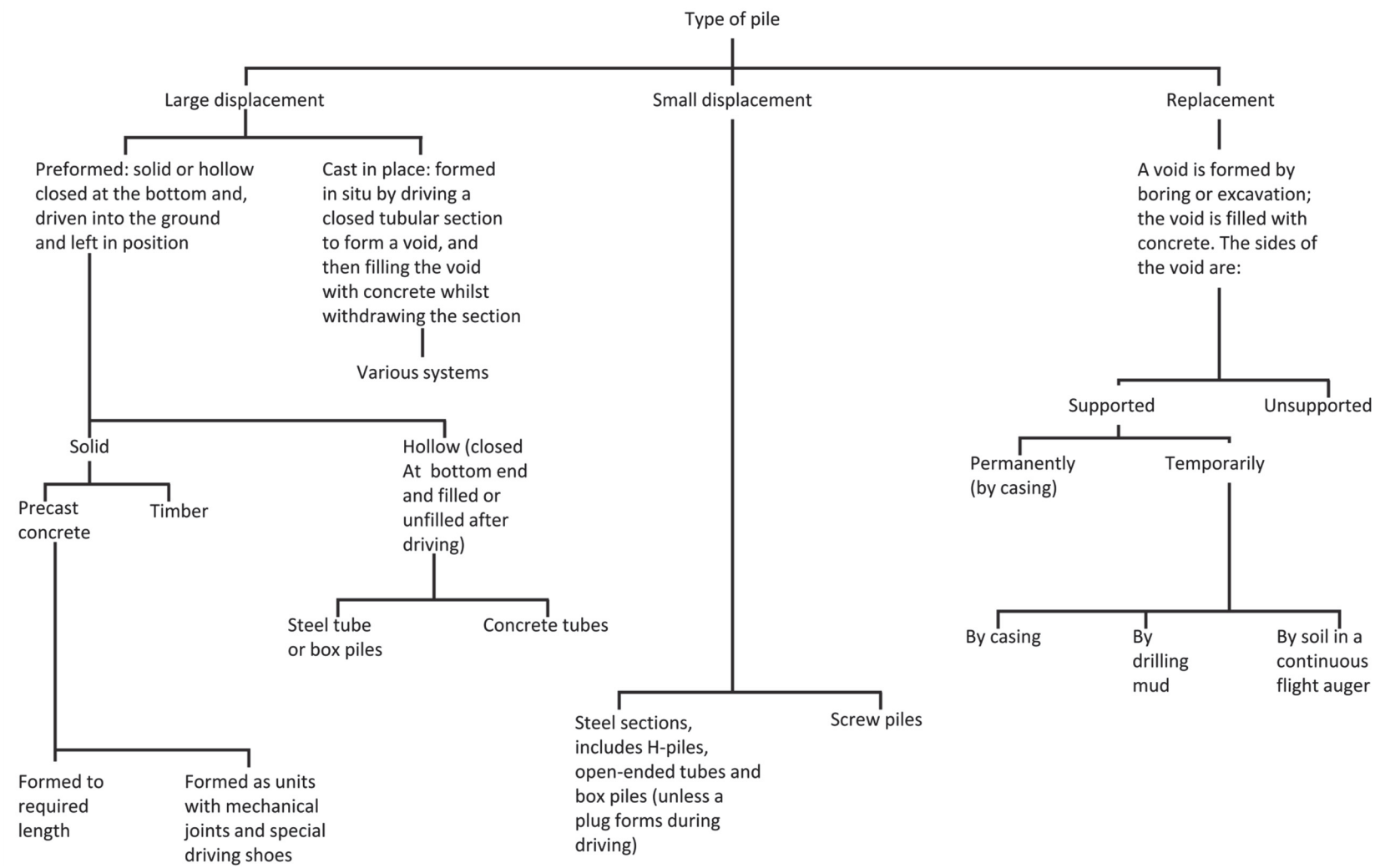

Figure 2.1 Summary of pile type (after BS8004:1986).

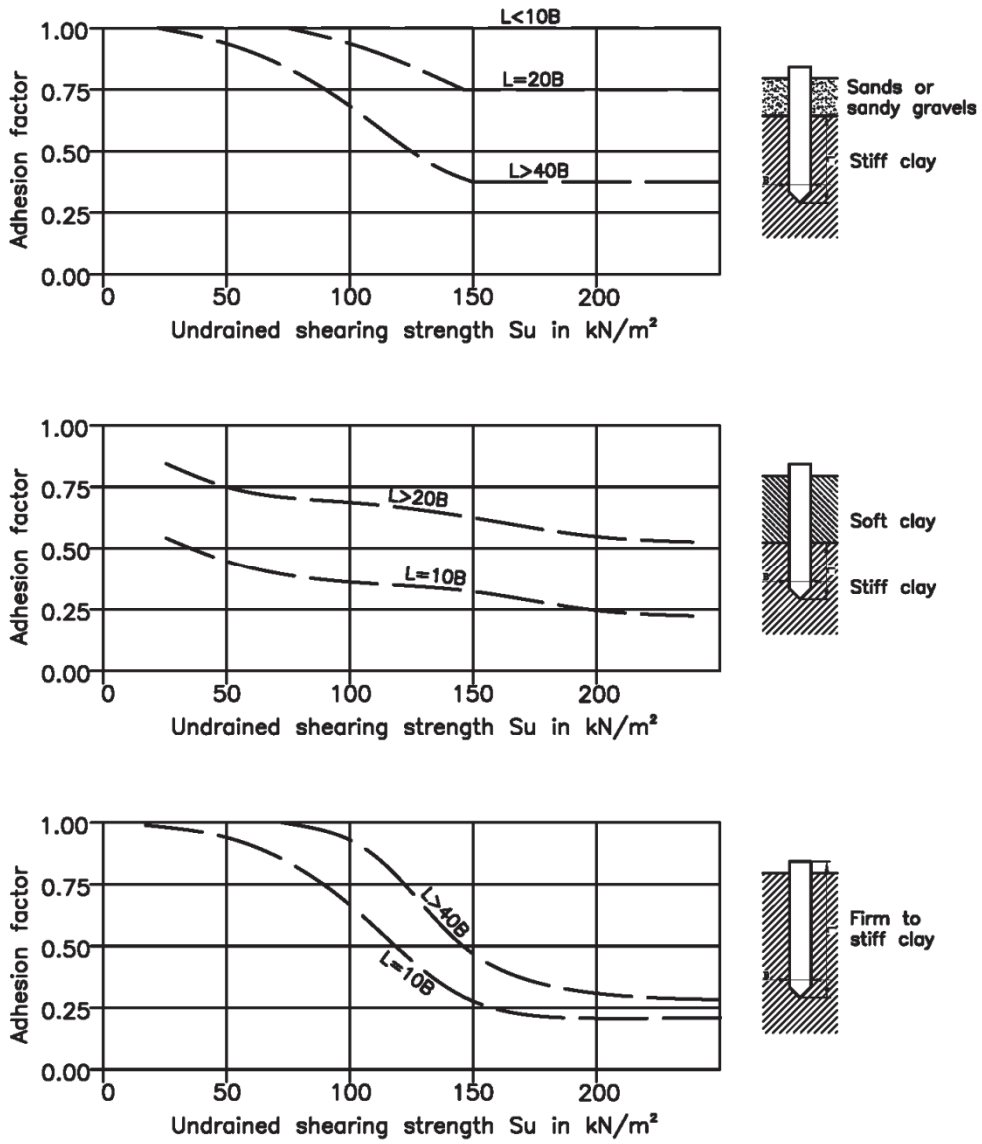

Figure 2.2 Adhesion factors for driven piles, after Tomlinson (1977).

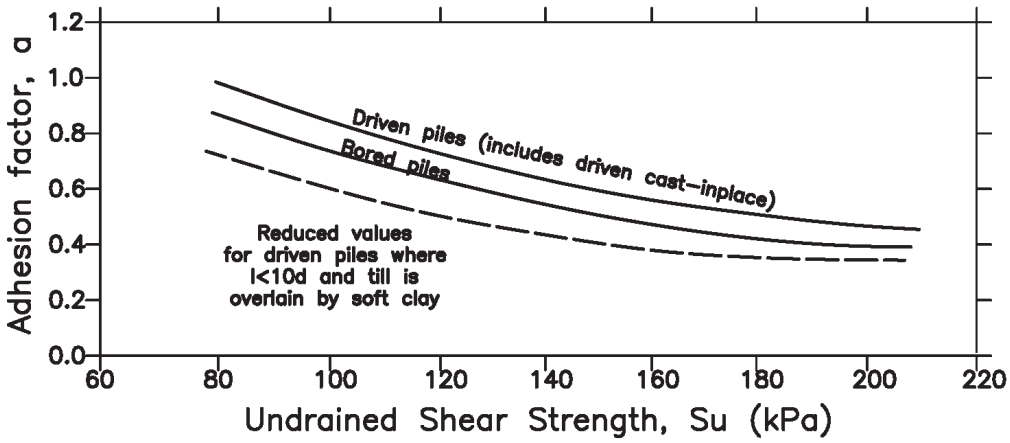

Figure 2.3 Adhesion factor for clay tills after Weltman and Healy (1973).

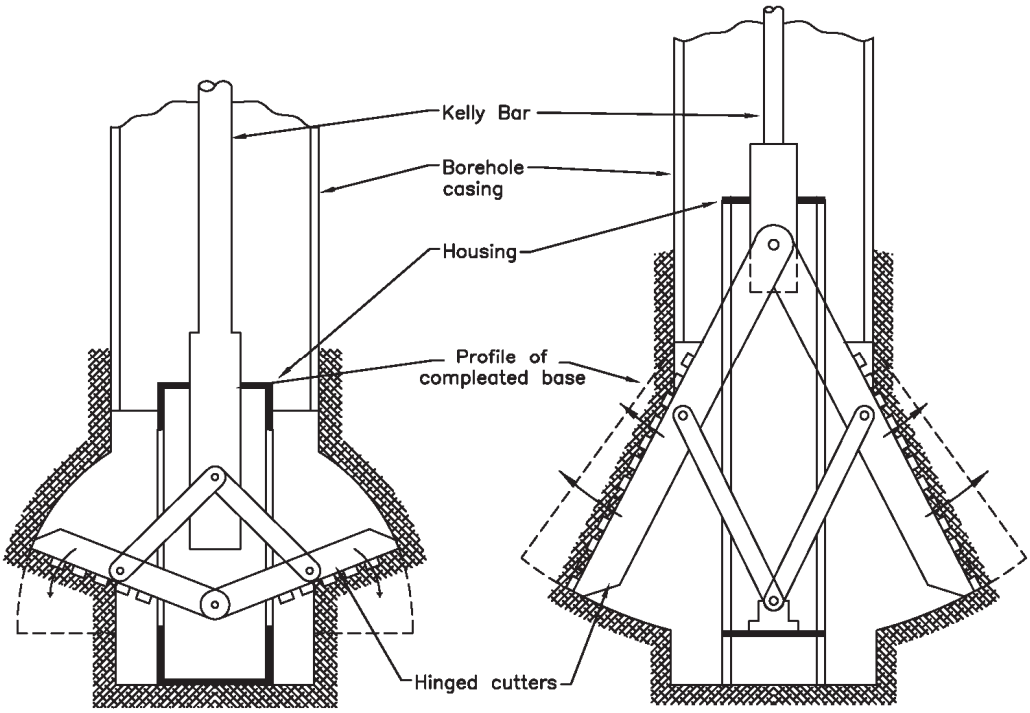

Figure 2.4 Schematic diagram of under reaming tool after Tomlinson (1977).

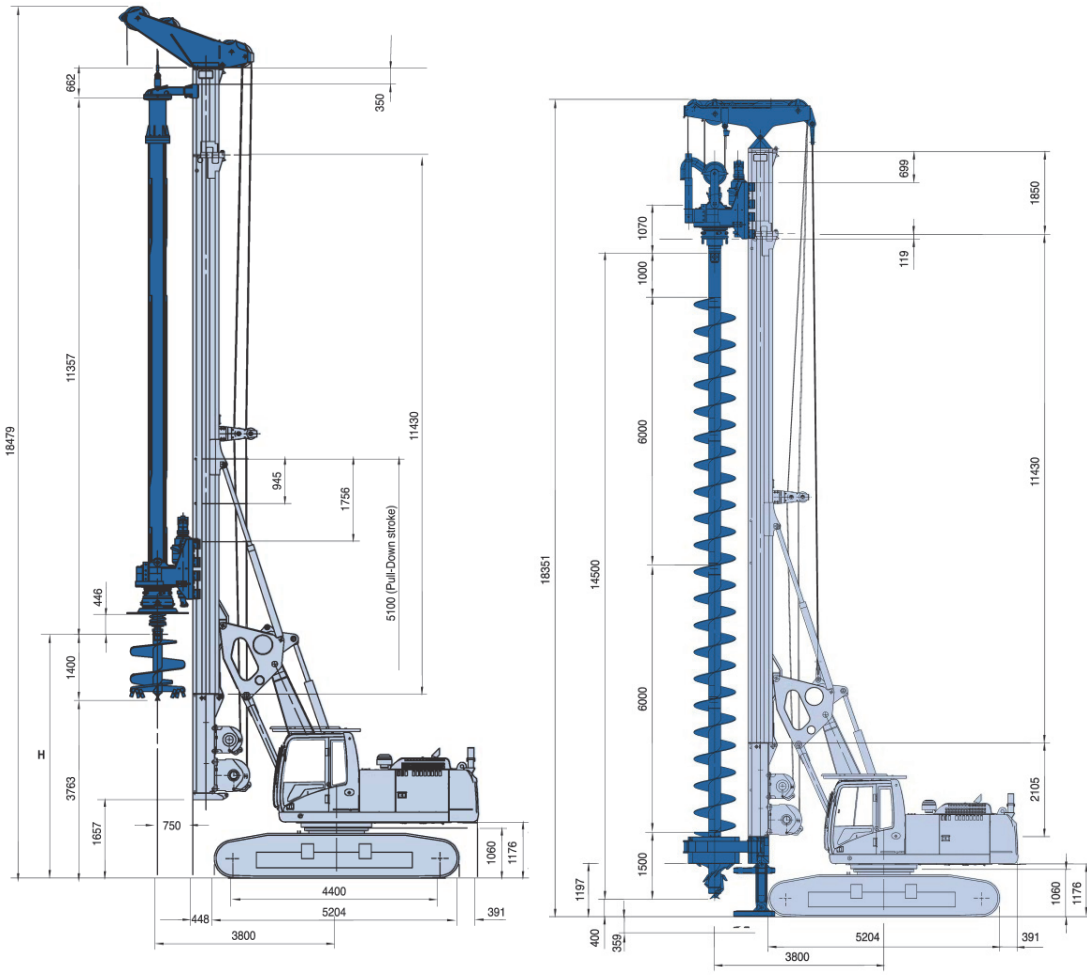

Figure 2.5 Soilmec SR40 CFA and rotary piling rig (courtesy of soilmec.com).

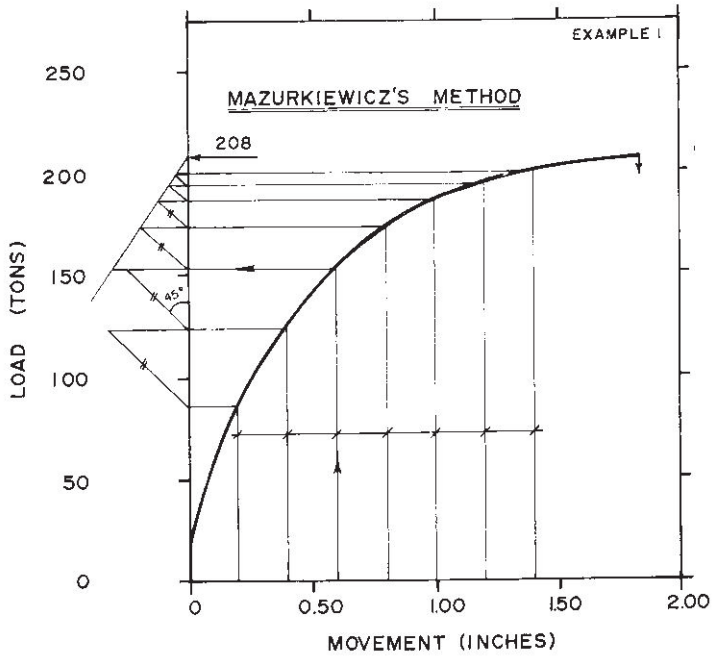

Figure 2.6 Pile ultimate failure according to Maxurkiewicz after Fellenius (1980).

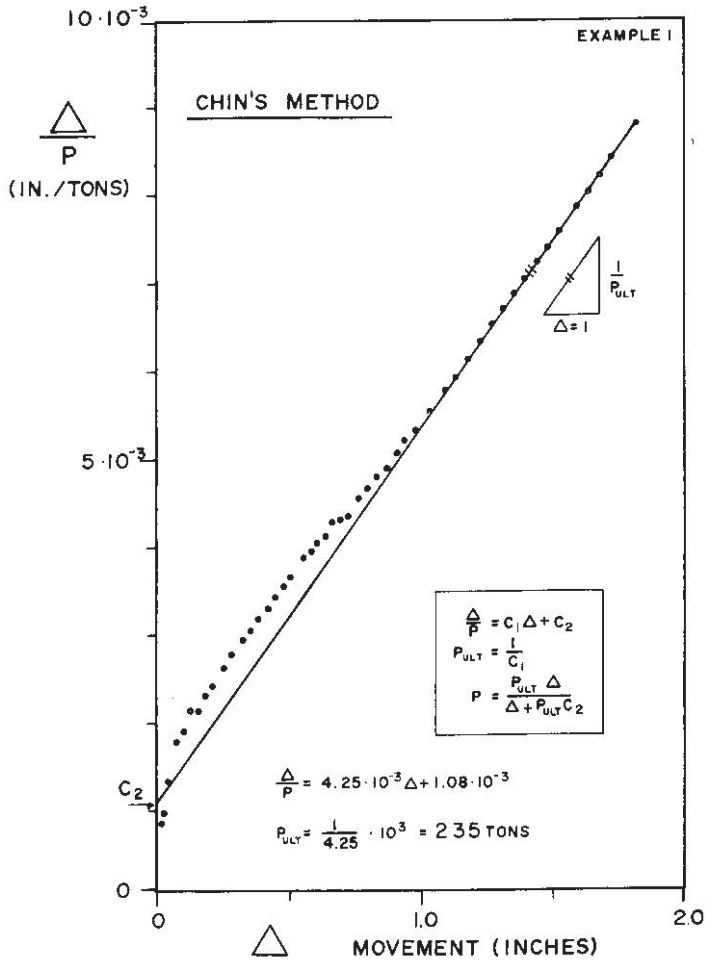

Figure 2.7 Pile ultimate failure according to Chin after Fellenius (1980).

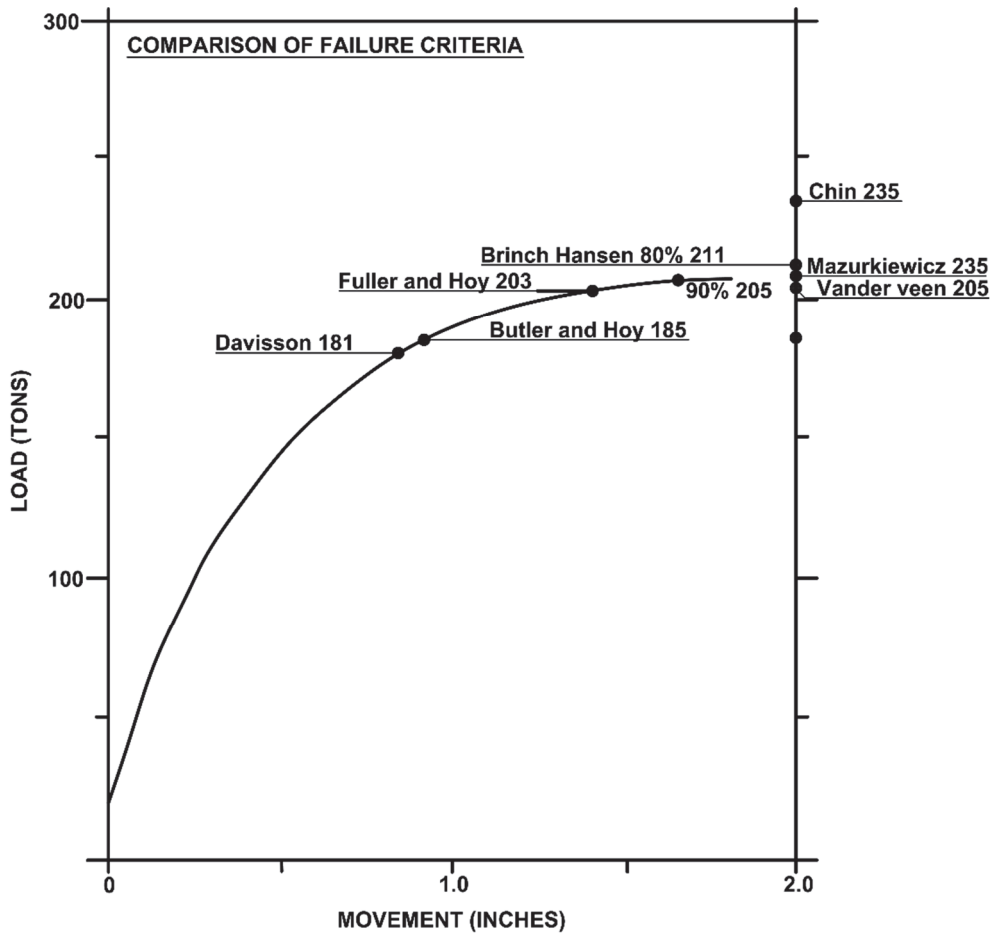

Figure 2.8 Comparison of nine failure criteria after Fellenius (1980)

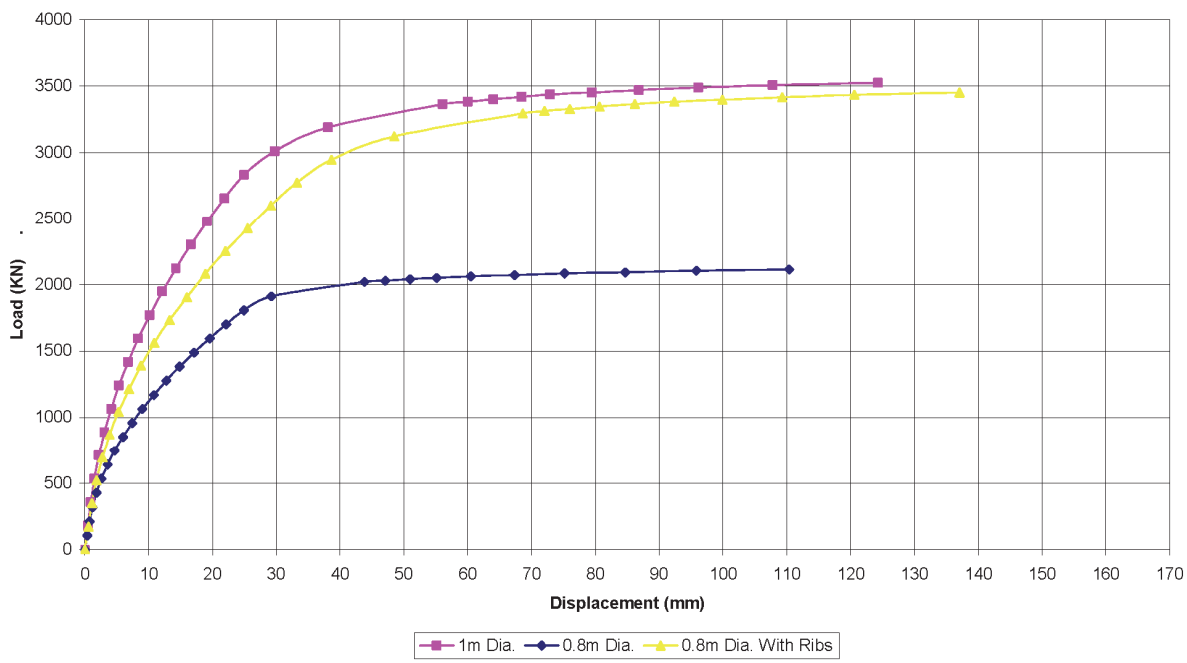

Figure 2.9 FEA load settlement curves after Senghani (2008).

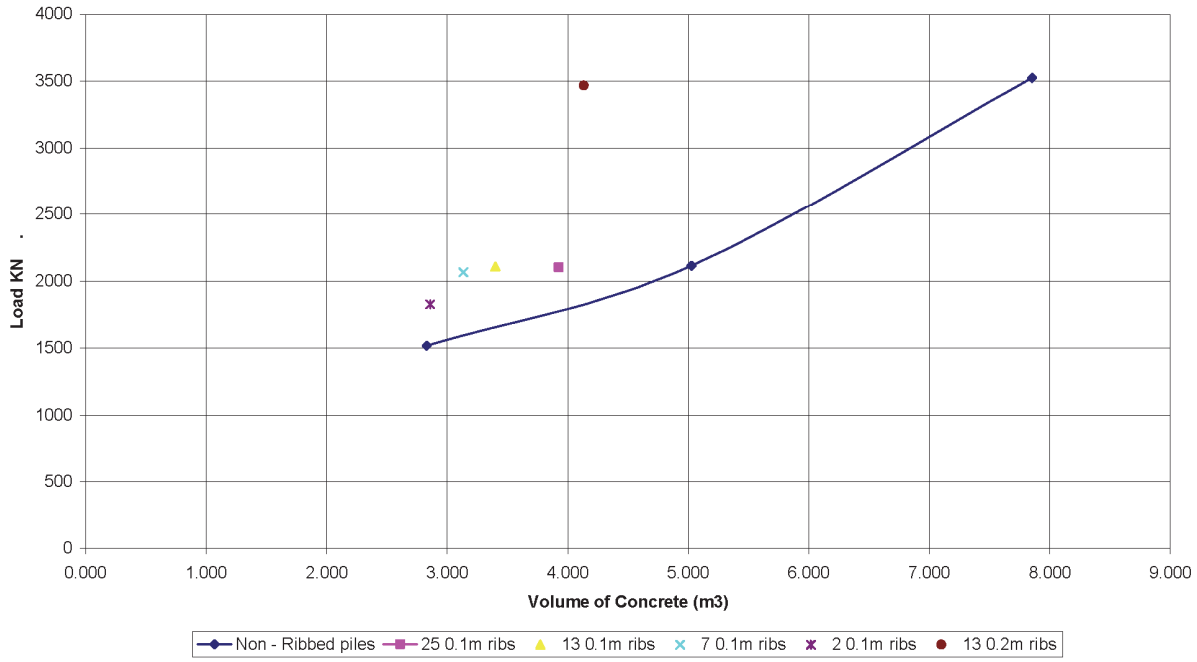

Figure 2.10 Predictions of volume of concrete for a given load from finite element analysis conducted by Senghani (2008).

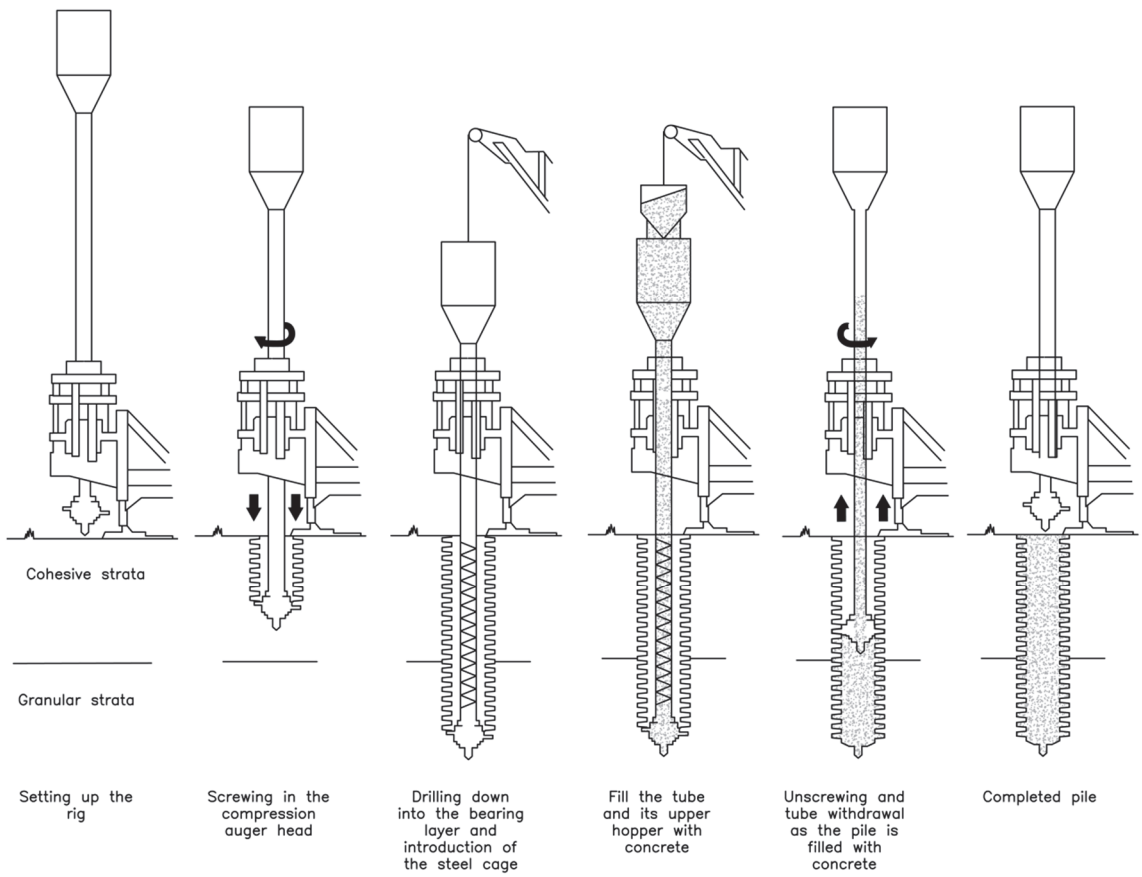

Figure 2.11 Atlas piling method after Tomlinson (1977).

Figure 2.12 Expanded Piling construction issue rib cutting tool.

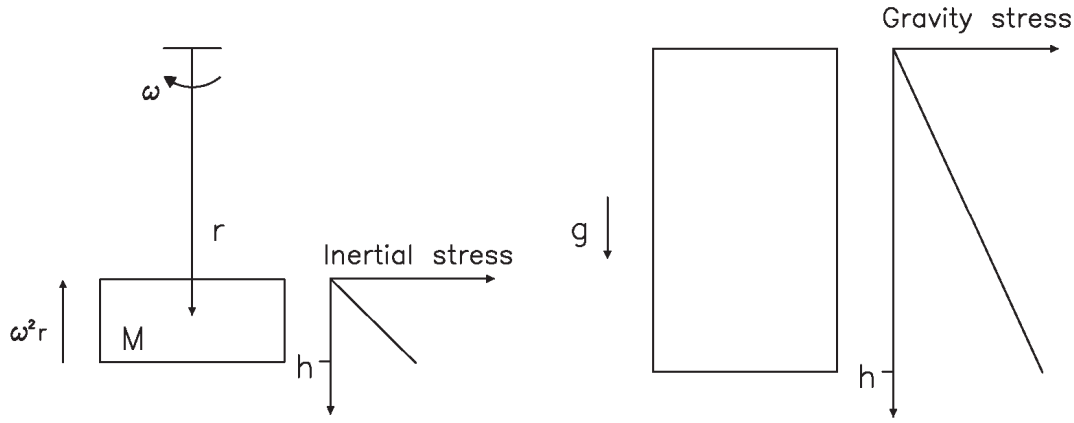

Figure 3.1 Inertial stress in a centrifuge model induced by rotation about a fixed axis and corresponding gravitational stresses in the prototype, after Taylor (1995).

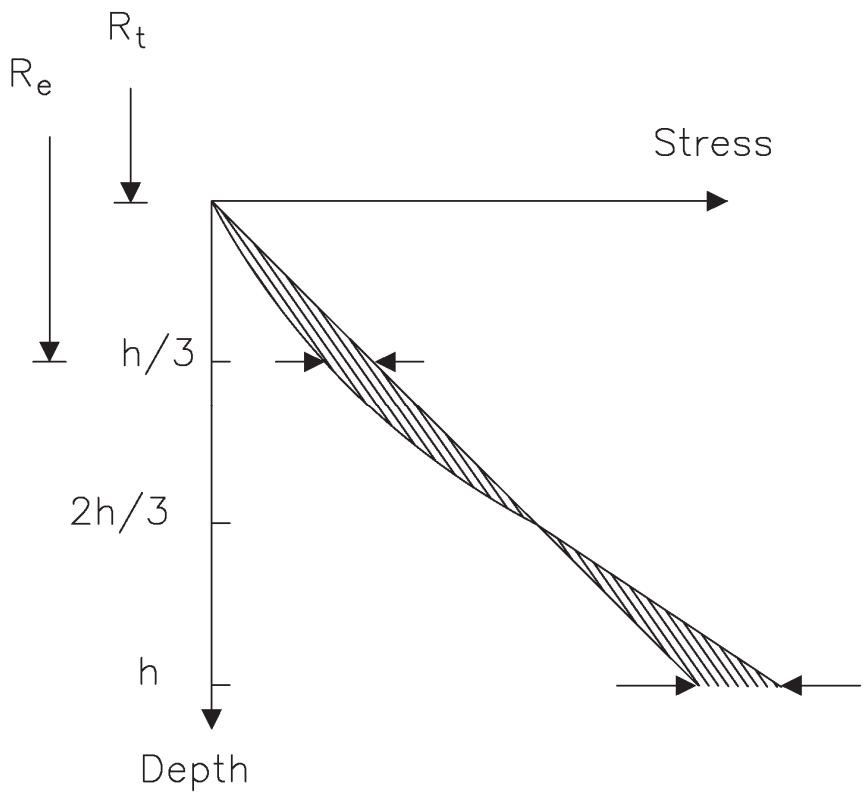

Figure 3.2 Comparison of stress variation with depth in a centrifuge model and its corresponding prototype, after Taylor (1995).

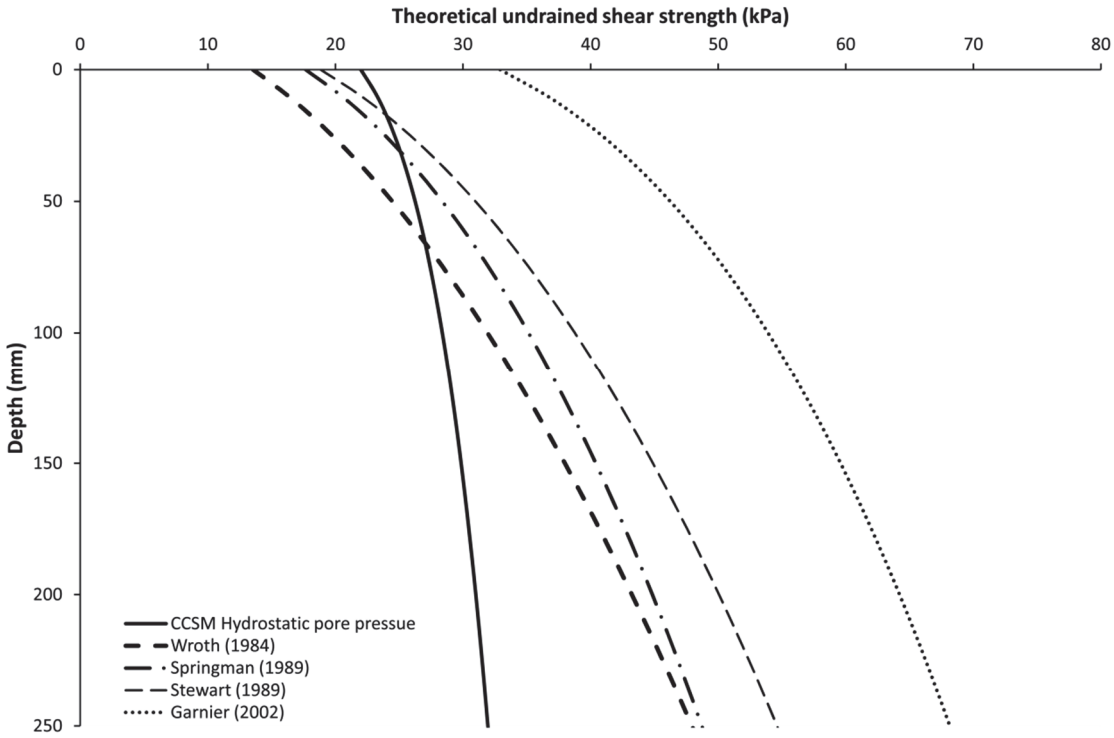

Figure 3.3 Estimated undrained shear strength profile with depth.

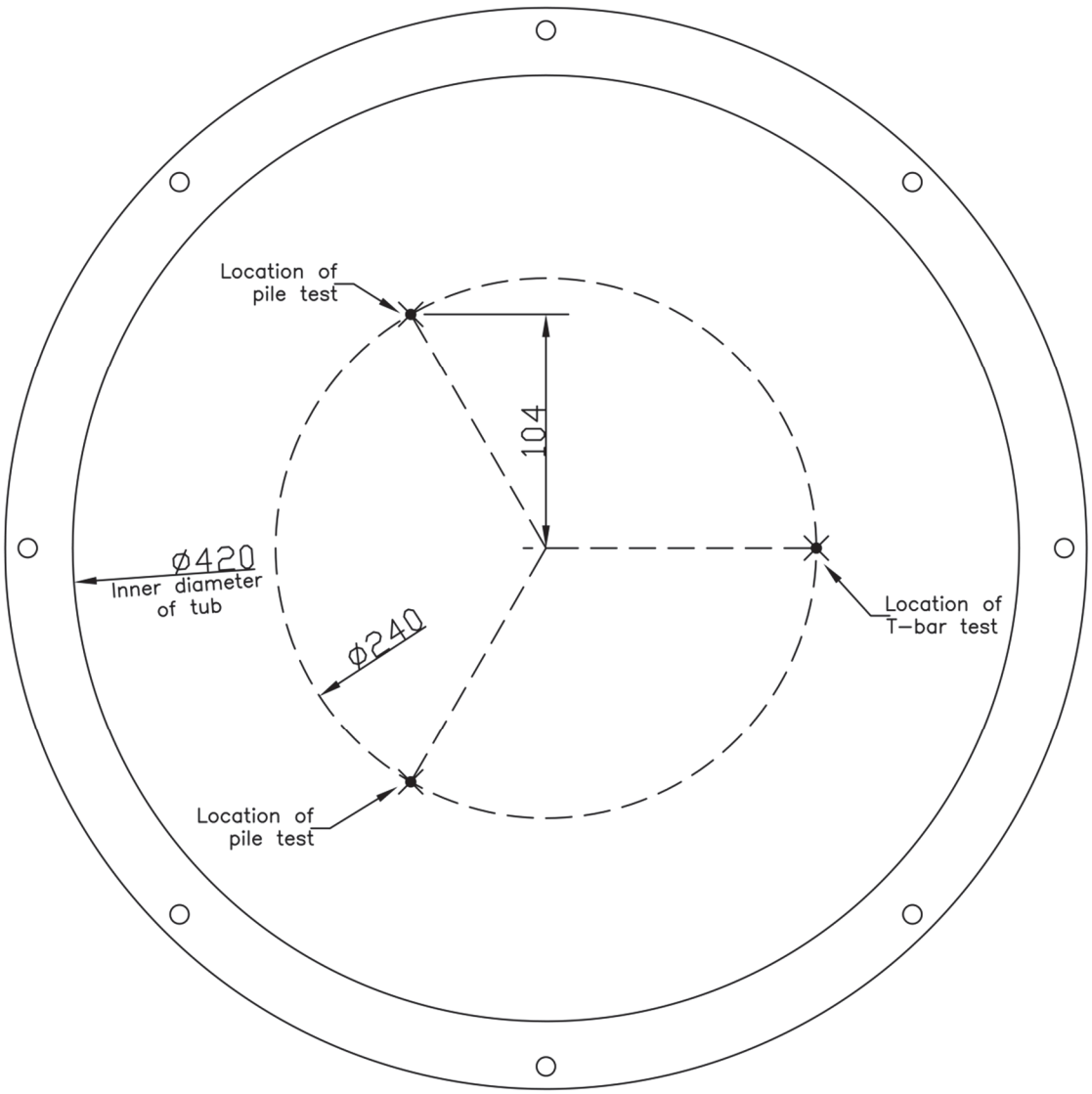

Figure 4.1 Test layout plan.

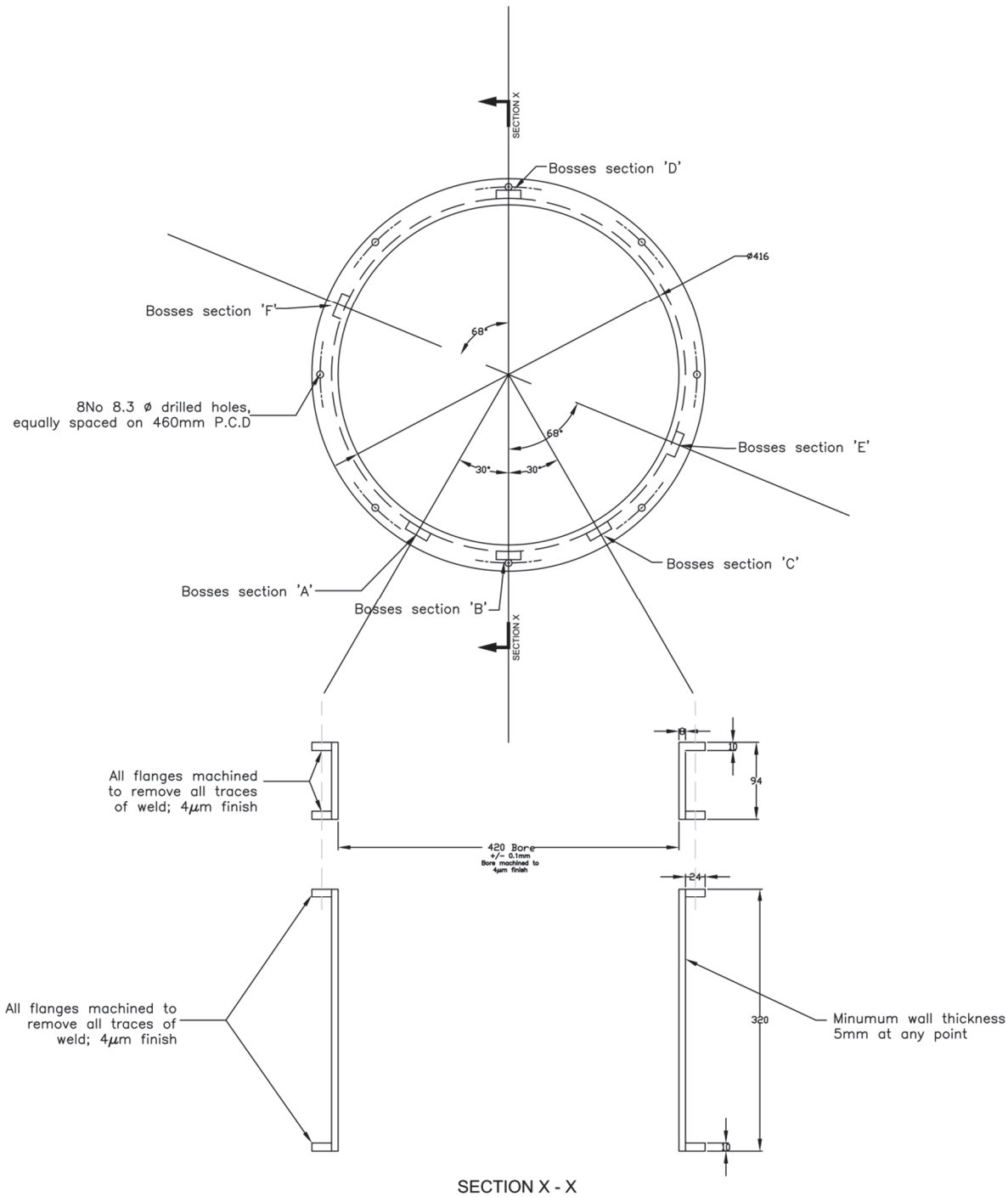

Figure 4.2 Construction details of new cylindrical soil container.

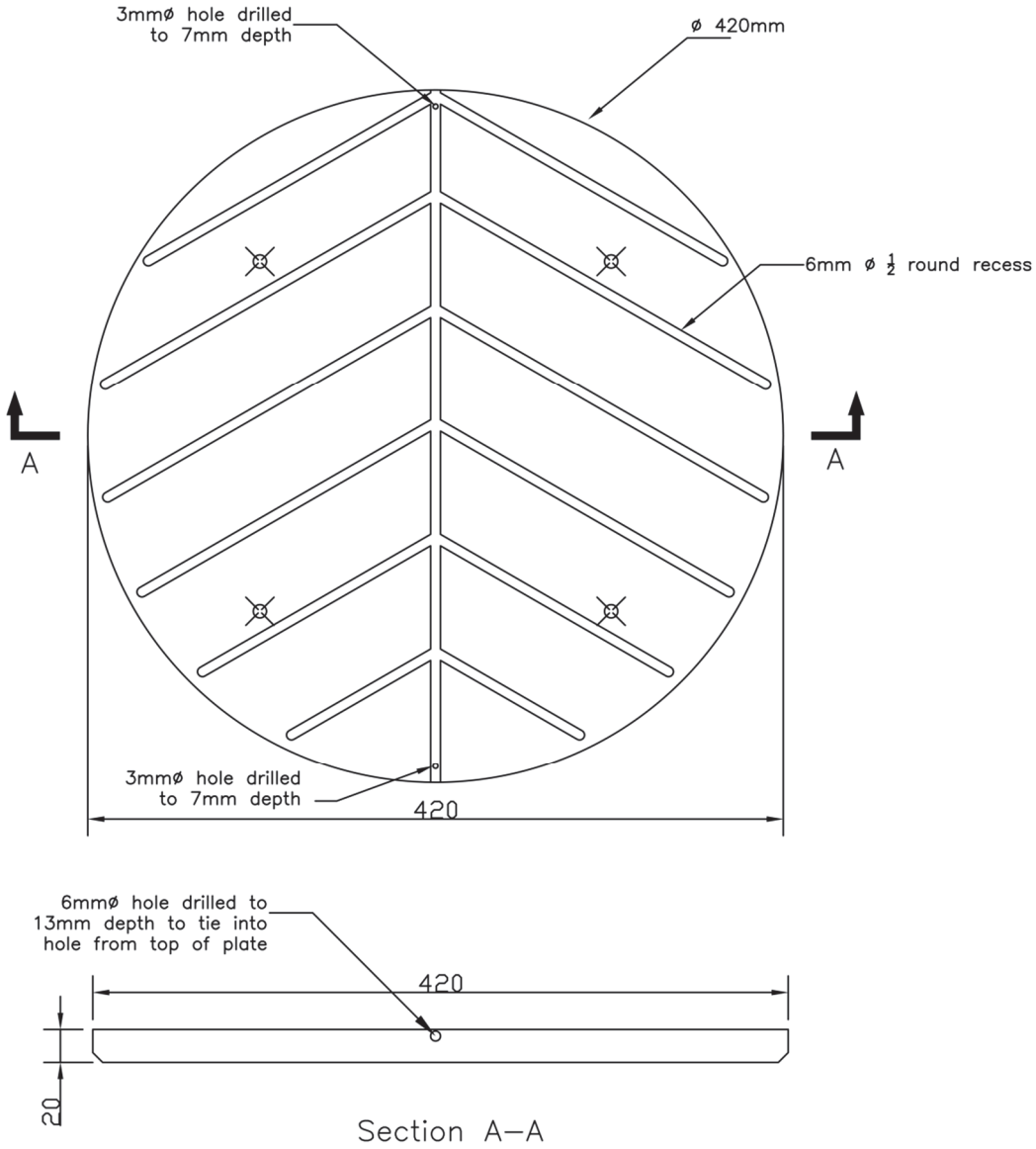

Figure 4.3 Drainage plate.

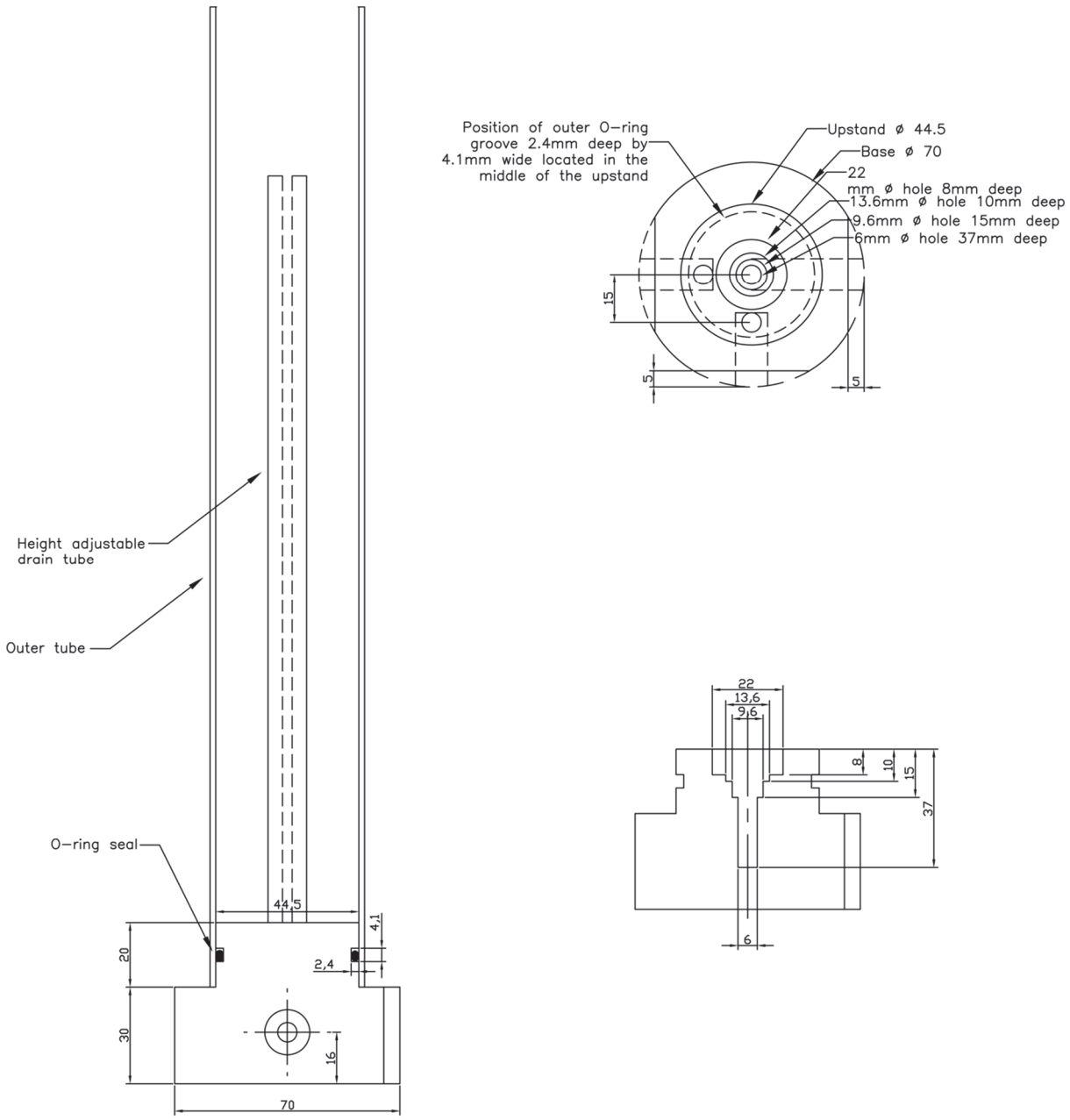

Figure 4.4 Adjustable brass standpipe.

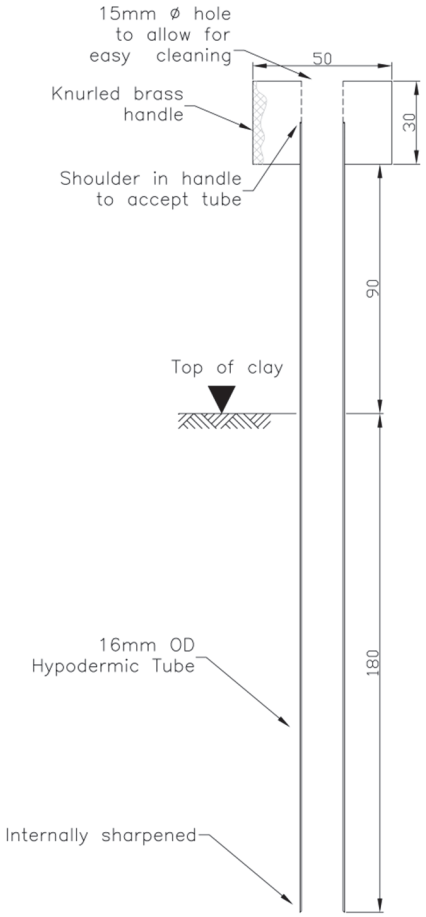

Figure 4.5 Straight shafted pile cutting tool.

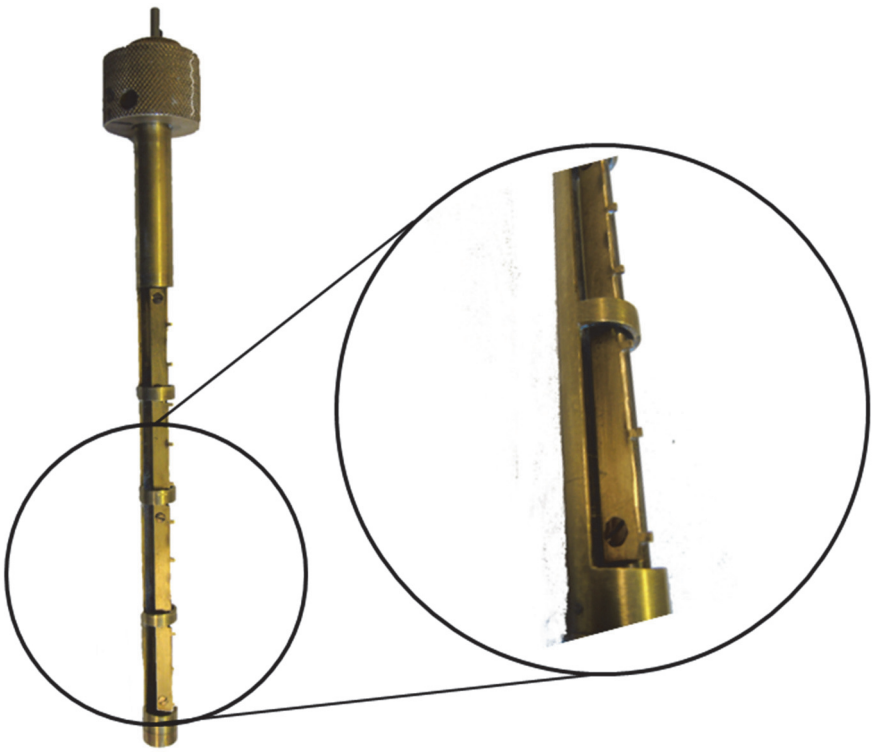

Figure 4.6 Rib cutting tool.

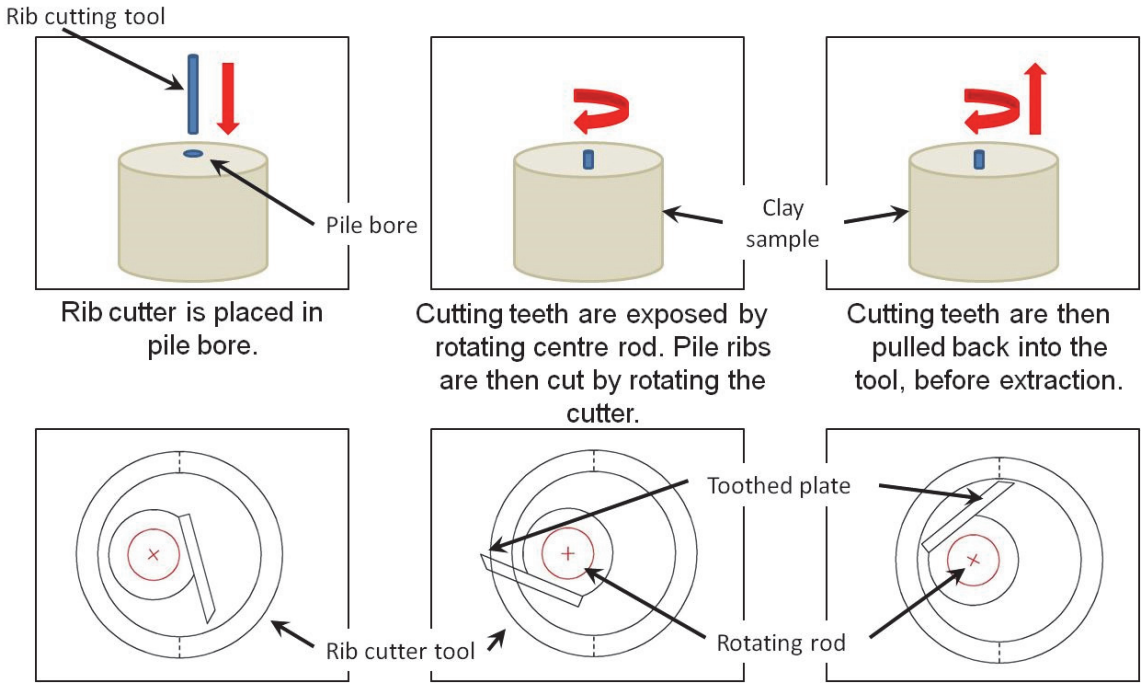

Figure 4.7 Rib cutting tool operation.

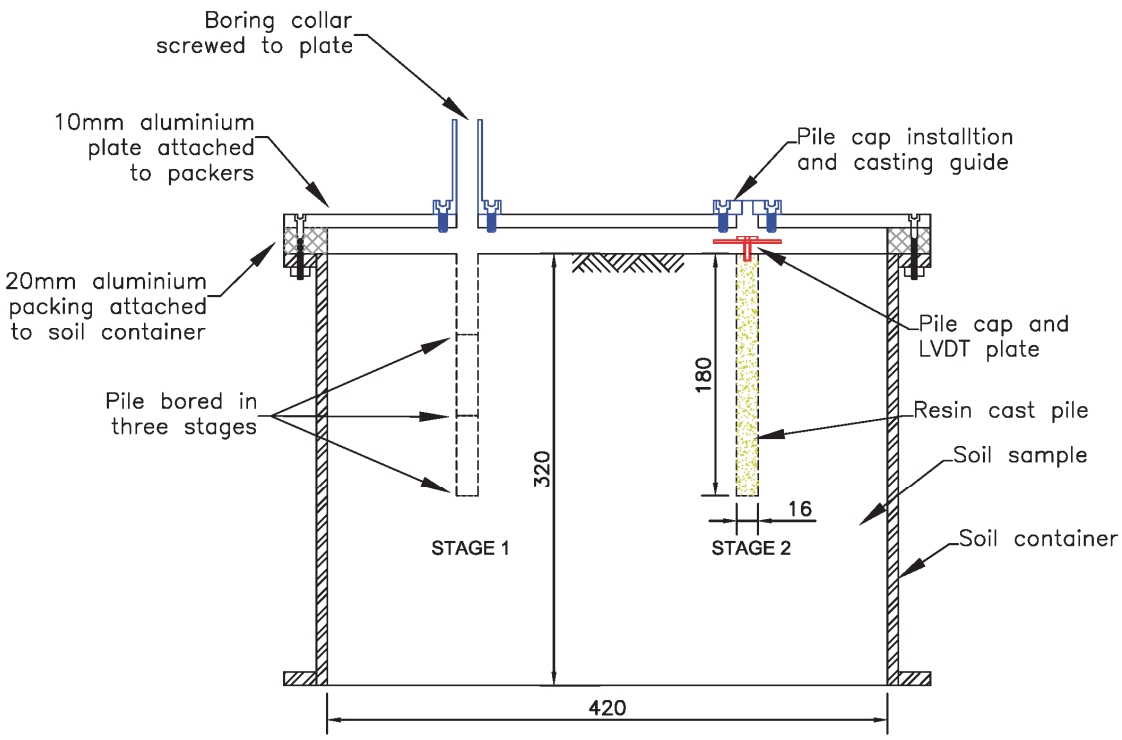

Figure 4.8 Pile cutting guide collars.

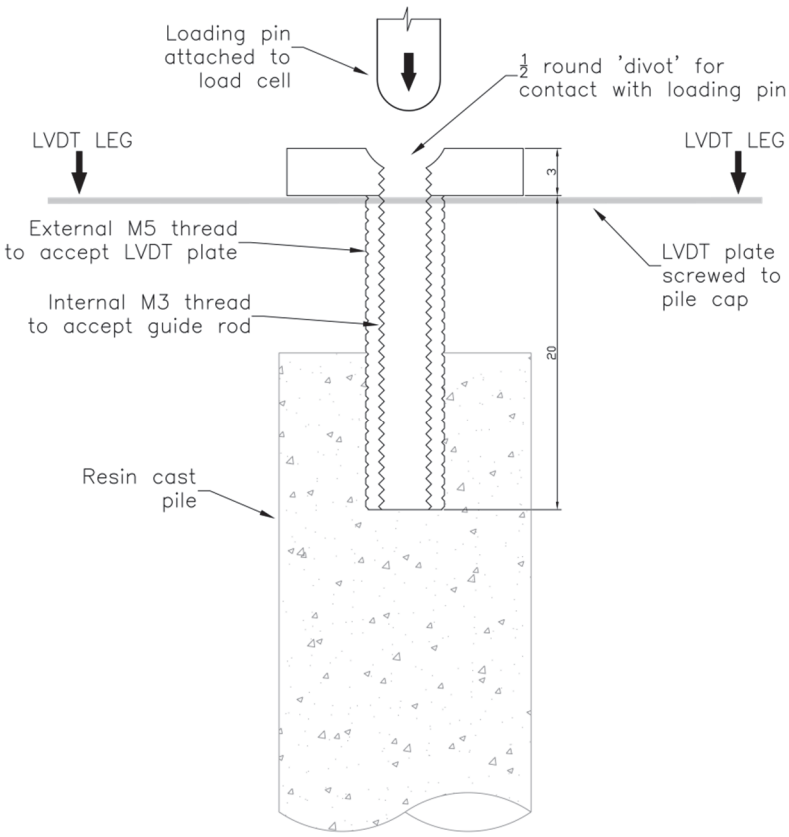

Figure 4.9 Pile cap (section).

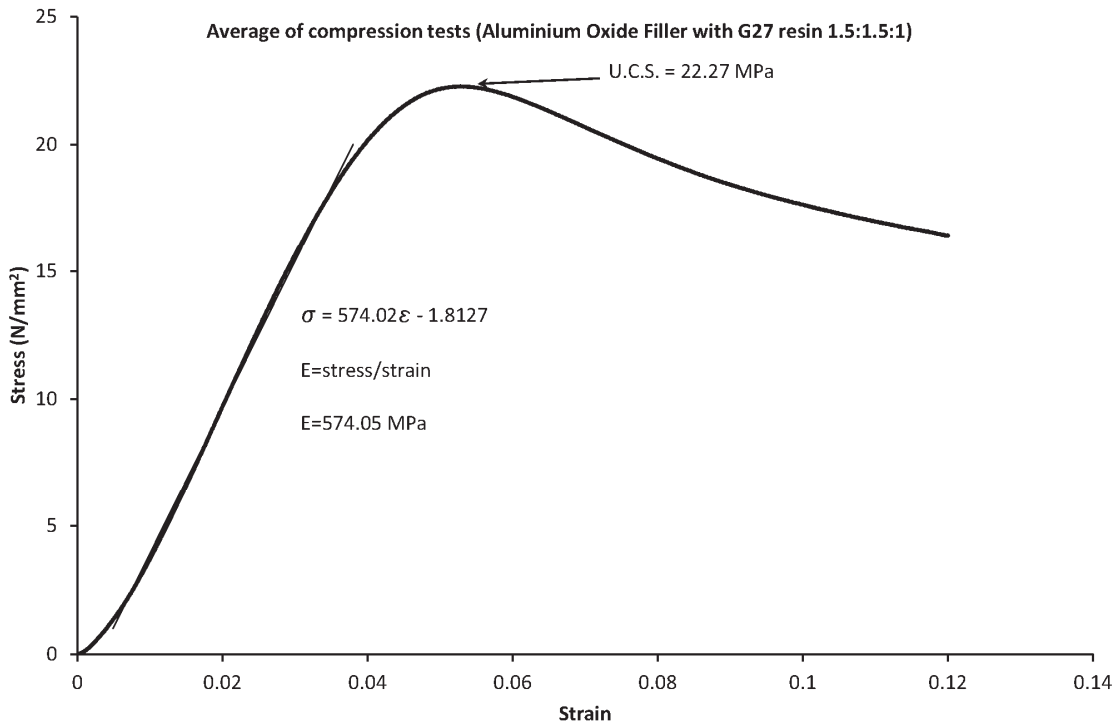

Figure 4.10 Compressive load tests on Sika Biresein G27 resin with Al_2O_3 filler.

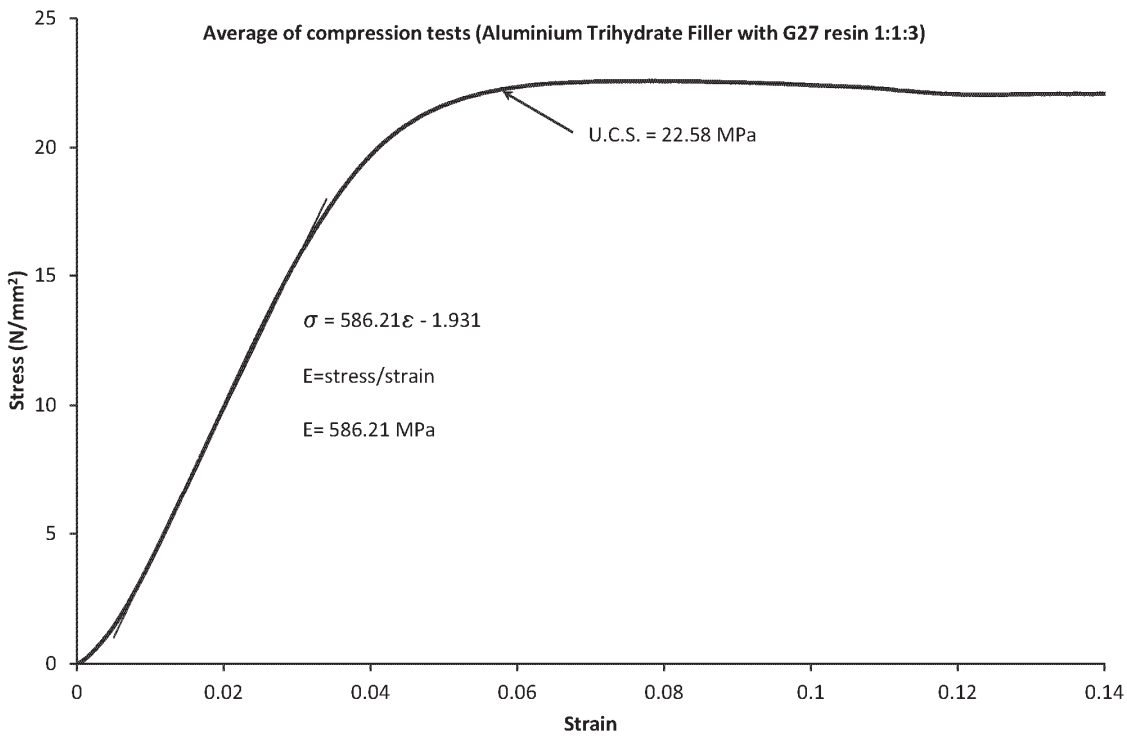

Figure 4.11 Compressive load tests on Sika Biresein G27 resin with $Al(OH)_3$ filler.

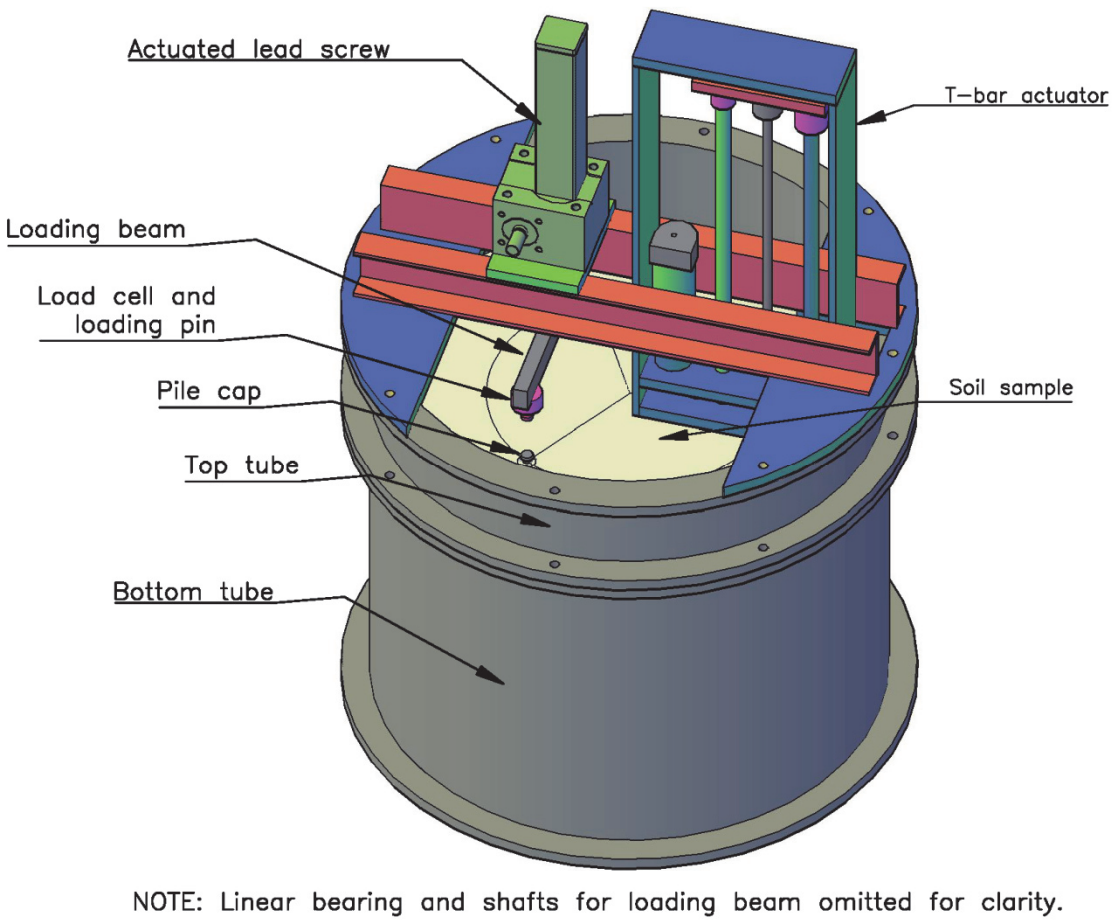

Figure 4.12 Actuated lead screw and loading beam.

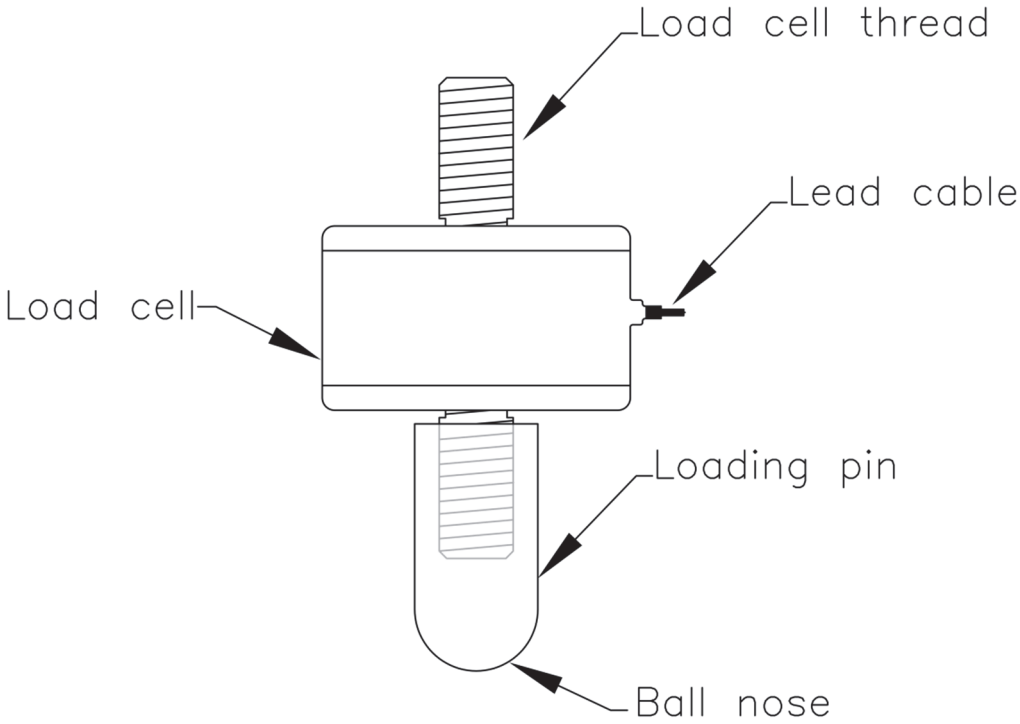

Figure 4.13 Load cell and loading pin assembly diagram.

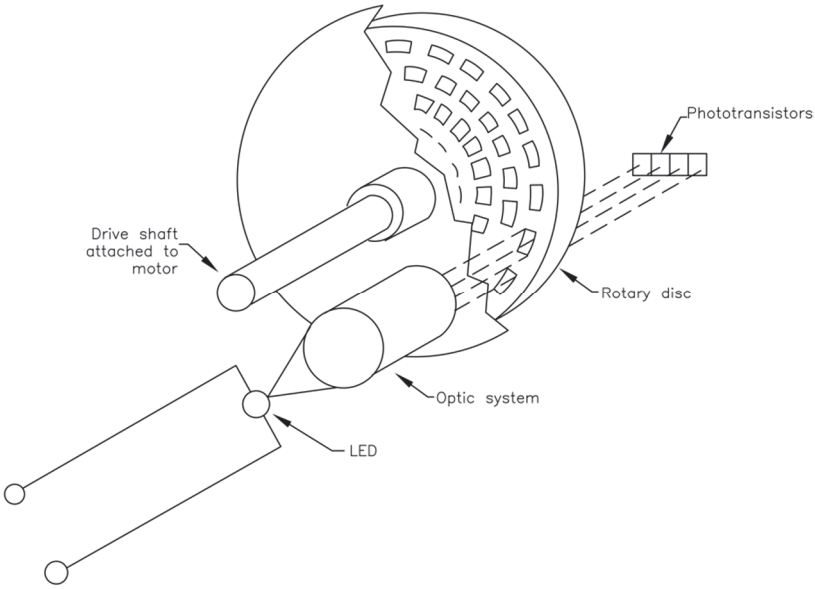

Figure 4.14 Optical rotary encoder exploded view.

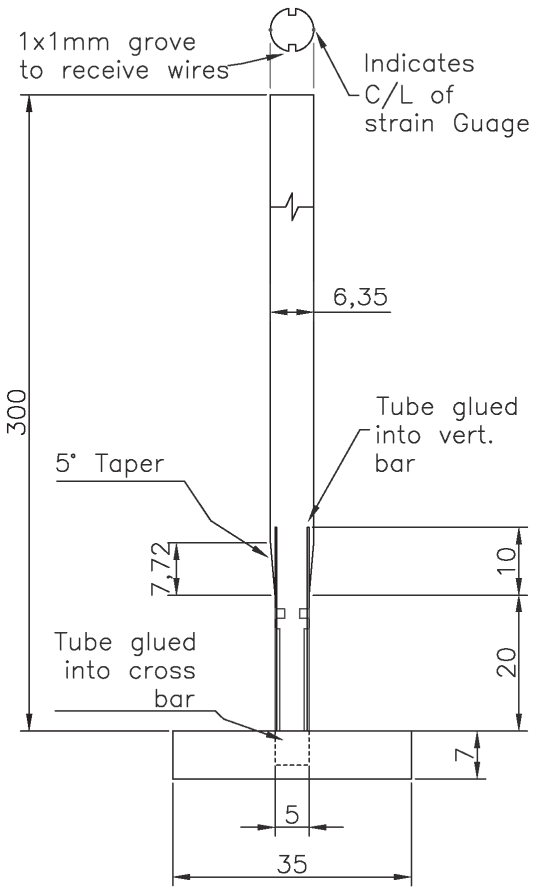

Figure 4.15 T-Bar Penetrometer construction detail.

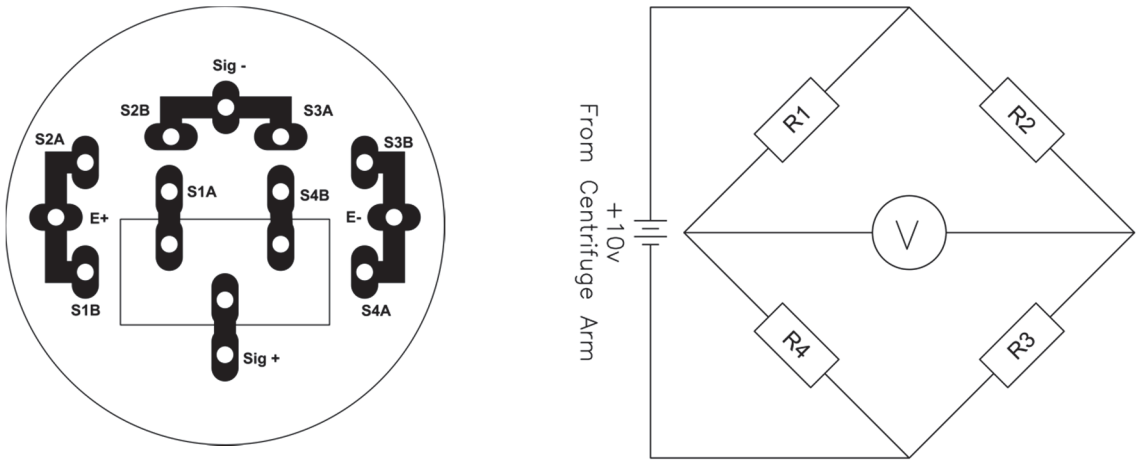

Figure 4.16 T-bar PCB layout and circuit diagram.

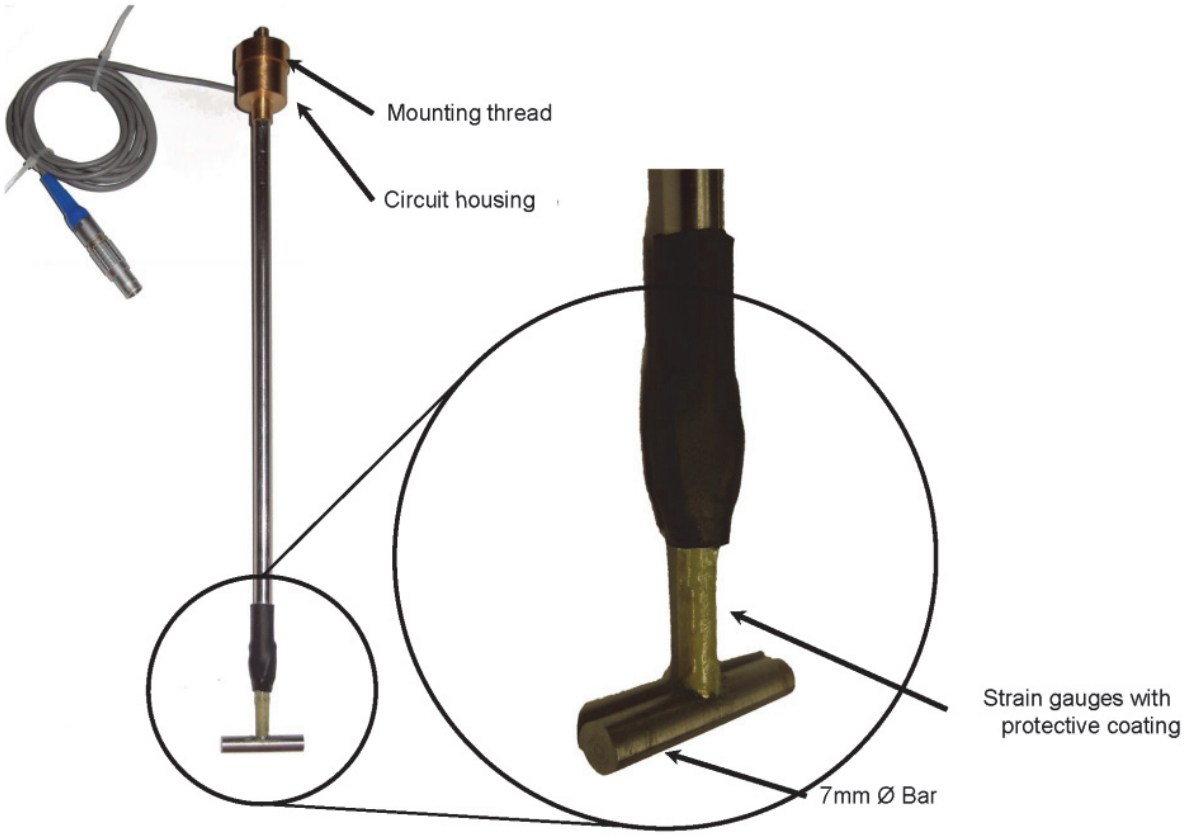

Figure 4.17 T-bar Penetrometer photograph.

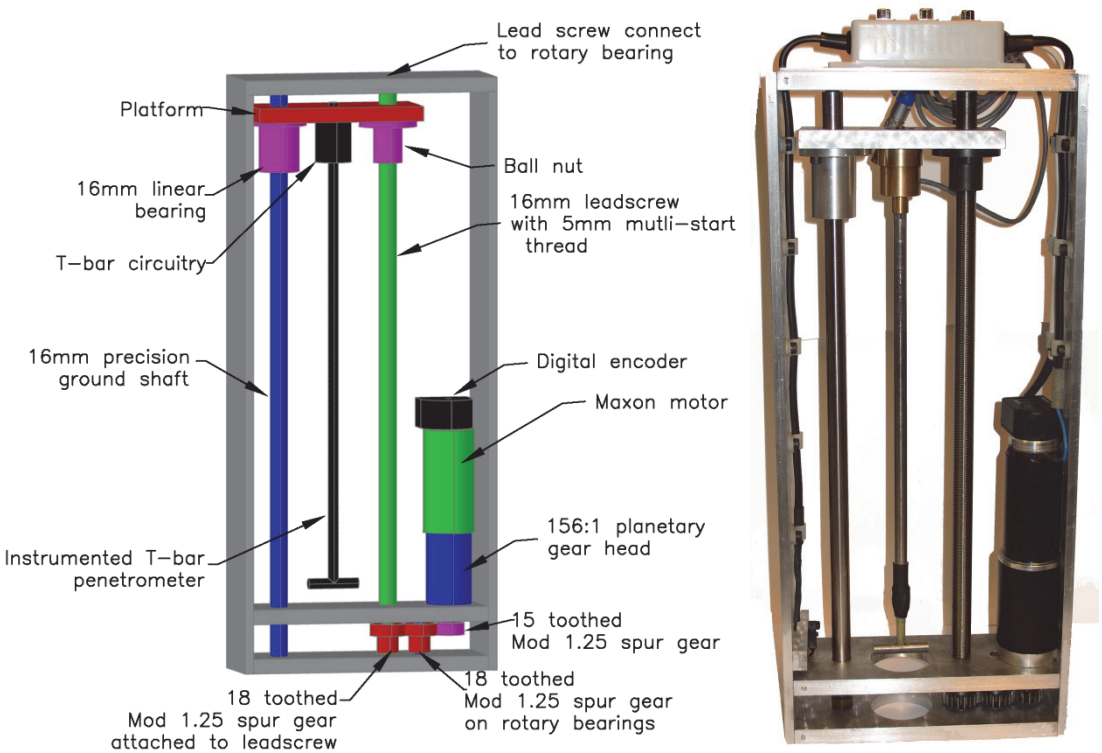

Figure 4.18 Construction detail and photograph of T-Bar actuator.

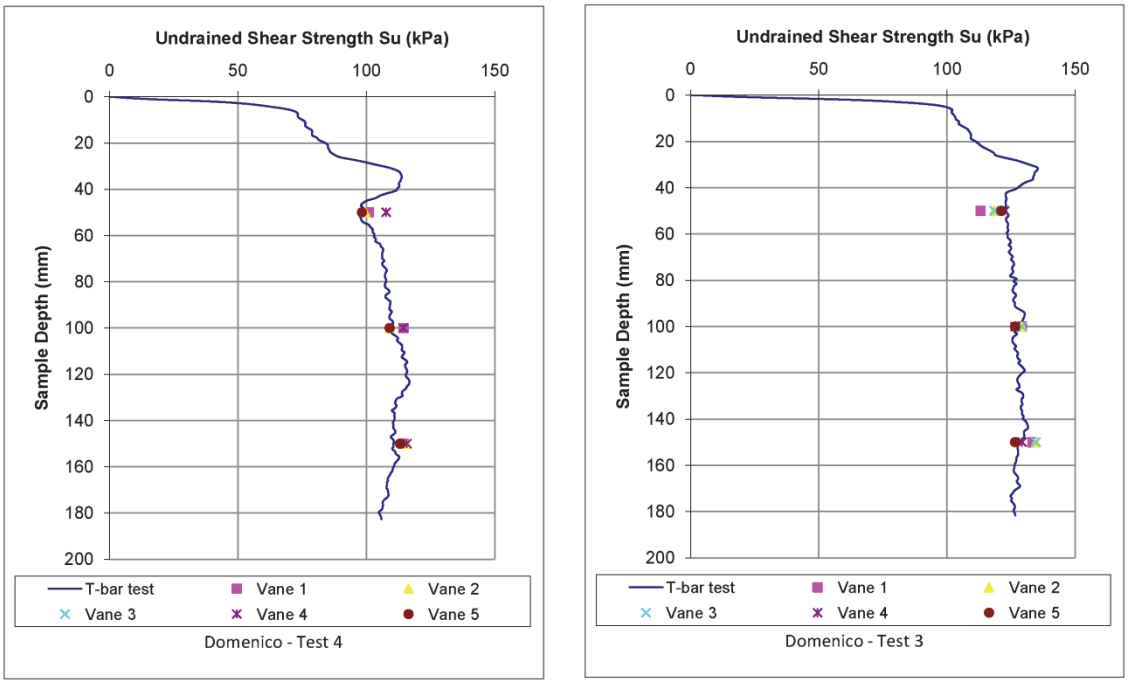

Figure 4.19 Undrained shear strength with depth for T-bar Penetrometer calibration, (McNamara, 2011).

Figure 4.20 Photograph of industrial ribbon blade mixer.

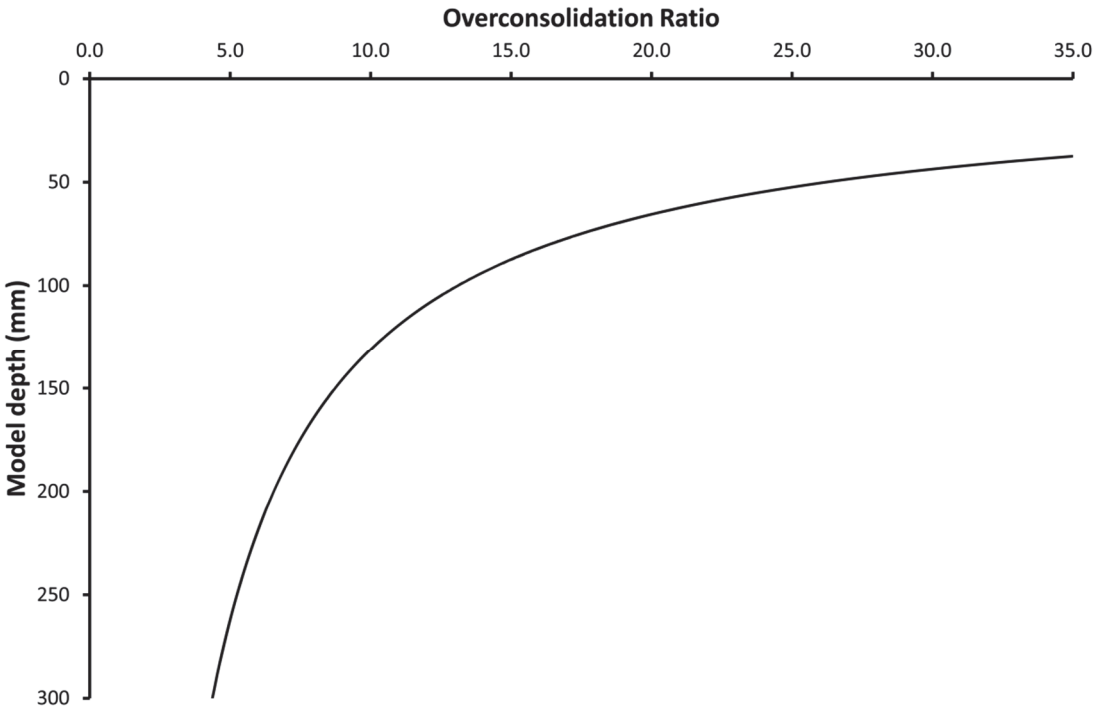

Figure 4.21 Variation of over-consolidation ratio with depth for a kaolin sample consolidated to 500kPa and allowed to swell under 250kPa.

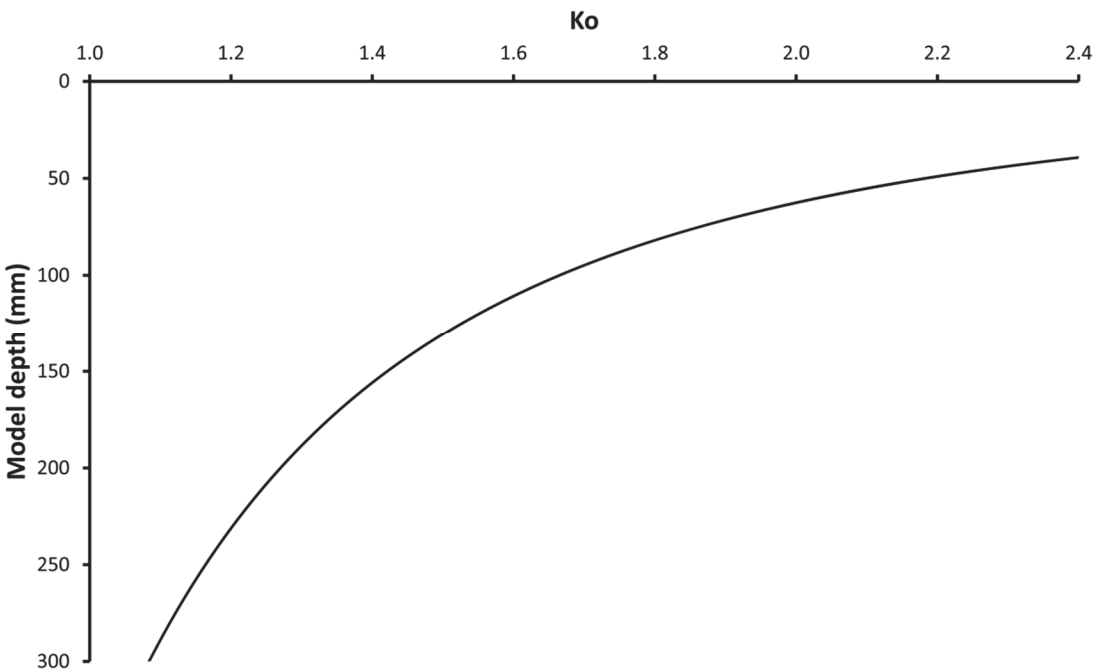

Figure 4.22 Variation of K_0 with depth for over-consolidated kaolin sample.

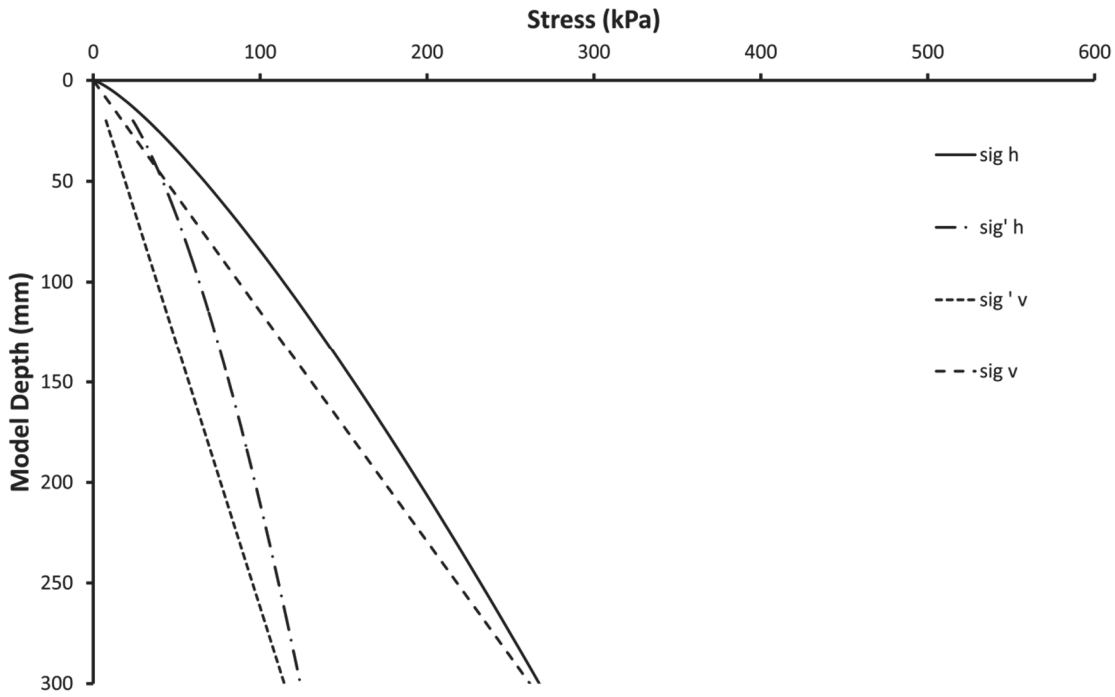

Figure 4.23 Theoretical vertical and horizontal total and effective stresses for over-consolidated kaolin sample.

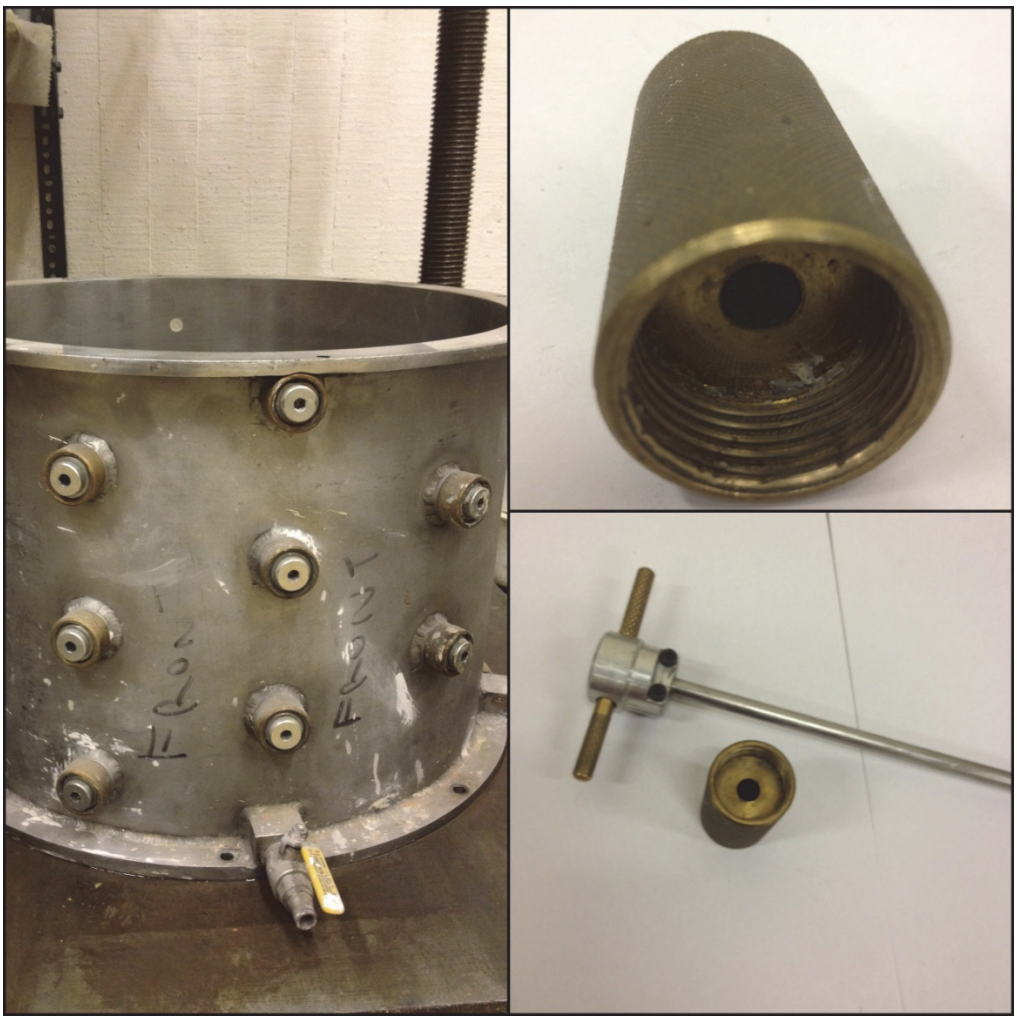

Figure 4.24 Pore pressure ports and transducer installation equipment.

Figure 4.25 Excess soil trimmed with wire cutter.

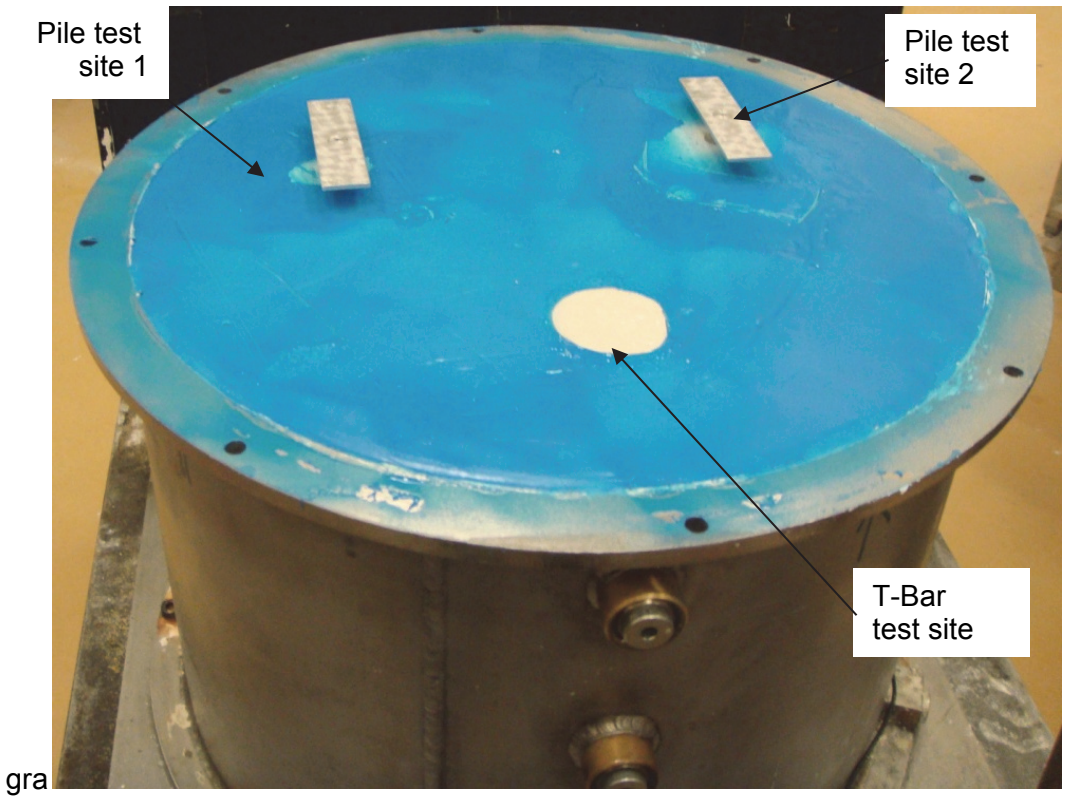

gra

Figure 4.26 PlastiDip used to seal top of soil model.

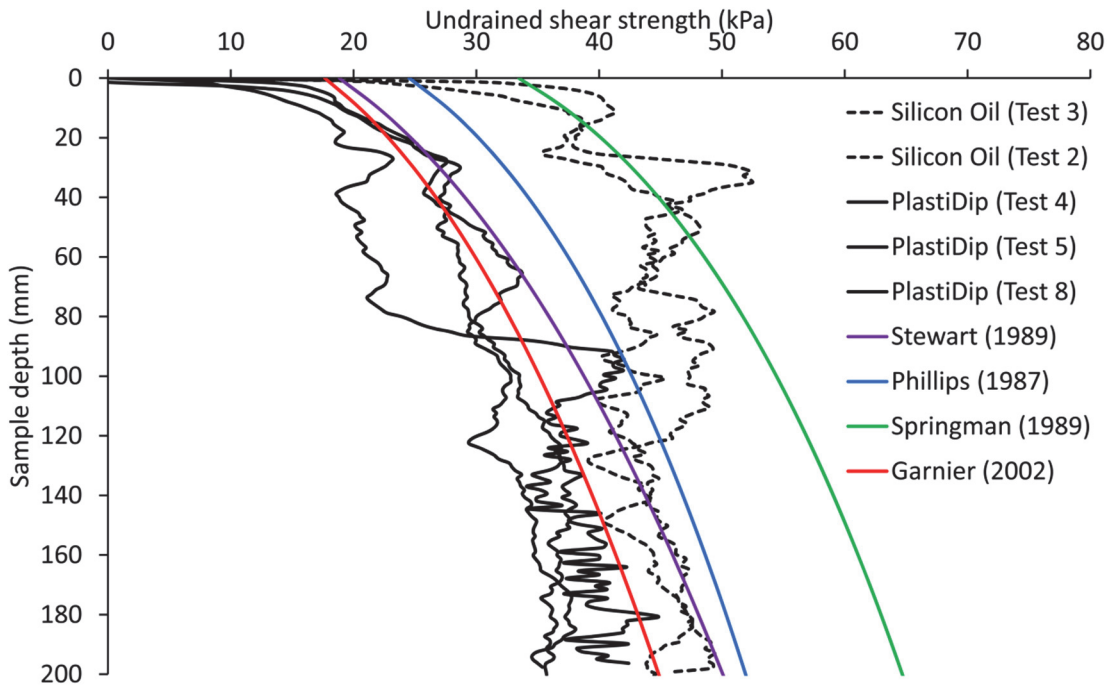

Figure 4.27 Undrained shear strength with depth for silicon oil and PlastiDip used as surface sealant.

Figure 4.28 Top tube mounted to soil container with instrumentation attached.

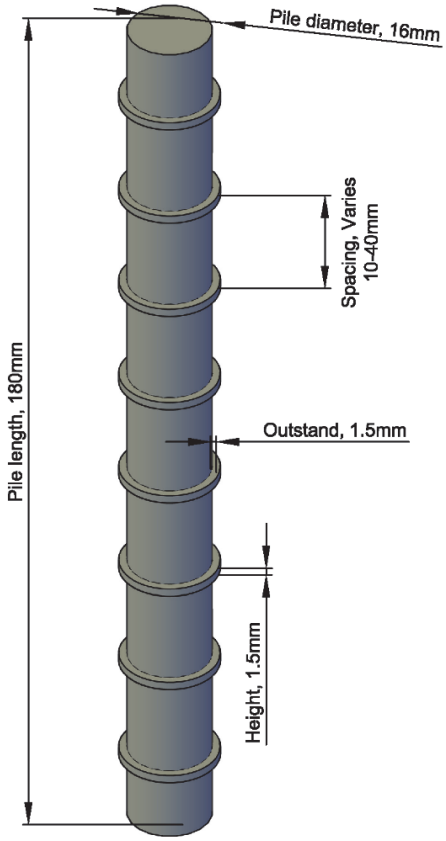

Figure 5.1 Typical pile dimensions.

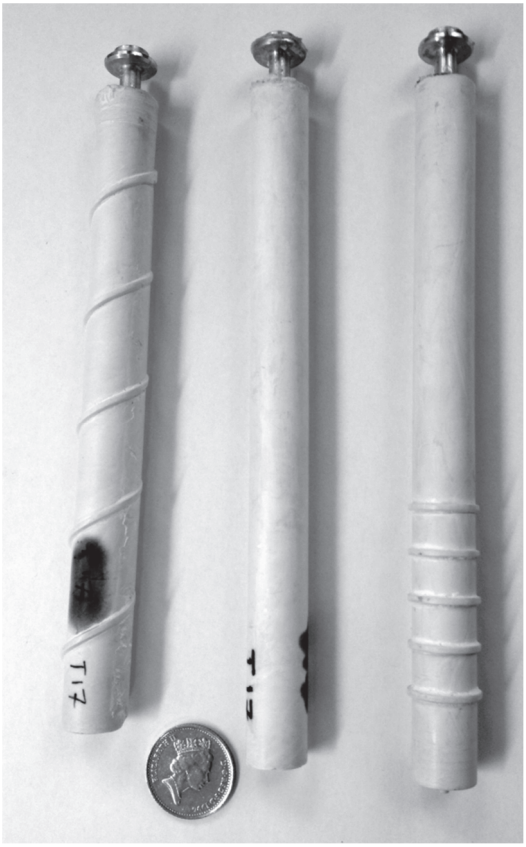

Figure 5.2 Typical exhumed piles (scaled to 10p).

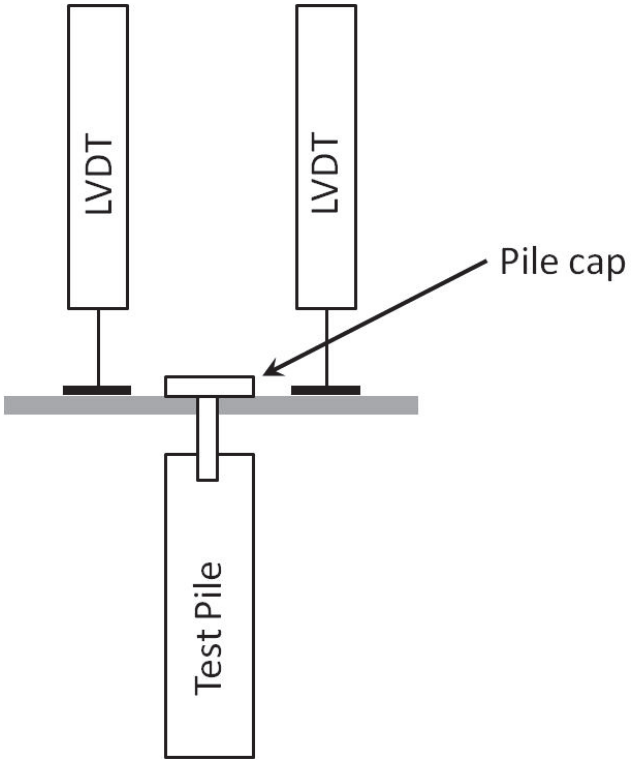

Figure 5.3 LVDT arrangement used to detect eccentric pile loading.

Figure 5.4 Rib cutting tool developed and used by Witton-Dauris (2008).

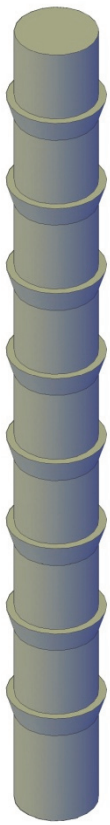

Figure 5.5 Isometric illustration of the tapered rib pile.

Figure 5.6 10mm helical rib cutter with ball nut and cutting bucket.

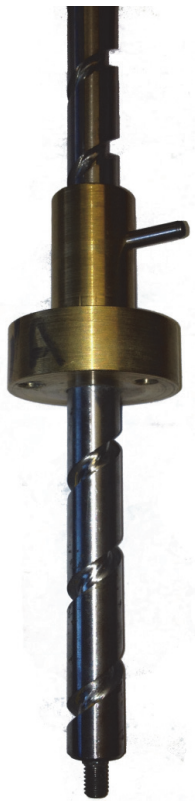

Figure 5.7 Manufactured lead screw and ball nut (30mm pitch).

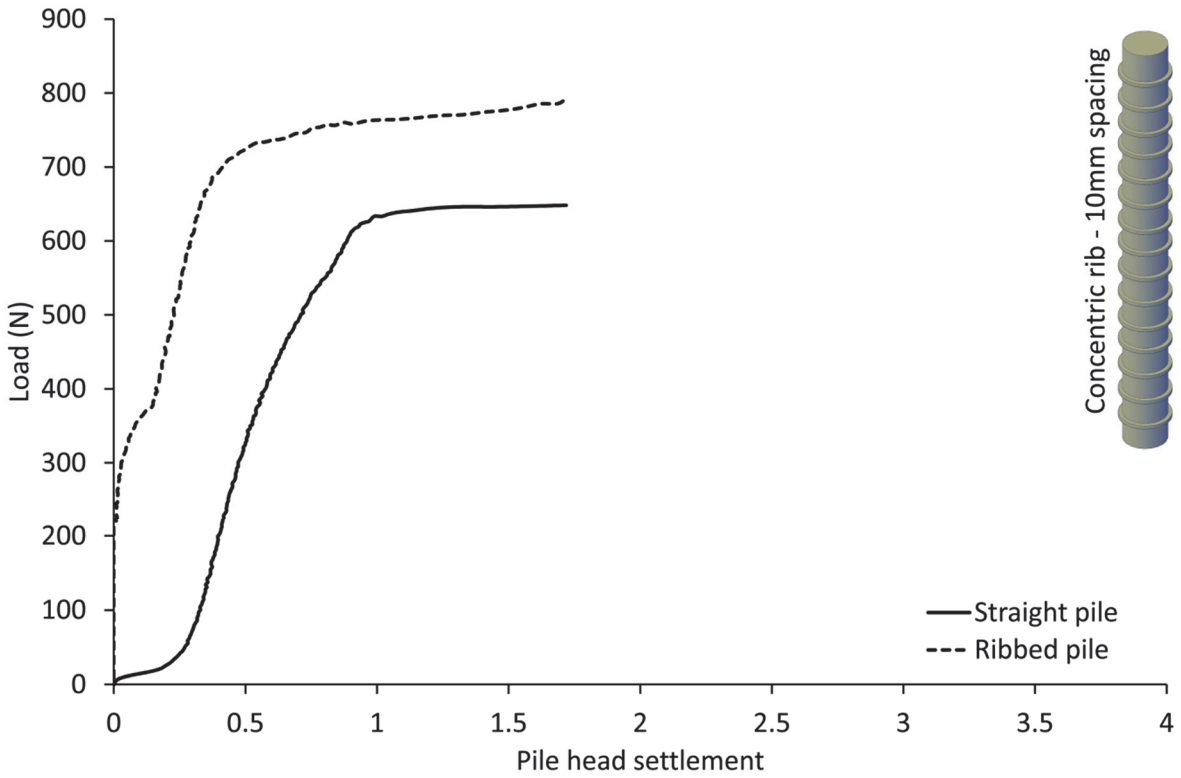

Figure 5.8 Load settlement curve, Test RJG0, concentrically ribbed pile with 10mm spacing using existing test equipment.

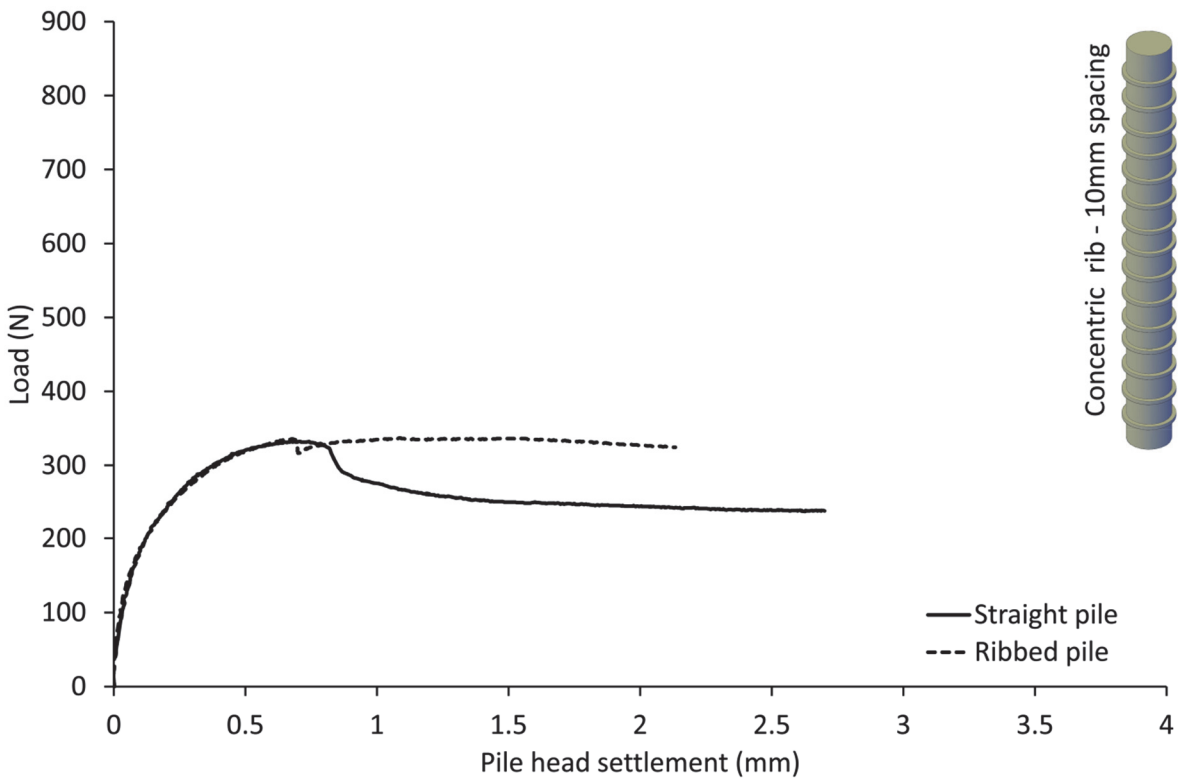

Figure 5.9 Load settlement curve, Test RJG2, concentrically ribbed pile with 10mm spacing.

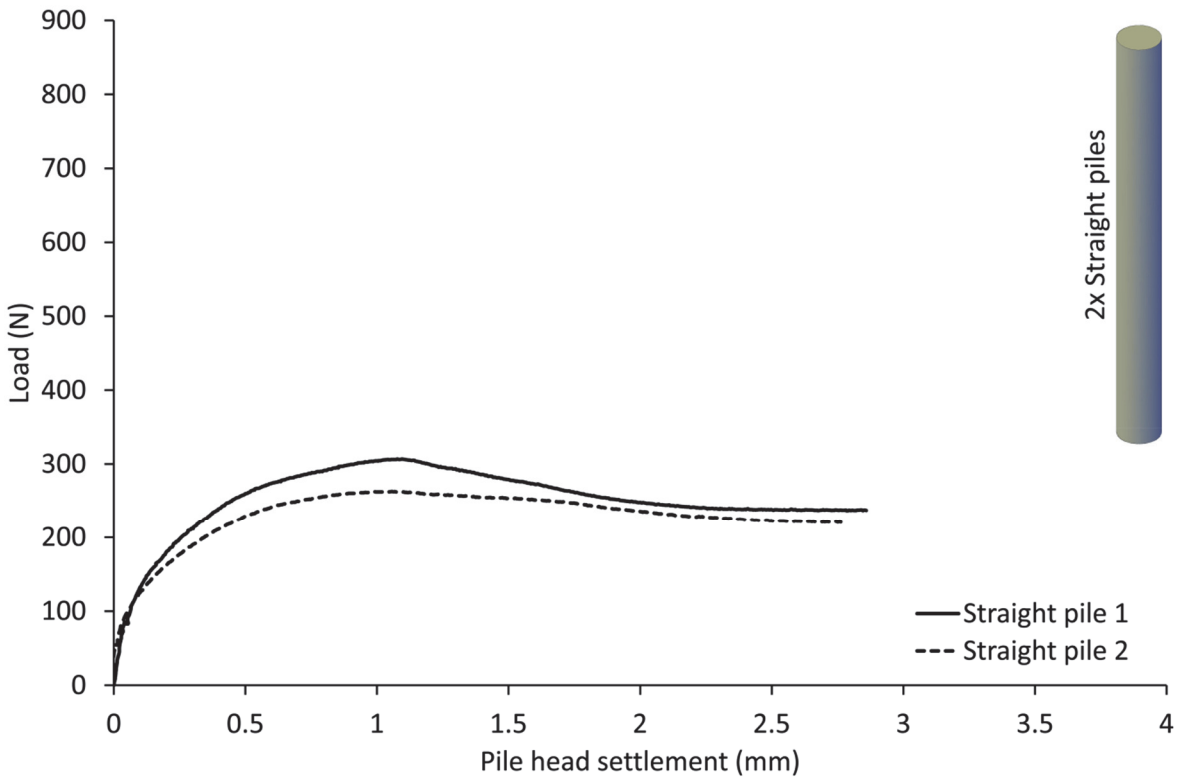

Figure 5.10 Load settlement curve, Test RJG5, 2 straight shafted piles.

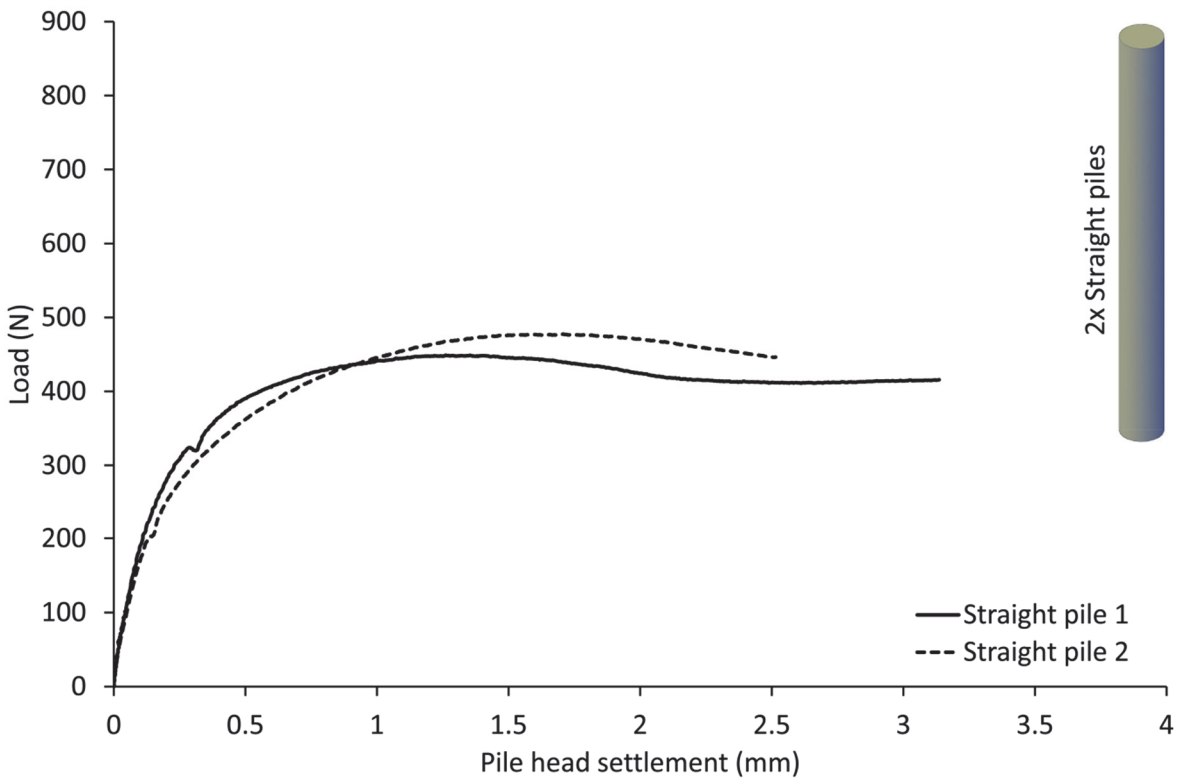

Figure 5.11 Load settlement curve, Test RJG6, 2 straight shafted piles.

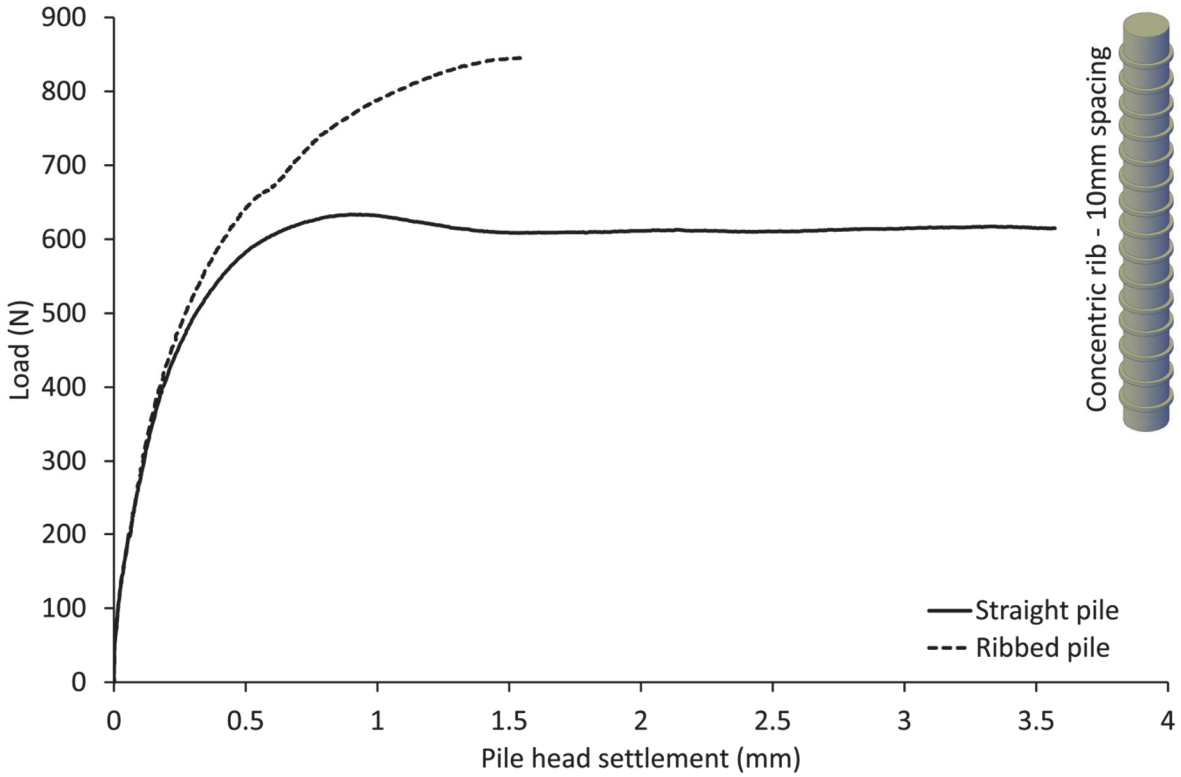

Figure 5.12 Load settlement curve, Test RJG3, concentrically ribbed pile with 10mm spacing.

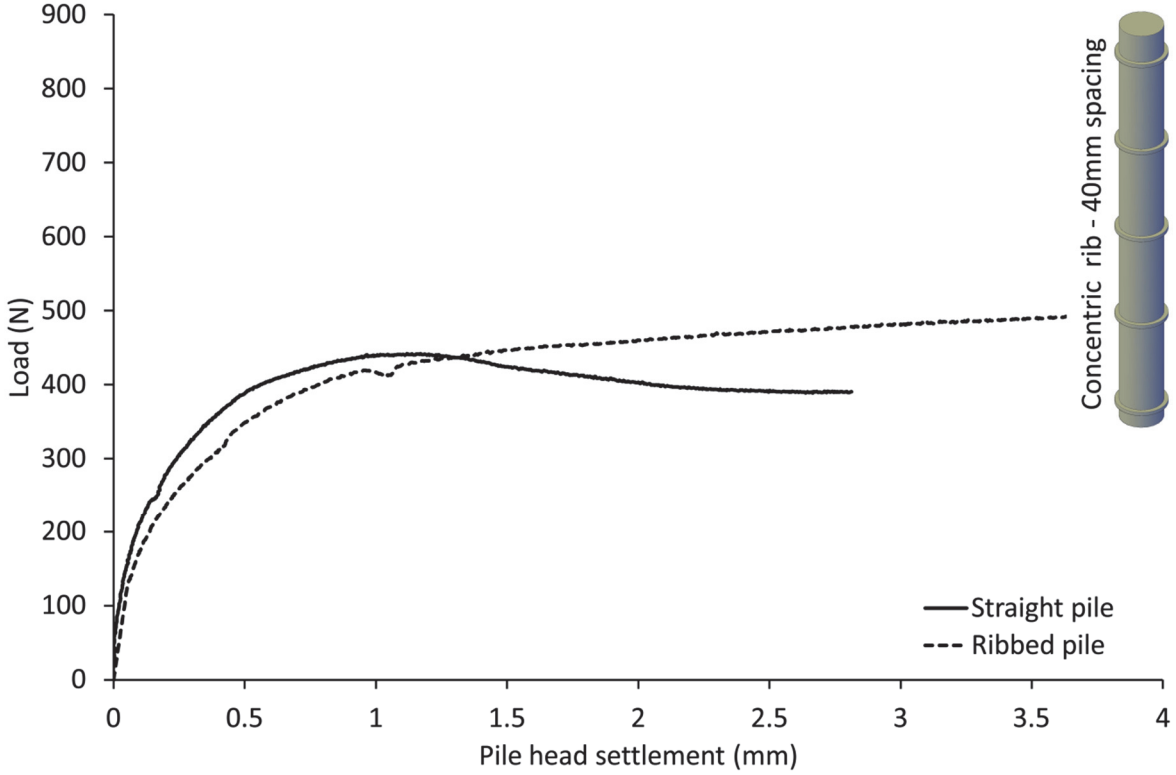

Figure 5.13 Load settlement curve, Test RJG13, concentrically ribbed pile with 40mm spacing.

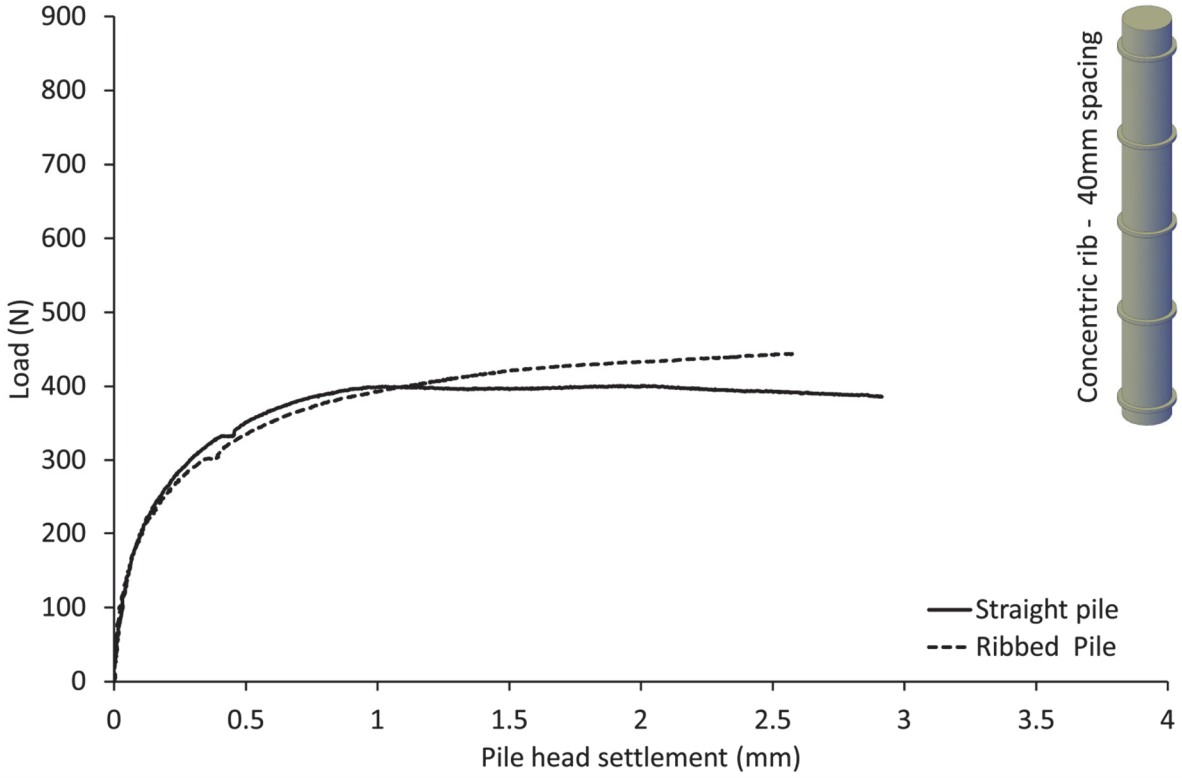

Figure 5.14 Load settlement curve, Test RJG21, concentrically ribbed pile with 40mm spacing.

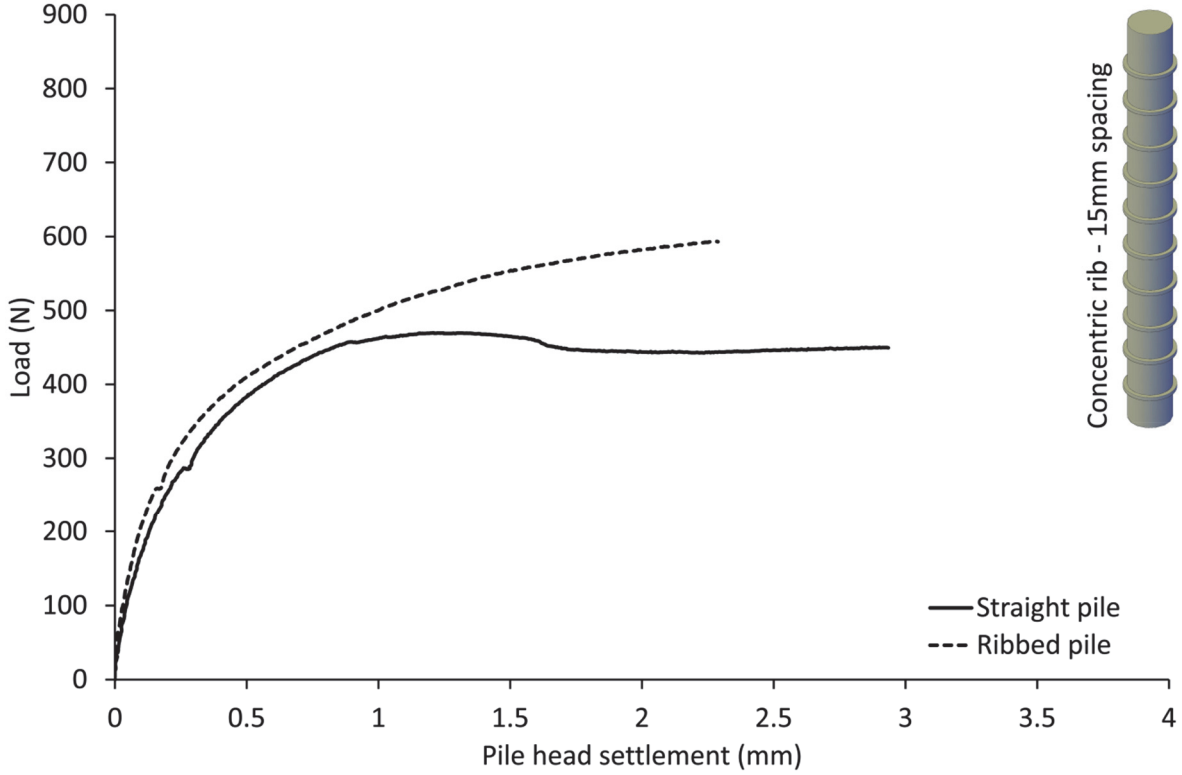

Figure 5.15 Load settlement curve, Test RJG4, concentrically ribbed pile with 15mm spacing.

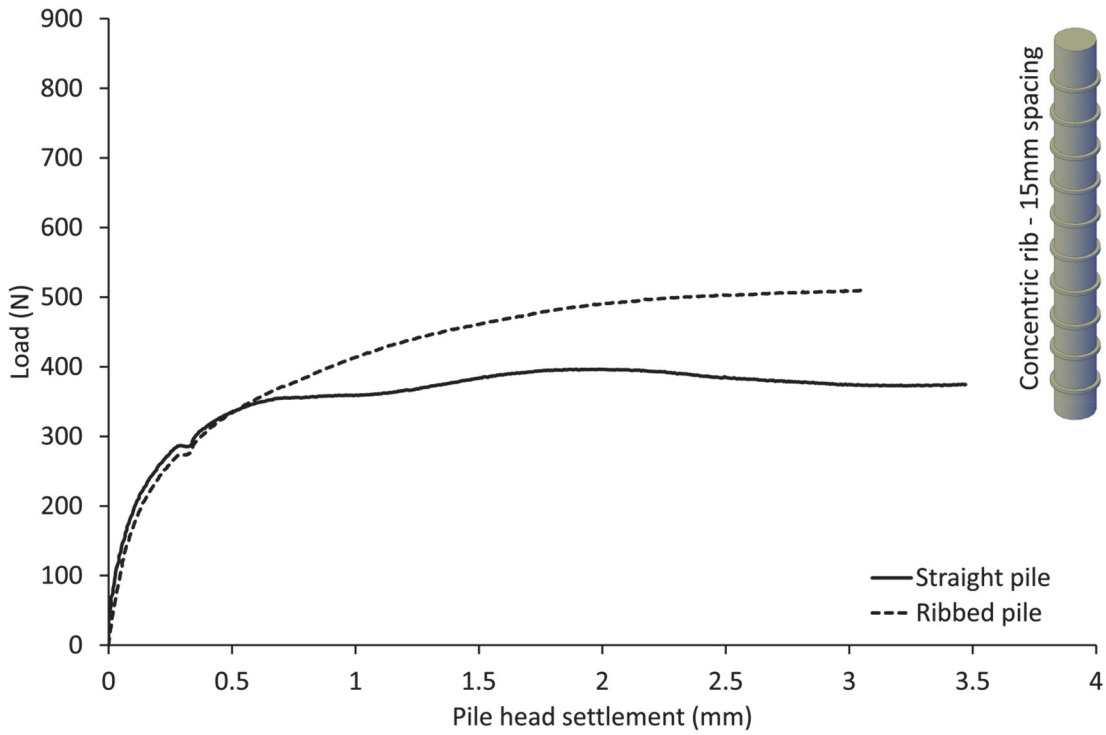

Figure 5.16 Load settlement curve, Test RJG7, concentrically ribbed pile with 15mm spacing.

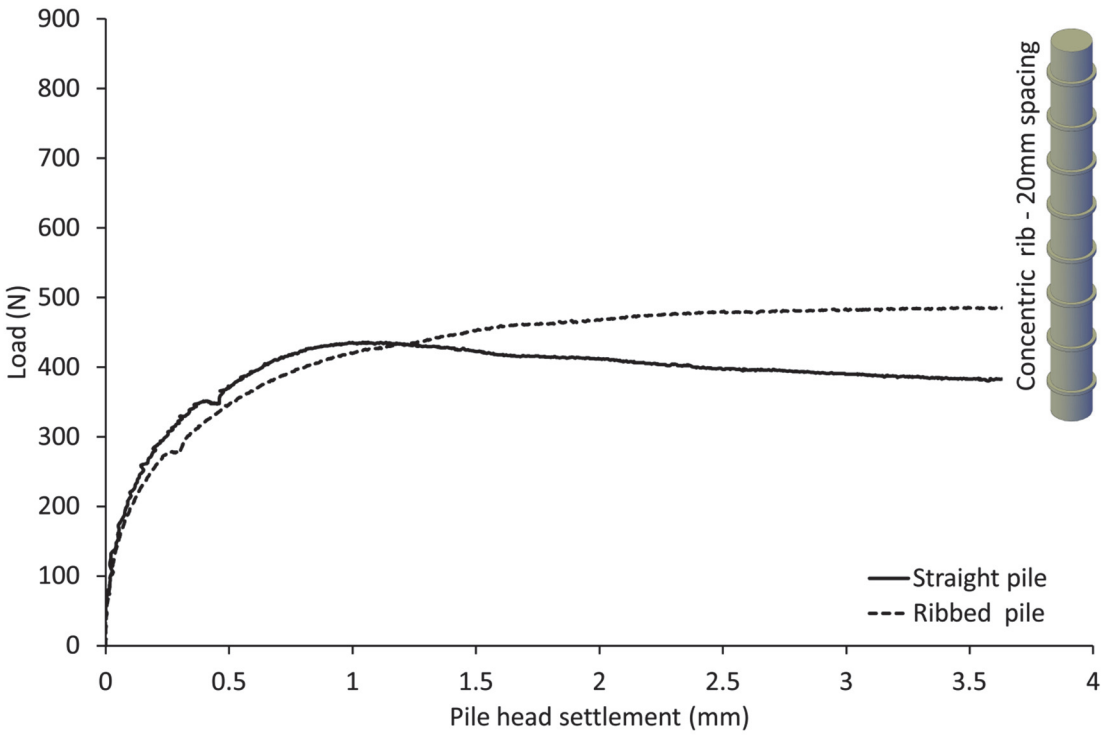

Figure 5.17 Load settlement curve, Test RJG10, concentrically ribbed pile with 20mm spacing.

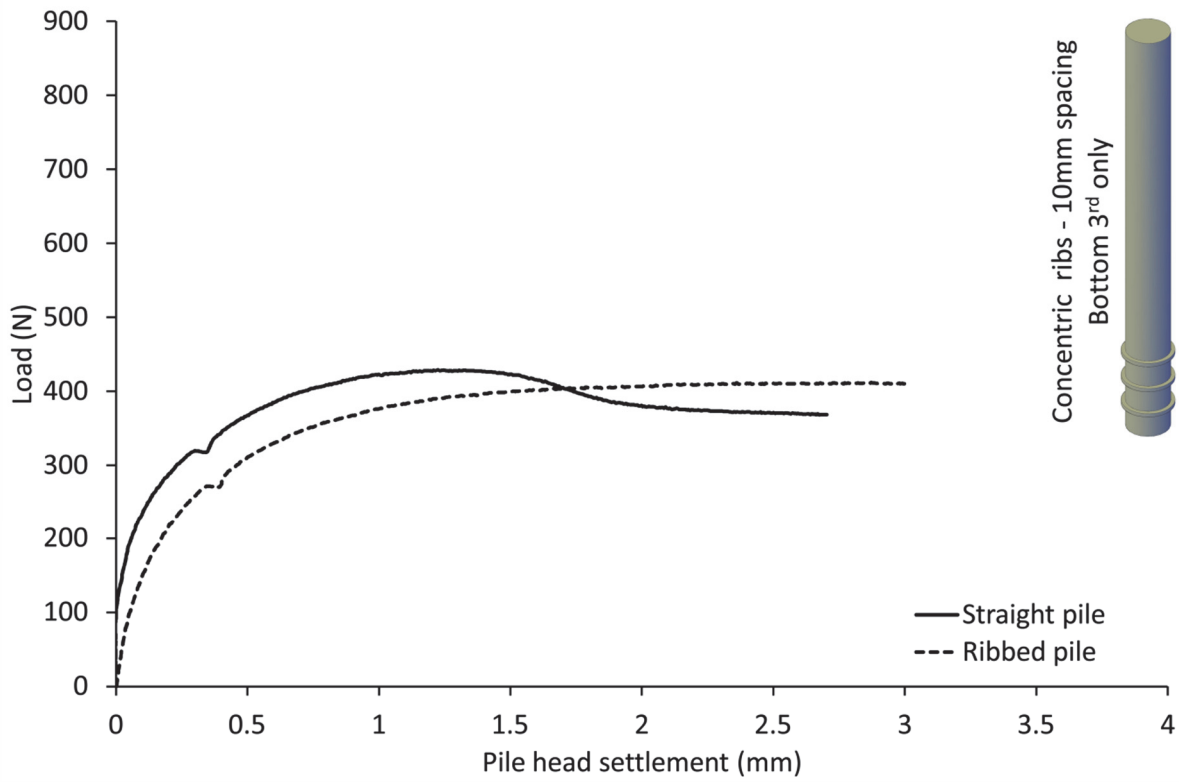

Figure 5.18 Load settlement curve, Test RJG14, concentrically ribbed pile with 10mm spacing with ribs only in bottom third of pile.

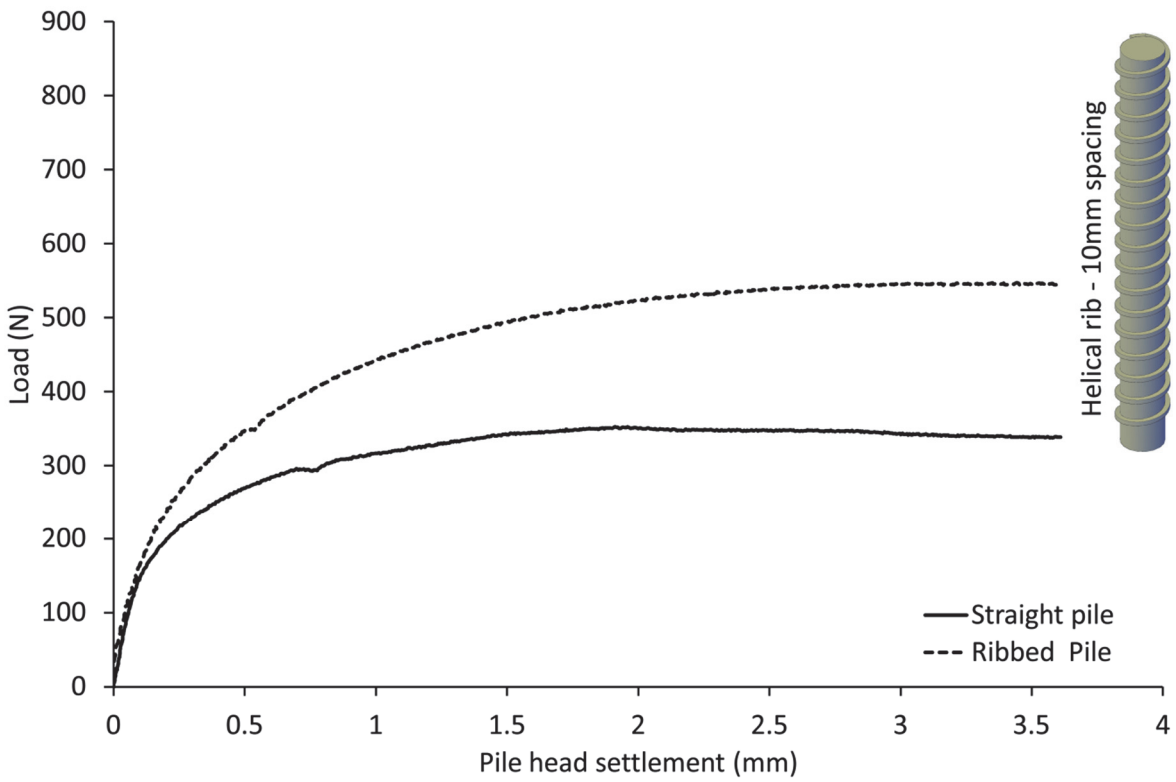

Figure 5.19 Load settlement curve, Test RJG8, helically ribbed pile with 10mm spacing.

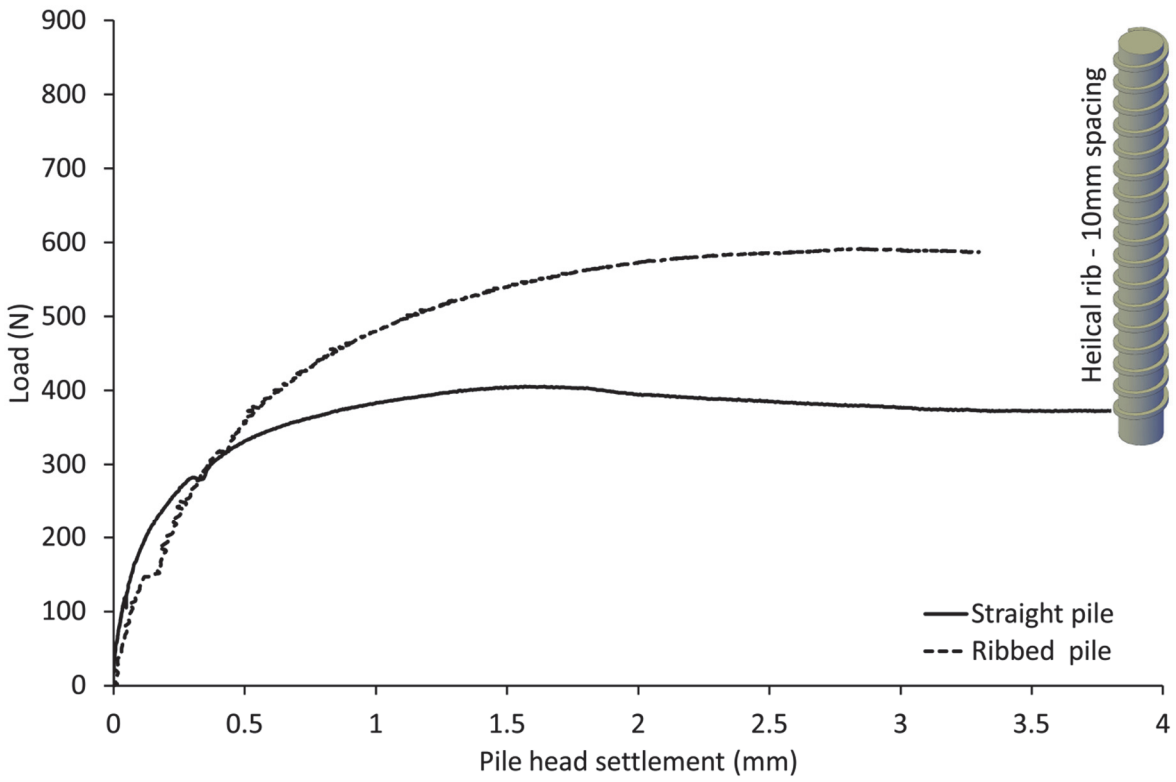

Figure 5.20 Load settlement curve, Test RJG9, helically ribbed pile with 10mm spacing.

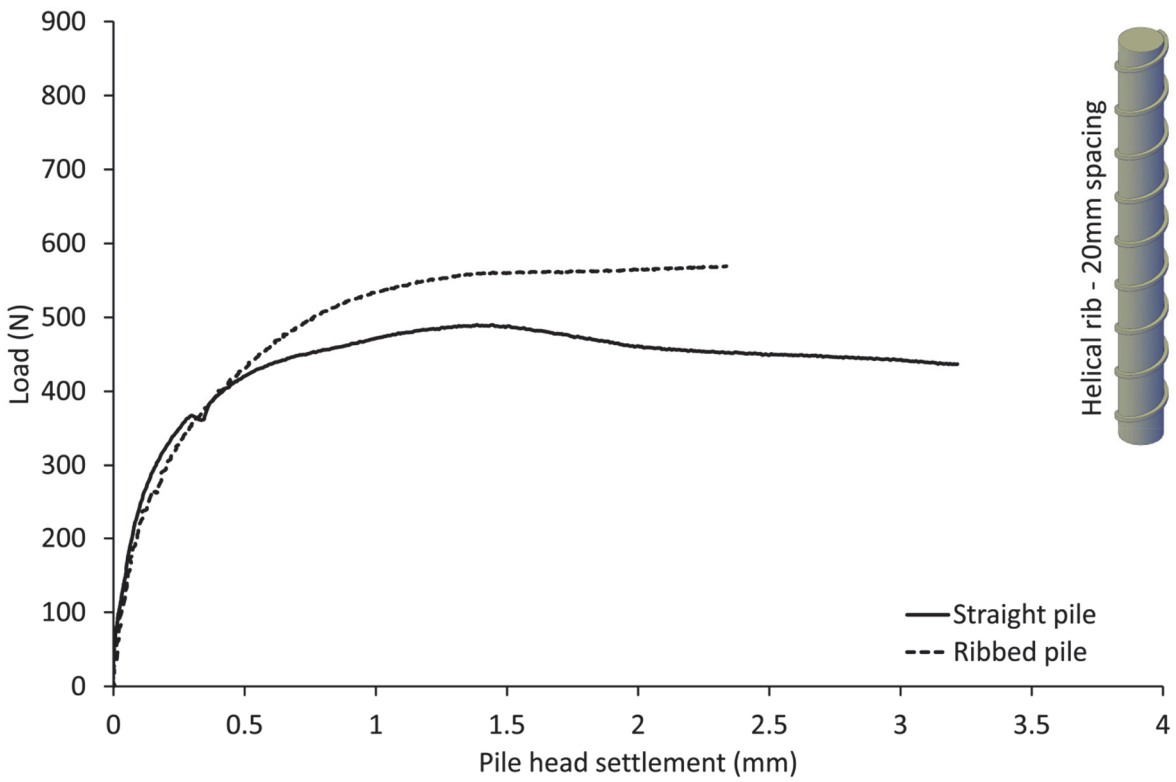

Figure 5.21 Load settlement curve, Test RJG16, helically ribbed pile with 20mm spacing.

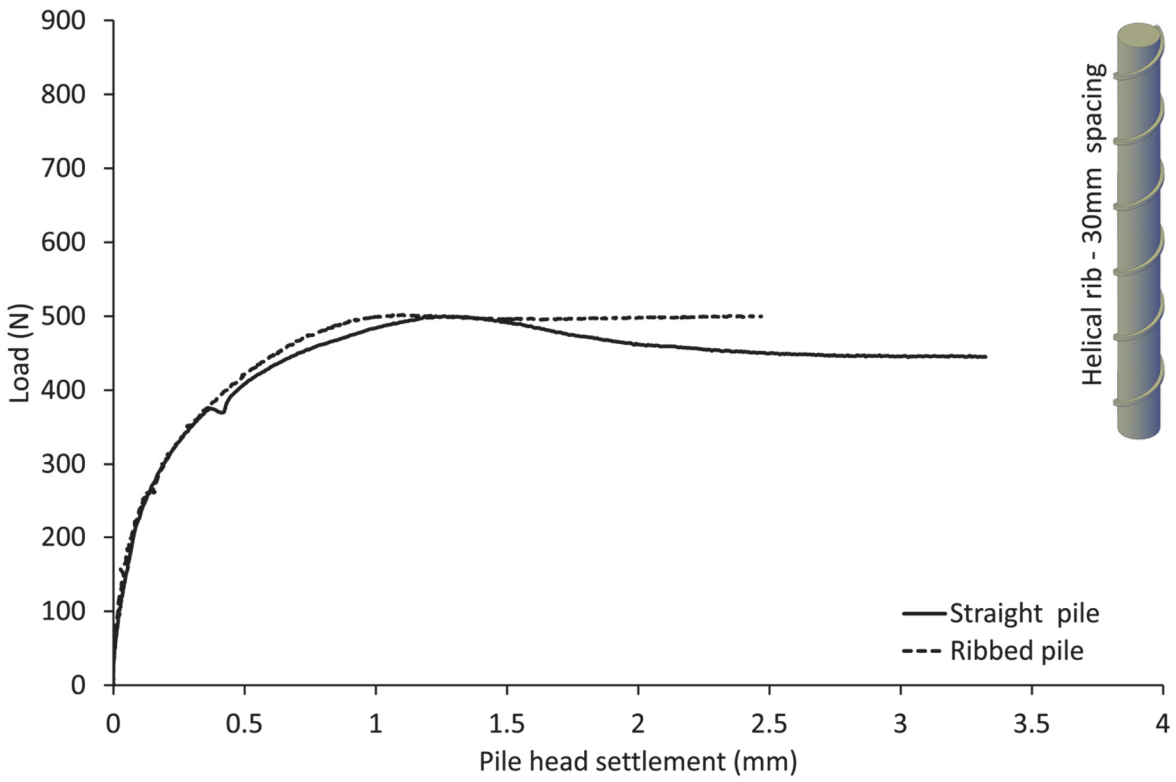

Figure 5.22 Load settlement curve, Test RJG17, helically ribbed pile with 30mm spacing.

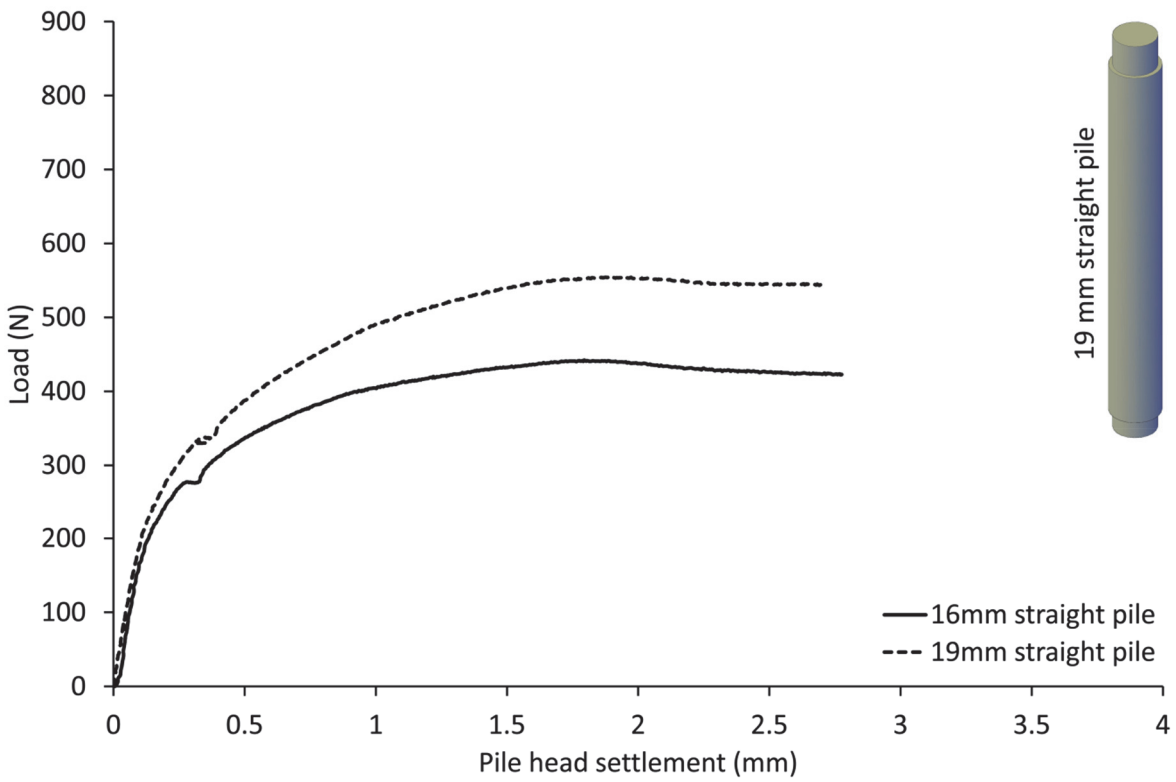

Figure 5.23 Load settlement curve, Test RJG11, 19mm diameter straight shafted pile.

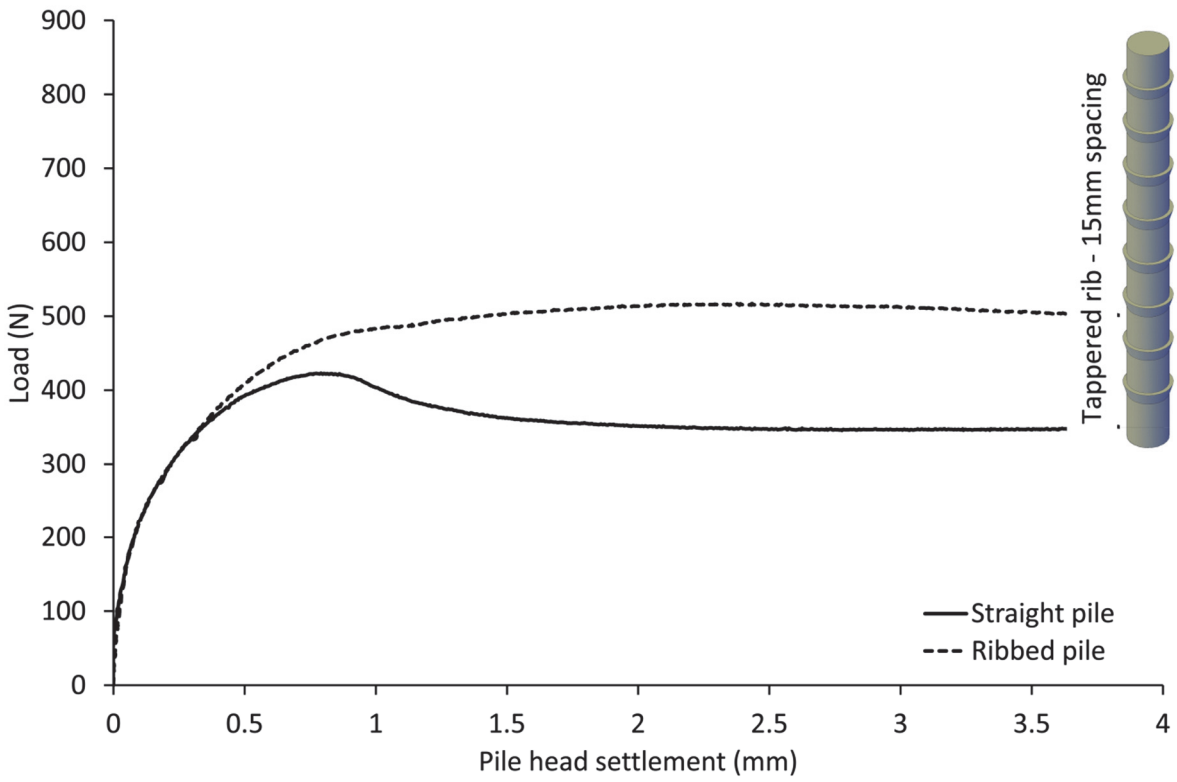

Figure 5.24 Load settlement curve, Test RJG15, tapered ribbed pile with 15mm spacing.

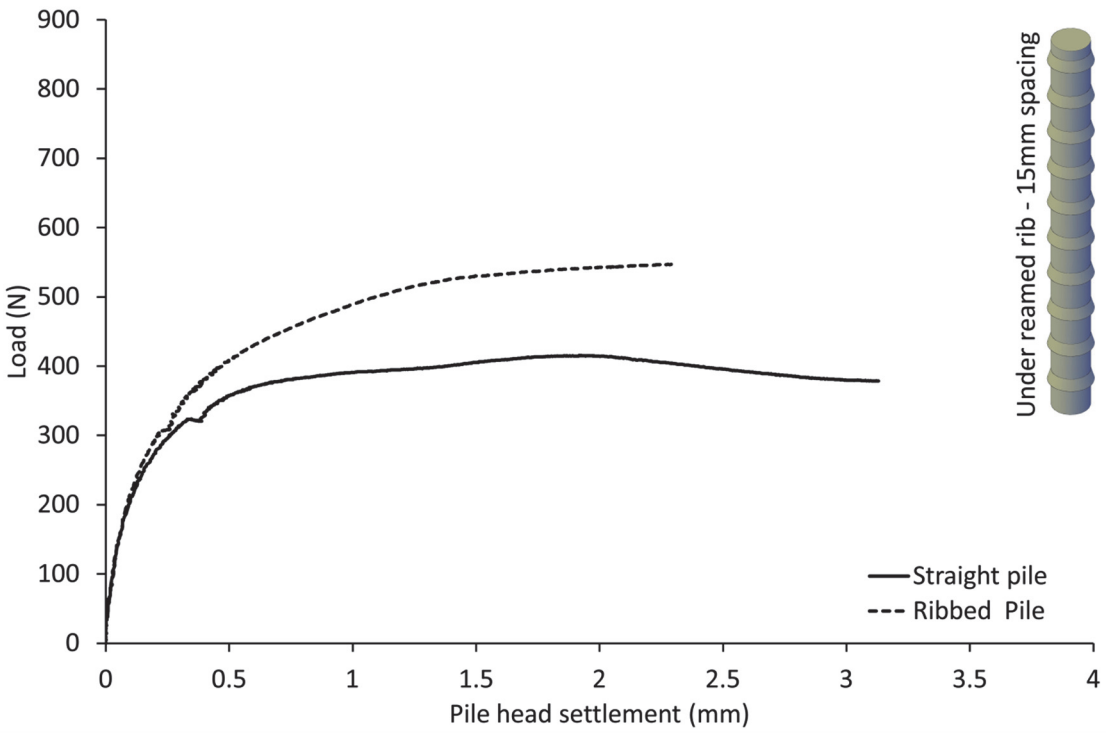

Figure 5.25 Load settlement curve, Test RJG22, under reamed pile with 15mm spacing.

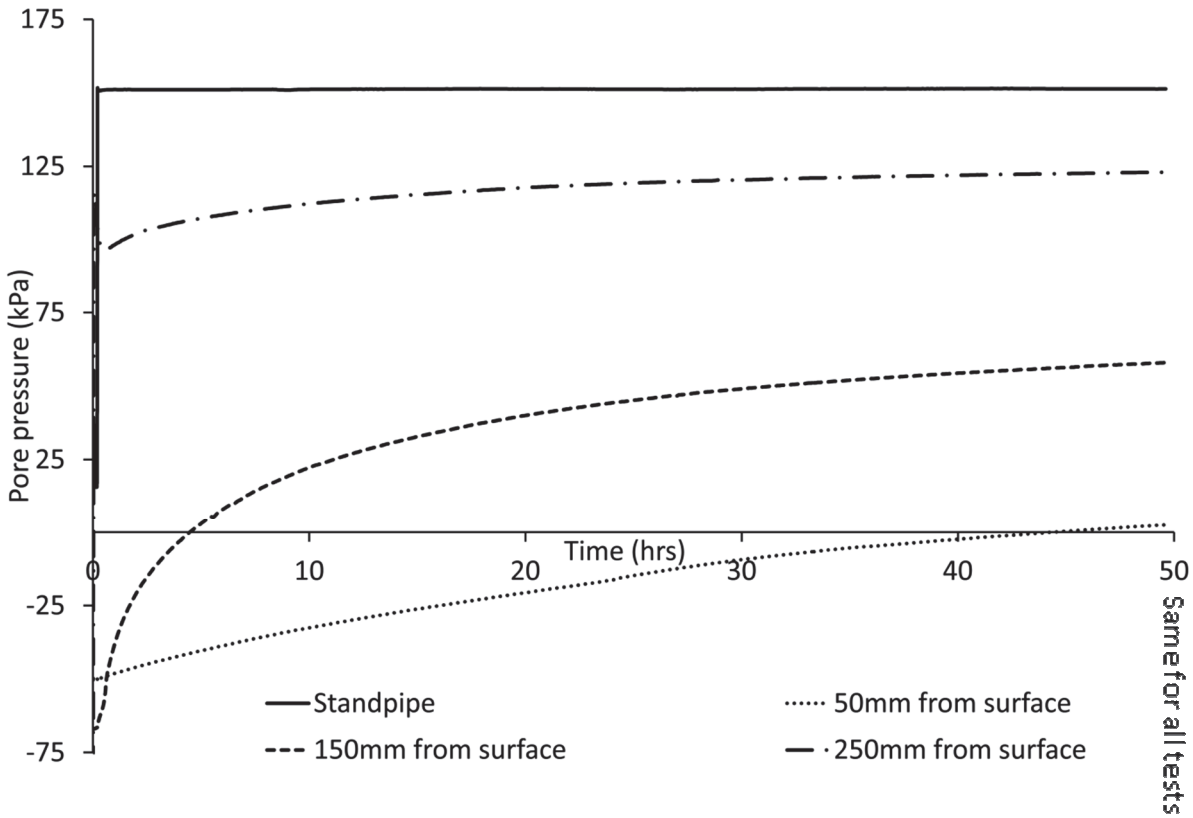

Figure 5.26 Typical PPT response during pore pressure equalisation.

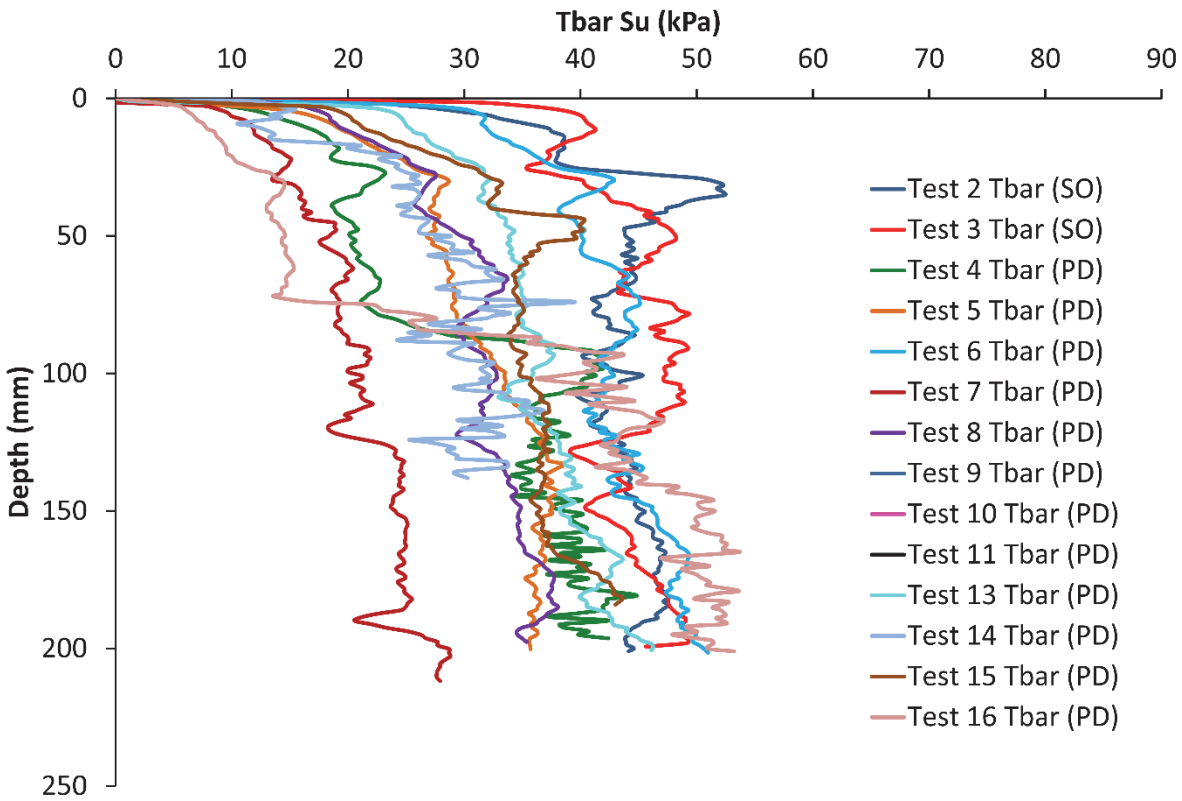

Figure 6.1 Undrained shear strength with depth as profiled by the T-bar

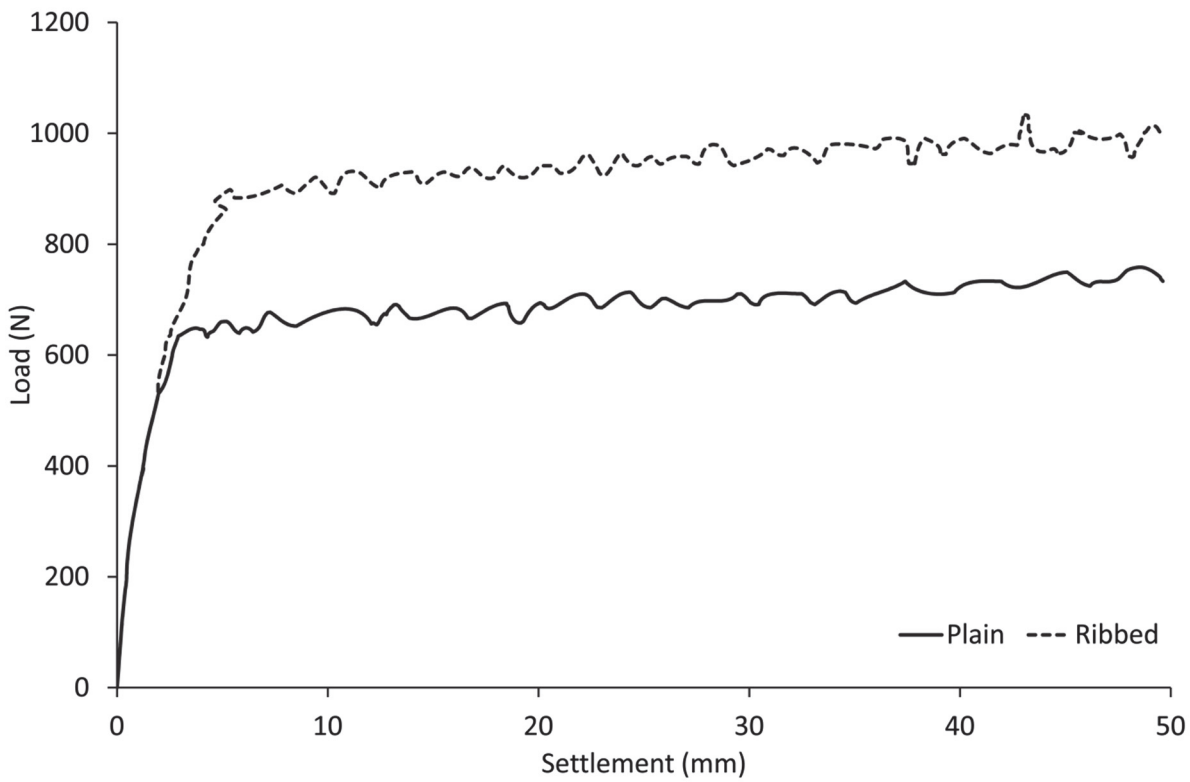

Figure 6.2 Load settlement curves from Expanded-Arup tests, Ground Engineering (2003).

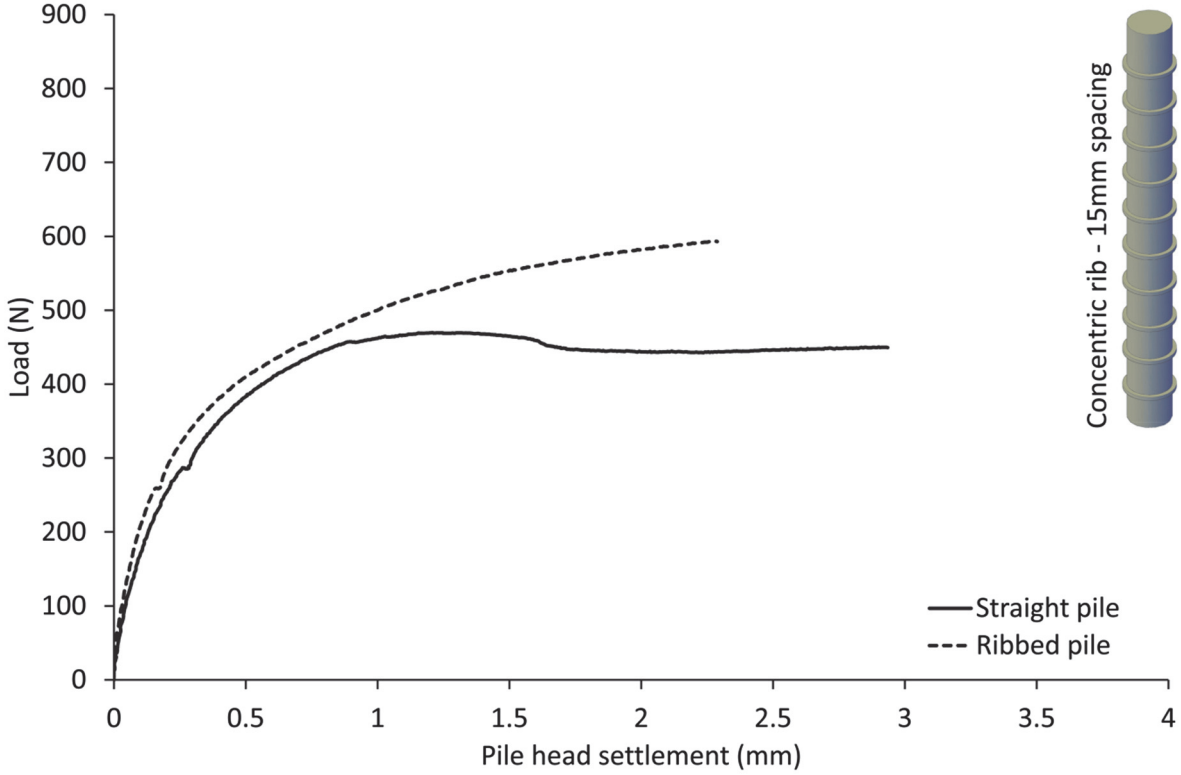

Figure 6.3 Load settlement curve, Test RJG4, concentrically ribbed pile with 15mm spacing.

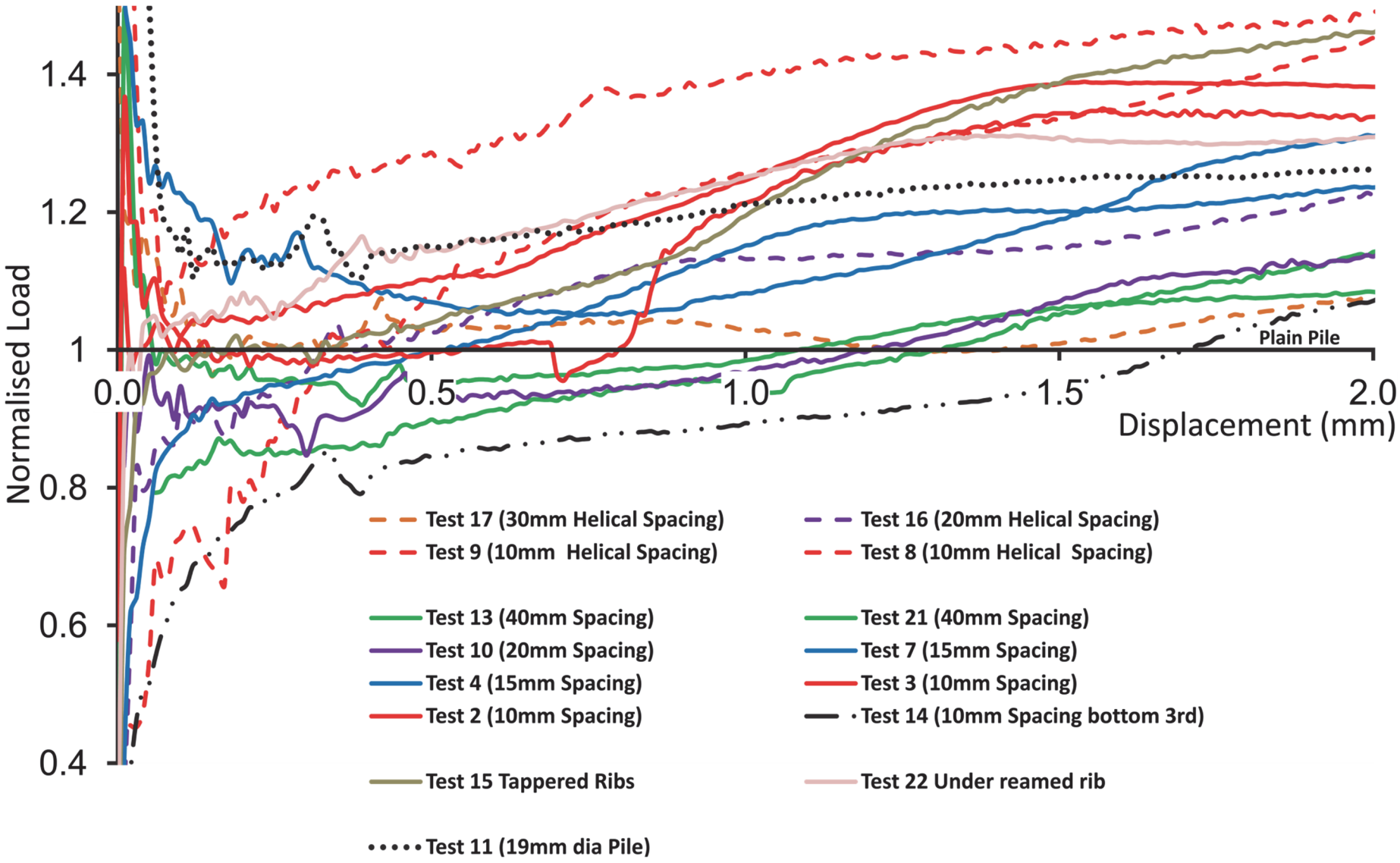

Figure 6.4 Normalised load settlement curves for all pile tests.

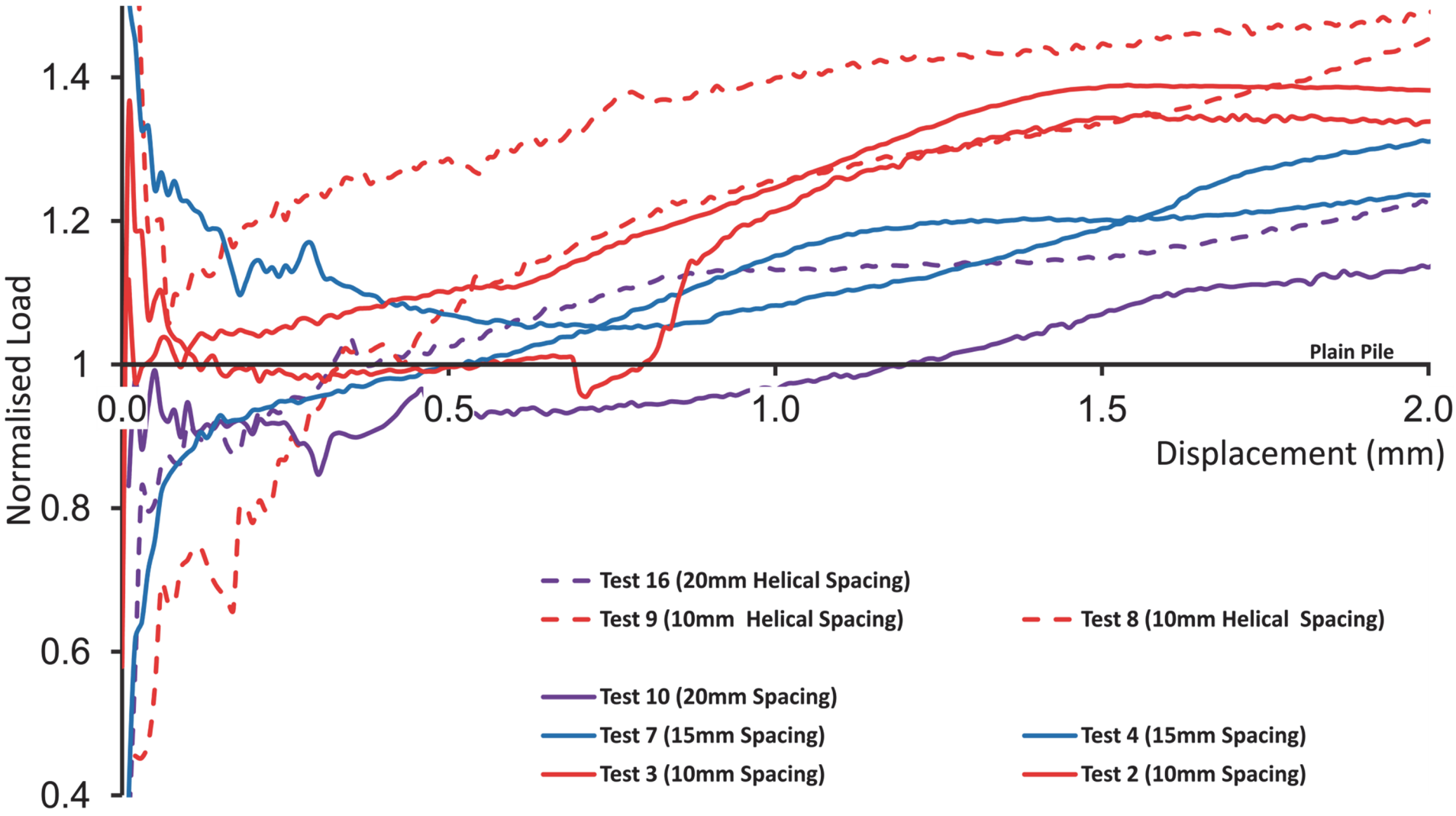

Figure 6.5 Normalised load settlement curves for concentric ribs and helical ribs with similar spacing.

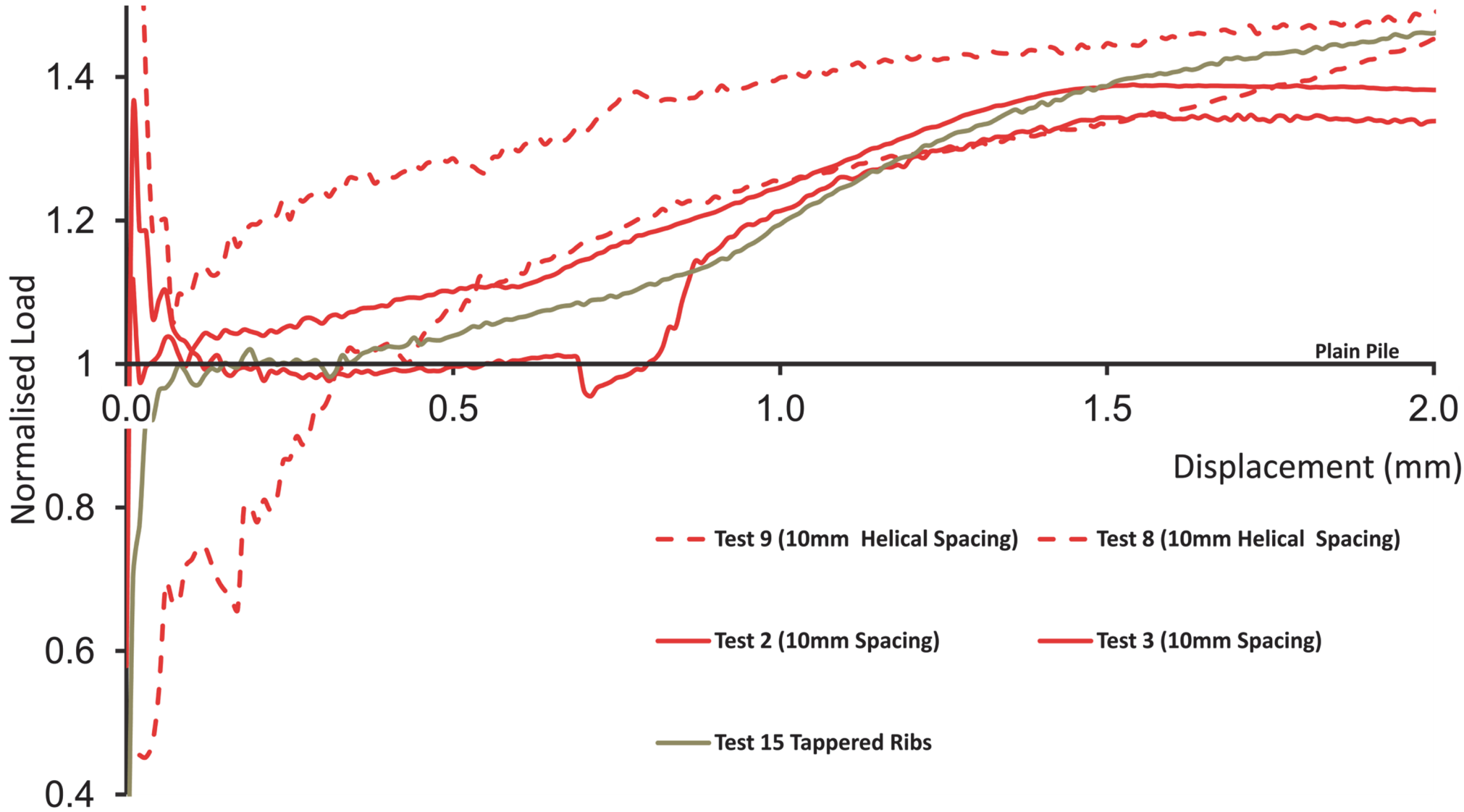

Figure 6.6 Normalised load settlement curves for 10mm spaced ribs and the tapered rib.

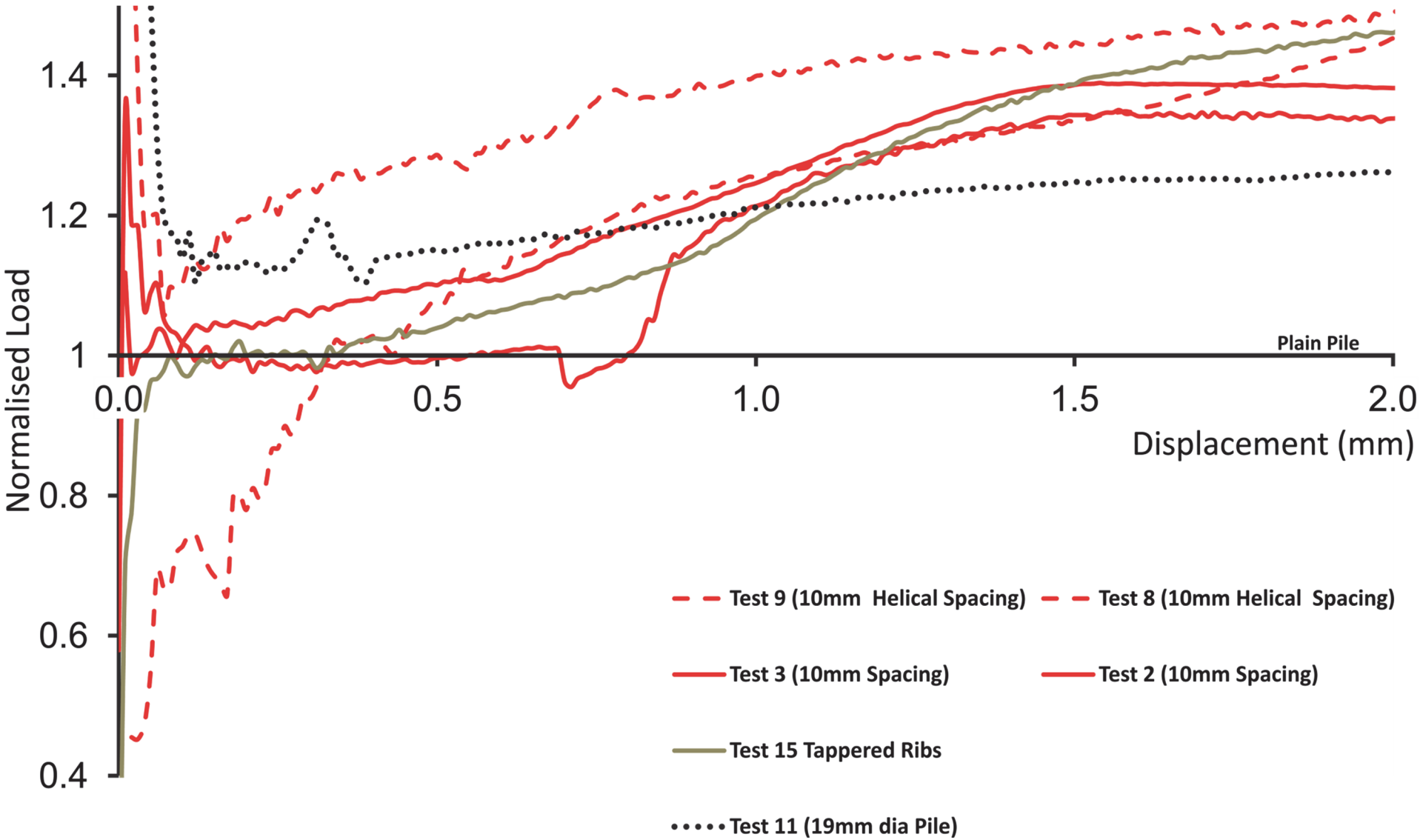

Figure 6.7 Normalised load settlement curves for the 19mm plain pile and the 10mm spaced ribbed piles.

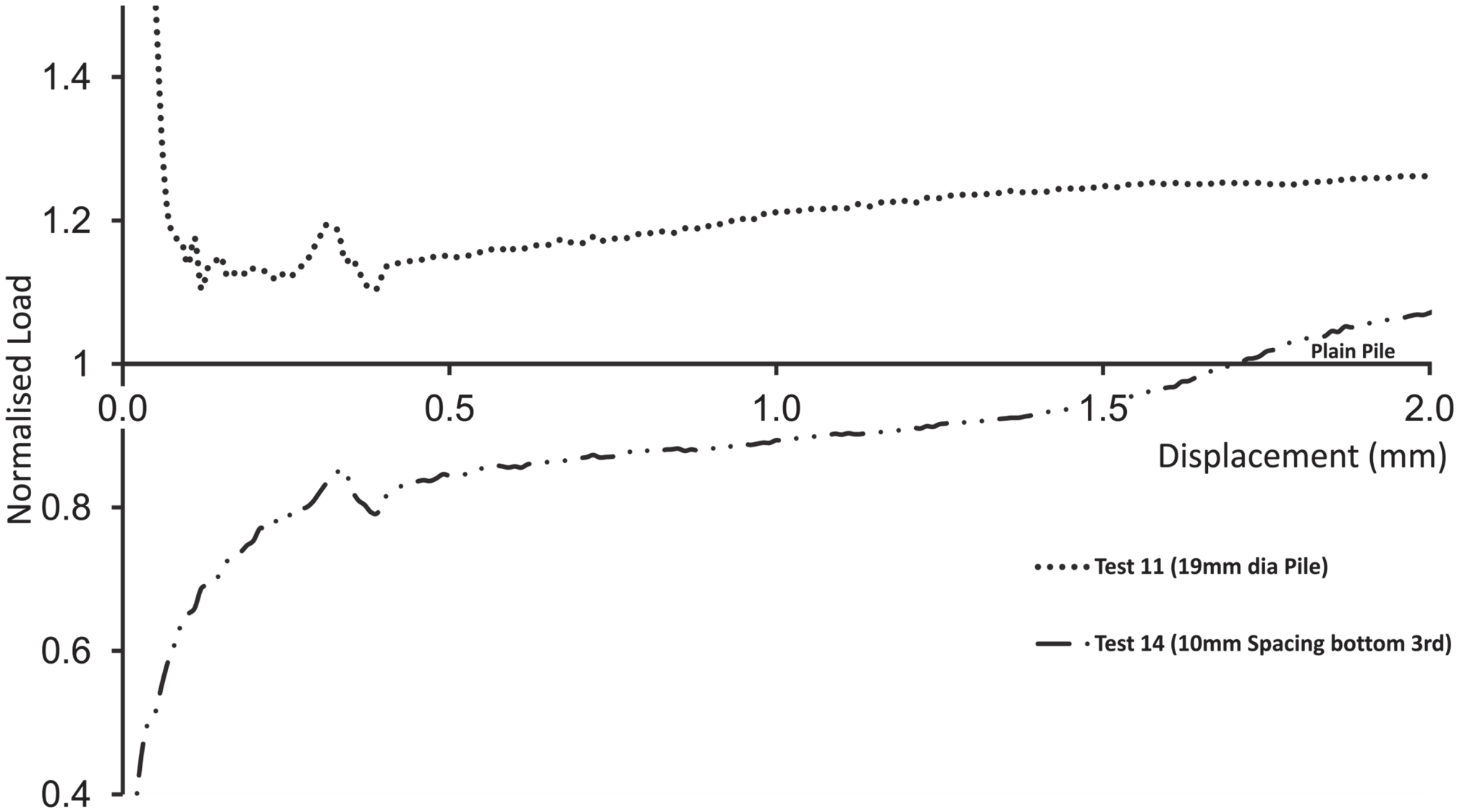

Figure 6.8 Normalised load settlement curves for the 19mm plain pile and a pile with the bottom third concentrically ribbed.

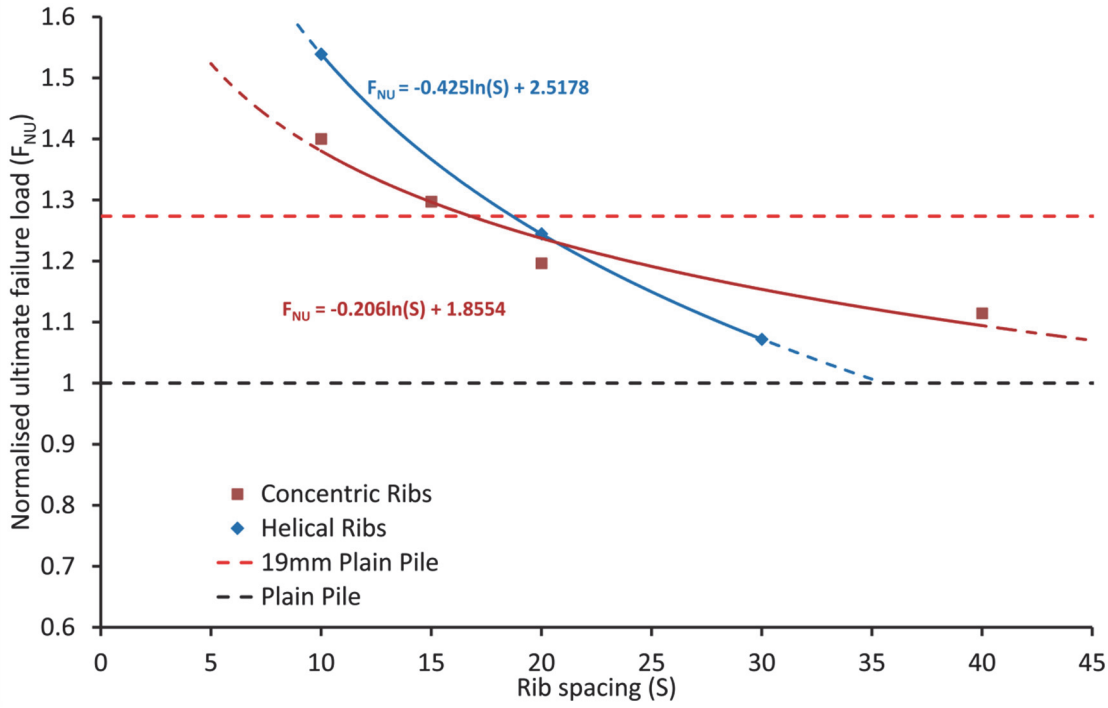

Figure 6.9 Average normalised load settlement curves for helical and concentric rib types.

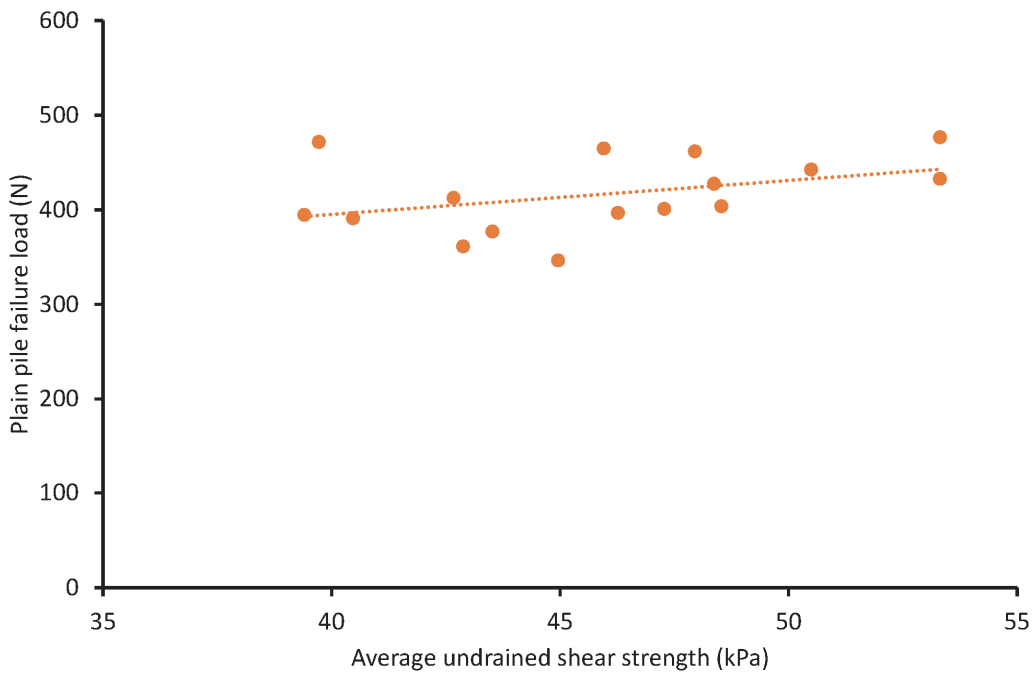

Figure 6.10 Plain pile ultimate capacity against soil sample average undrained shear strength for all successful tests.

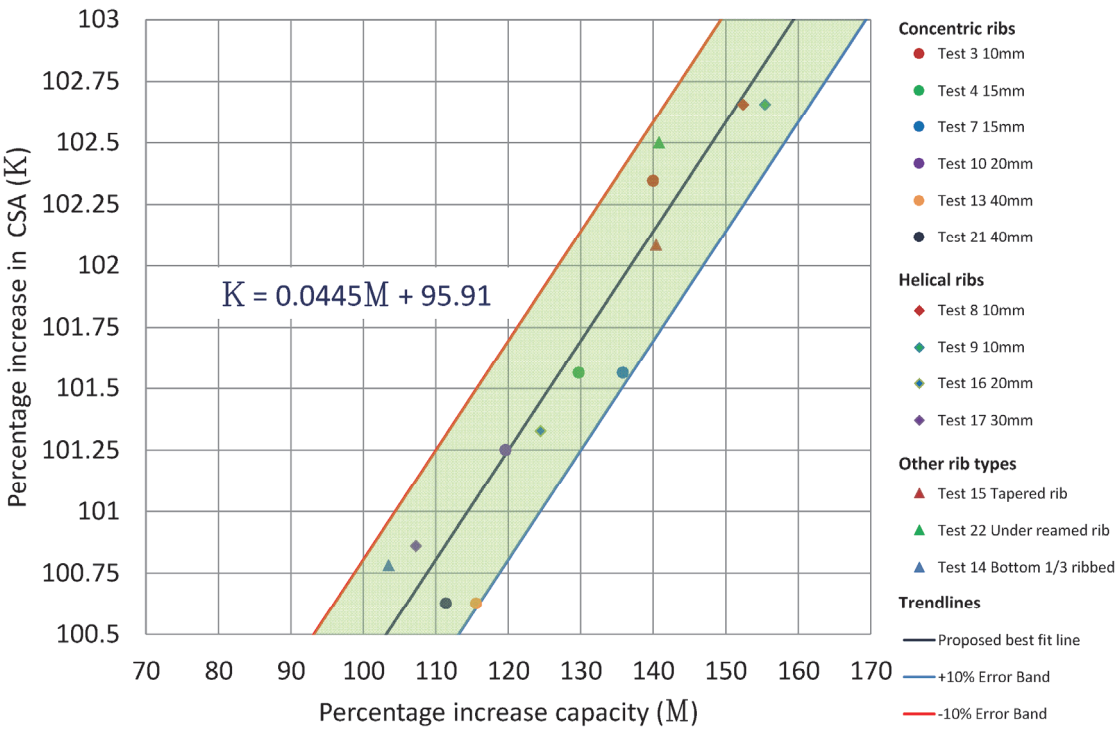

Figure 6.11 Percentage increase in pile cross sectional area (K) against the percentage increase in ultimate bearing capacity (M).

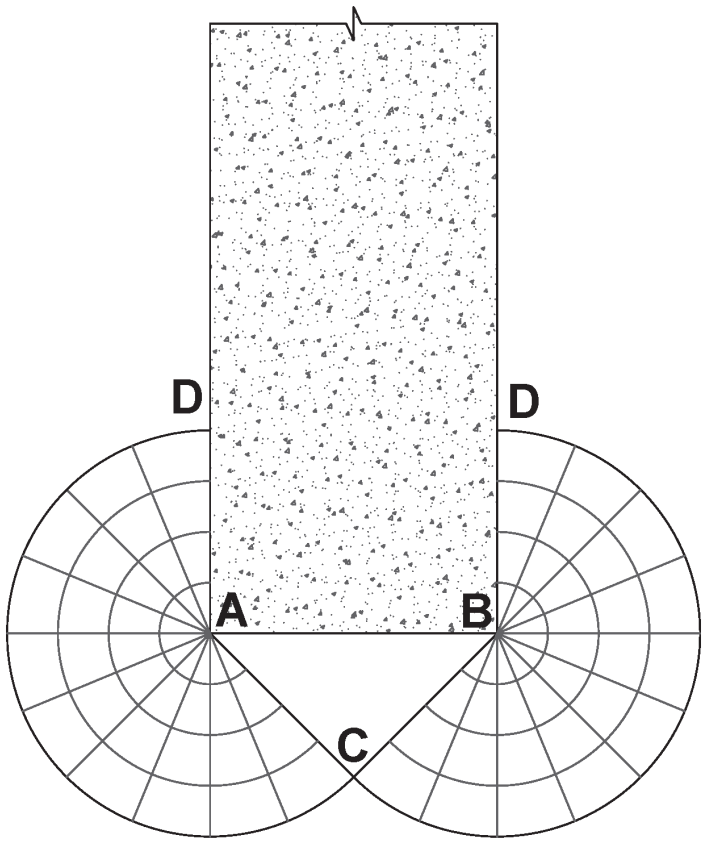

Figure 6.12 The end bearing plastic failure envelope for perfectly rough deep piles as presented by Meyerhof (1951).

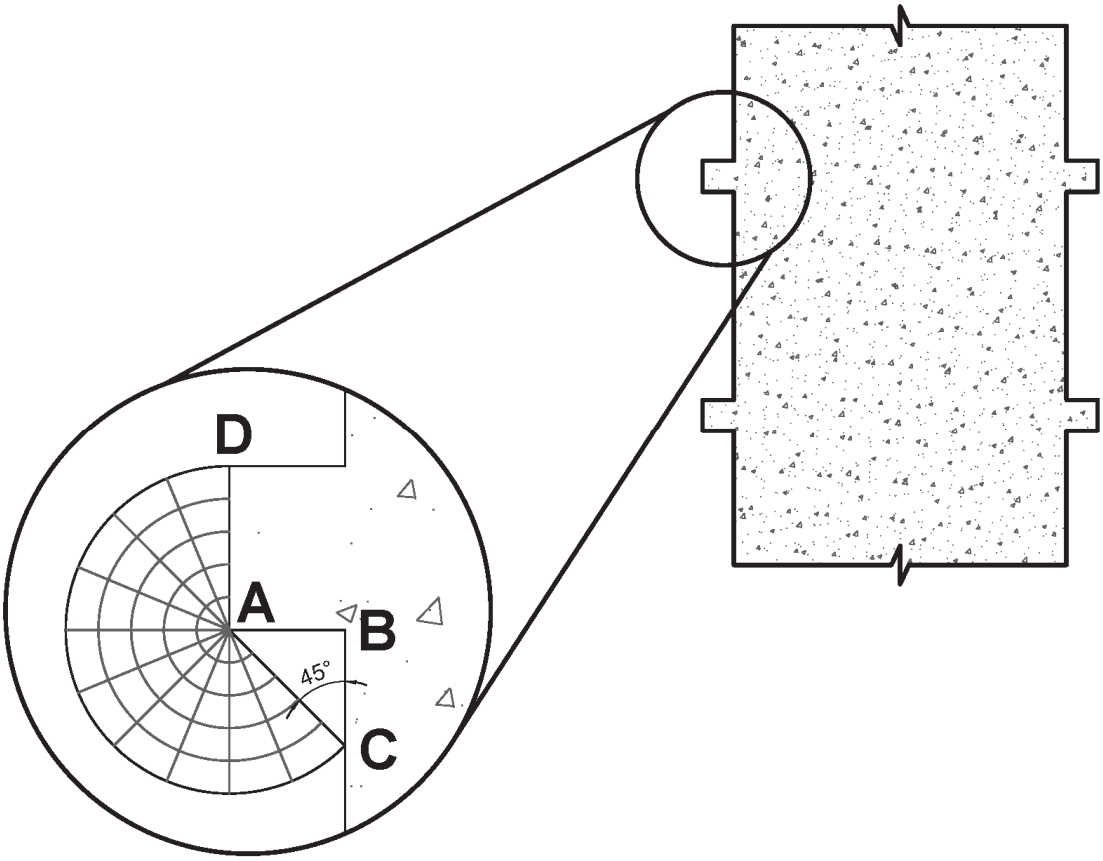

Figure 6.13 The proposed end bearing plastic failure envelope for concentric ribs.

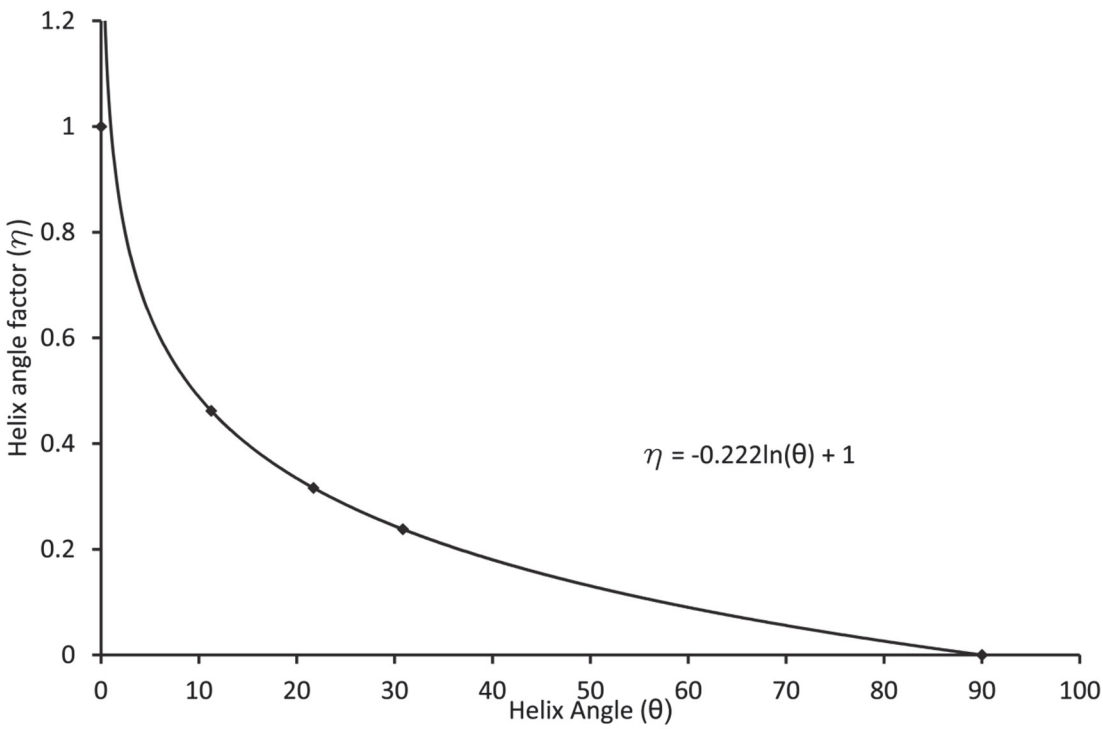

Figure 6.14 Helix angle factor (η) against the helix angle (θ) for helical ribs.

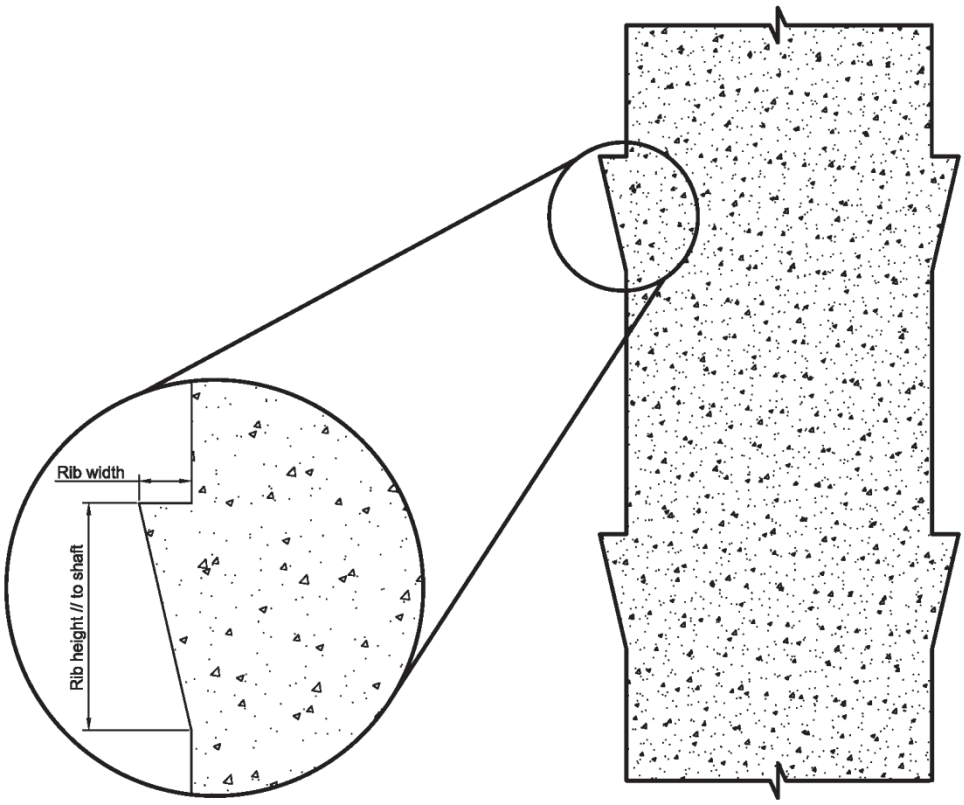

Figure 6.15 Tapered rib pile – rib height for shear calculation.

Appendix A: Example pile capacity calculation

For each ribbed pile tested a theoretical capacity was calculated using the detailed design method presented in Chapter 6.0. An example of this calculation for test RJG4 (15 mm concentrically ribbed pile) is presented here.

Soil strength profile

A soil strength profile based on the measured undrained shear strength is identified as:

$$S_u = 36.7 + 0.125Z \tag{A.1}$$

Where Z is the model scale depth in mm and S_U is the undrained shear strength in kPa.

Plain pile capacity

The failure load (Q_u) of the plain pile in test RJG4 is 1154.66kN, at prototype scale. This value has been derived from back analysis of the load settlement data (see Table 6.1).

The end bearing capacity Q_b is calculated by first calculating the undrained shear strength at the depth of the pile base (180mm).

$$S_u = 36.7 + 0.125 \times 180 = 59.20\ kPa \tag{A.2}$$

Q_b can then be calculated as:

$$Q_b = N_C \times S_{u\,(base)} \times A_b + w$$
$$Q_b = 6 \times 59.2 + 0.502 = 178.6\ kN \tag{A.3}$$

Where:

- N_C is the bearing capacity factor,
- A_b is the cross section area of the pile base at prototype scale in m^2, and
- w is the prototype weight of the pile in kN.

The shaft friction (Q_S) of the pile can be calculated from:

$$Q_s = \alpha \times S_{u(AVG)} \times A_s \tag{A.4}$$

Where:

- $S_{u(AVG)}$ is the average undrained shear strength,
- A_s is the area of pile shaft at prototype scale in m^2, and
- α is the adhesion factor.

As α is currently unknown $\frac{Q_s}{\alpha}$ must be calculated first:

$$\frac{Q_s}{\alpha} = 59.2\ kPa \times 22.62\ m = 1084.6\ kN \tag{A.5}$$

The adhesion factor α can then be calculated from the measure failure load and the calculated base capacity:

$$\alpha = \frac{Q_u - Q_b}{Q_s/\alpha}$$

$$\alpha = \frac{1154.66 - 178.6}{1084.6} = 0.9 \tag{A.6}$$

This value of α can be assumed for the ribbed pile in test RJG4 since both piles were installed under the same conditions in the same soil sample with identical resin.

Ribbed pile capacity

The capacity of a ribbed pile can be calculated from the following equation:

$$Q_u = \sum Q_s + Q_b + \sum Q_{rs} + \sum Q_{rb} \tag{A.7}$$

Where: Q_u – ultimate loading capacity of the pile,

Q_s – ultimate skin friction along the plain shaft,

Q_b – ultimate base resistance,

Q_{rs} – ultimate skin friction along the rib shaft,

Q_{rb} – ultimate base resistance from each rib and,

The end bearing capacity of the ribbed pile is the same as the plain pile, hence

$$Q_b = 178.6\ kN \tag{A.8}$$

The rib base capacity is calculated for each rib using the following equation:

$$Q_{rb} = S_{u(rb)} \times N_C \times A_{rb} \tag{A.9}$$

Where: $S_{u(rb)}$ is the soil undrained shear strength at the rib base,

N_C is the bearing capacity factor and,

A_{rb} is the prototype area of the rib base in m^2.

The rib shaft capacity is calculated for each rib using the following equation:

$$Q_{rs} = S_{u(rs)} \times \alpha \times A_{rs} \tag{A.10}$$

Where: $S_{u(rs)}$ is the soil undrained shear strength at the centre of the rib,

α is the adhesion factor back calculated from the plain pile and,

A_{rs} is the prototype area of the rib shaft in m^2.

Table A.1 shows the calculated rib base and shaft capacities for test RJG4 using equations A.9 and A.10.

Rib No:	Rib base capacity (Q_{rb})	Rib shaft capacity (Q_{rs})
Rib 1	46.86	7.61
Rib 2	50.19	8.15
Rib 3	53.51	8.70
Rib 4	56.84	9.24
Rib 5	60.16	9.78
Rib 6	63.49	10.32
Rib 7	66.82	10.86
Rib 8	70.17	11.40
TOTAL	468.01 kN	76.06 kN

Table A.1 calculated rib base and shaft capacities

The shaft capacity from the plain shaft was calculated using the following equation:

$$Q_s = S_{u(s)} \times \alpha \times A_s \tag{A.11}$$

Where: $S_{u(s)}$ is the soil undrained shear strength at the centre of the portion of shaft,

α is the adhesion factor back calculated from the plain pile and,

A_s is the prototype area of the shaft in m^2.

Table A.2 shows the calculated plain shaft capacity for test RJG4 using equations A.11.

Shaft No:	Plain shaft capacity (Q_s)
Shaft 1	47.37
Shaft 2	55.44
Shaft 3	58.36
Shaft 4	61.28
Shaft 5	64.20
Shaft 6	67.11
Shaft 7	70.03
Shaft 8	72.95
Shaft 9	75.86
Shaft 10	78.78
Shaft 11	101.72
TOTAL	753.10 kN

Table A.2 calculated plain shaft capacities

In order to calculate the ultimate capacity the constitutive components are summated:

$$Q_u = \sum Q_s + Q_b + \sum Q_{rs} + \sum Q_{rb}$$
$$Q_u = 753.10 + 178.6 + 76.06 + 468.01 \tag{A.12}$$
$$Q_u = 1475.77\ kN$$

The actual failure load of this pile was 1498.17 kN. The theoretical and actual capacities are within 2%.